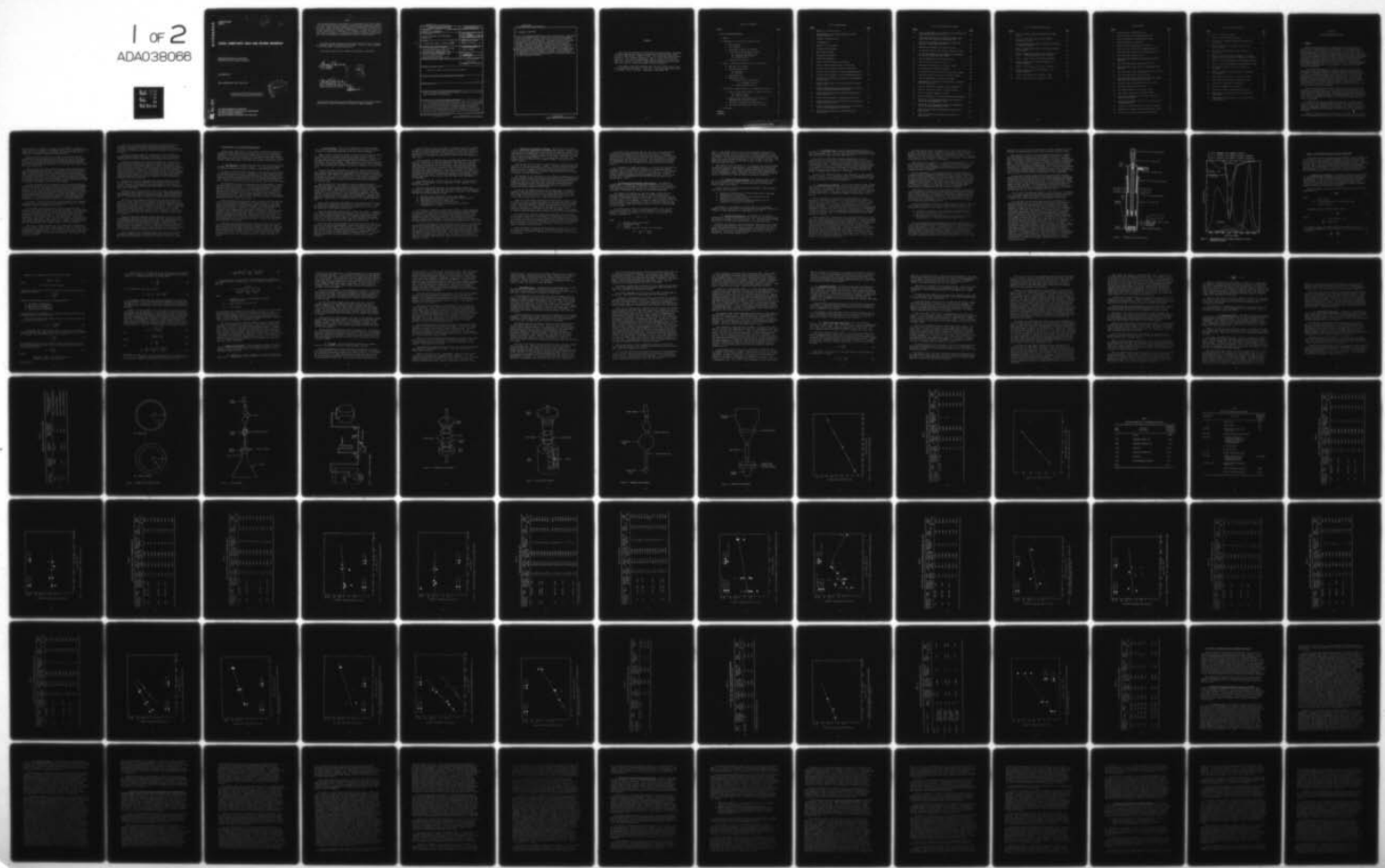


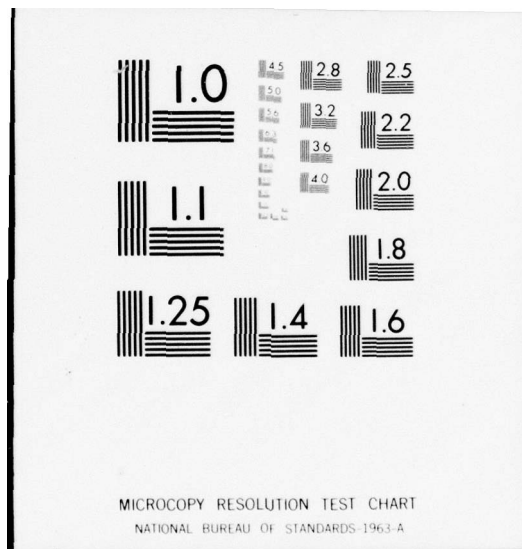
AD-A038 066

PENNSYLVANIA STATE UNIV UNIVERSITY PARK PETROLEUM RE--ETC F/G 11/8  
FLUIDS, LUBRICANTS, FUELS AND RELATED MATERIALS. (U)  
NOV 76 E E KLAUS, E J TEWKSBURY, E CVITKOVIC F33615-73-C-5101  
AFML-TR-74-201-PT-3 NL

UNCLASSIFIED

1 of 2  
ADA038066





ADA 038066

AFML-TR-74-201  
Part III

(12)

JK

## FLUIDS, LUBRICANTS, FUELS AND RELATED MATERIALS

*PETROLEUM REFINING LABORATORY*  
*THE PENNSYLVANIA STATE UNIVERSITY*

NOVEMBER 1976

FINAL REPORT MAY 1975 - APRIL 1976

Approved for public release; distribution unlimited



AIR FORCE MATERIALS LABORATORY  
AIR FORCE WRIGHT AERONAUTICAL LABORATORIES  
AIR FORCE SYSTEMS COMMAND  
WRIGHT-PATTERSON AIR FORCE BASE, OHIO 45433

FILE COPY

NOTICE

When Government drawings, specifications, or other data are used for any purpose other than in connection with a definitely related Government procurement operation, the United States Government thereby incurs no responsibility nor any obligation whatsoever; and the fact that the government may have formulated, furnished, or in any way supplied the said drawings, specifications, or other data, is not to be regarded by implication or otherwise as in any manner licensing the holder or any other person or corporation, or conveying any rights or permission to manufacture, use, or sell any patented invention that may in any way be related thereto.

This report has been reviewed by the Information Office (OI) and is releasable to the National Technical Information Service (NTIS). At NTIS, it will be available to the general public, including foreign nations.

This technical report has been reviewed and is approved for publication.

*George J. Morris*  
GEORGE J. MORRIS  
Project Engineer



*Larry L. Fehrenbacher*  
LARRY L. FEHRENBACHER, Major, USAF  
Chief, Lubricants and Tribology Branch  
Nonmetallic Materials Division

Copies of this report should not be returned unless return is required by security considerations, contractual obligations, or notice on a specific document.

Unclassified

SECURITY CLASSIFICATION OF THIS PAGE (When Data Entered)

REPORT DOCUMENTATION PAGE		READ INSTRUCTIONS BEFORE COMPLETING FORM
1. REPORT NUMBER AFML-TR-74-201, Part III	2. GOVT ACCESSION NO.	3. RECIPIENT'S CATALOG NUMBER
4. TITLE (and Subtitle) FLUIDS, LUBRICANTS, FUELS AND RELATED MATERIALS		5. TYPE OF REPORT & PERIOD COVERED Final Report 1 May 75 through 30 April 76
7. AUTHOR(s) E. Erwin Klaus, Elmer J. Tewksbury, et al.		6. PERFORMING ORG. REPORT NUMBER AF33615-73-C-5101
9. PERFORMING ORGANIZATION NAME AND ADDRESS Petroleum Refining Lab., Chem. Engr. Dept. The Pennsylvania State University University Park, PENNSYLVANIA 16802		10. PROGRAM ELEMENT, PROJECT, TASK AREA & WORK UNIT NUMBERS 7343 - 734303
11. CONTROLLING OFFICE NAME AND ADDRESS Air Force Materials Laboratory (MBT) Air Force Systems Command Wright-Patterson AFB, OHIO 45433		12. REPORT DATE November 1976
14. MONITORING AGENCY NAME & ADDRESS (if different from Controlling Office)		13. NUMBER OF PAGES 168
16. DISTRIBUTION STATEMENT (of this Report) Approved for public release, distribution unlimited.		15. SECURITY CLASS. (of this report) Unclassified
17. DISTRIBUTION STATEMENT (of the abstract entered in Block 20, if different from Report)		15a. DECLASSIFICATION/DOWNGRADING SCHEDULE 280 450
18. SUPPLEMENTARY NOTES		
19. KEY WORDS (Continue on reverse side if necessary and identify by block number) Fluids, Lubricants, Lubrication, Small Capillary Viscometer, Micro Oxidation Test, Gel Permeation Chromatography		
20. ABSTRACT (Continue on reverse side if necessary and identify by block number) A new microtest for the evaluation of the oxidative and thermal degradation of fluids and lubricants has been developed. This test, in conjunction with gel permeation chromatography, promises to provide a means for the rapid determination of the extent of oxidative and additive degradation. The effects of base fluid viscosity, mean pore diameter, and additive concentration on the formation of thin films on a capillary wall are examined. Mean pore diameters of 0.2 to 1.2 microns are used. These thin films are (cont on p 1473 B)		

DD FORM 1 JAN 73 1473A EDITION OF 1 NOV 65 IS OBSOLETE  
S/N 0102-014-6601

Unclassified

SECURITY CLASSIFICATION OF THIS PAGE (When Data Entered)

bpg

UNCLASSIFIED

SECURITY CLASSIFICATION OF THIS PAGE(When Data Entered)

20. Abstract (concluded)

*(cont'd p 1473A)*  
shown to have different properties than those of the bulk fluid. Competition of additives is shown to have an effect on the formation and thickness of these surface films. Cellulose type filters as well as metal filters are used to provide the micro capillaries. Techniques which allow the accurate determination of wear debris from the four-ball wear tester have been developed. Preferential and competitive adsorption of polar species on the metal surface and the subsequent chemical reactions are shown to be the key process in boundary lubrication. Additive competition is apparent. Commercial phosphorus-containing antiwear additives are investigated using the experimental technique developed in this study. Surface temperatures are demonstrated to be a key parameter in boundary surface interactions both physically and chemically. The importance of the chemical interactions in boundary conditions is shown.

1473B

UNCLASSIFIED

SECURITY CLASSIFICATION OF THIS PAGE(When Data Entered)

## FOREWORD

This report was prepared by the Petroleum Refining Laboratory, Department of Chemical Engineering, College of Engineering at The Pennsylvania State University under Contract F33615-73-C-5101. This project was initiated under Project No. 7343 "Aerospace Lubricants," Task No. 734303 "Fluid Lubricant Materials." This work was administered under the direction of the Air Force Materials Laboratory, Air Force Systems Command, Wright-Patterson Air Force Base, Ohio, with Mr. George Morris (MBT) as Project Engineer.

This report covers work conducted from 1 May 1975 through 30 April 1976. It was submitted by the authors 15 June 1976. They are E. Erwin Klaus, Elmer J. Tewksbury, Emilio Cvitkovic, Joseph Maskew, and Stephen Hsu.

TABLE OF CONTENTS

<u>Section</u>	<u>Page</u>
I. FLUID AND LUBRICANT STUDIES . . . . .	1
1. Summary . . . . .	1
2. Development of a 40 Microliter Oxidation Test . . . . .	4
a. Test Apparatus . . . . .	4
b. Test Procedures . . . . .	5
c. Preparation of Analytical Solutions . . . . .	7
d. Gel Permeation Chromatography Analysis . . . . .	8
(1) Solvent-Solute Interactions . . . . .	9
(2) Gel-Solute Interactions . . . . .	9
(3) Analytical Unit . . . . .	10
e. Interpretation of Results . . . . .	10
3. Effect of Lubrication Additives on Flow in Thin Films . . . . .	15
a. Modeling of Porous Media . . . . .	15
b. Apparatus and Procedure . . . . .	18
(1) Apparatus . . . . .	18
(2) Procedure . . . . .	19
c. Experimental Error . . . . .	21
d. Experimental Results . . . . .	24
(1) Results with Cellulose Filters . . . . .	24
(a) Modeling Fluid Flow . . . . .	28
(2) Studies with Metal Filters . . . . .	29
4. The Effects of Chemical Reactions in Boundary Lubrications . .	70
a. Effects of Operating Parameters on Chemical Reactions .	70
(1) Effects of Load . . . . .	70
(2) Effects of Speed . . . . .	72
b. Effects of Functional Groups on the Formation of Organometallics as Related to Wear . . . . .	73
c. The Study of Phosphorus-Containing Additives . . . . .	78
d. The Lubrication Mechanism of Tributyl Phosphite . . . .	83
5. Conclusions . . . . .	136
APPENDIX . . . . .	139
REFERENCES . . . . .	155

LIST OF ILLUSTRATIONS

<u>Figure</u>		<u>Page</u>
1	Apparatus for Oxidation Tests . . . . .	13
2	Chromatograms of the Oxidation Products of Ester-Inhibitor Solutions . . . . .	14
3	Schematic of Restricted Pore . . . . .	31
4	Test Apparatus . . . . .	32
5	Schematic of Test Assembly . . . . .	33
6	Millipore Filter Assembly . . . . .	34
7	Metal Filter Assembly . . . . .	35
8	Measuring Bulb Assembly . . . . .	36
9	Prefiltration Apparatus . . . . .	37
10	Effect of Fluid Viscosity on Efflux Time . . . . .	38
11	Effect of Applied Pressure Drop on Efflux Time . . . . .	40
12	Effective Film Thickness of Dimer Acid (PRL 3697) . . . . .	44
13	Effective Film Thickness of n-Octyl Polymethacrylate-25 . .	47
14	Effective Film Thickness of n-Octyl Polymethacrylate-55 . .	48
15	Effective Film Thickness as a Function of Pore Diameter for Oleic Acid . . . . .	51
16	Effect of Shear Stress on the Effective Film Thickness of Oleic Acid . . . . .	52
17	Effect of Shear Stress on the Effective Film Thickness of a Barium Sulfonated Hydrocarbon (PRL 3530) . . . . .	54
18	Effective Film Thickness for a Barium Sulfonated Hydrocarbon (PRL 3530) . . . . .	55
19	Effective Film Thickness of a Heavy Resin (ML) 7779) . .	59
20	Effect of Shear Stress on the Effective Film Thickness of a Heavy Resin (MLO 7779) . . . . .	60
21	Effect of Shear Stress on the Effective Film Thickness of a Partially Hydrogenated Resin (MLO 7760) . . . . .	61
22	Effective Film Thickness for a Hydrogenated Resin (LH 136, 137) . . . . .	62

LIST OF ILLUSTRATIONS (Continued)

<u>Figure</u>		<u>Page</u>
23	Effect of Shear Stress on the Effective Film Thickness for a Hydrogenated Resin (LH 136, 137) . . . . .	63
24	Effective Film Thickness of a Barium Sulfonated Hydrocarbon (PRL 3530) and a Heavy Resin (MLO 7779) . . . . .	66
25	Effective Film Thickness as a Function of Mean Pore Radius for a Heavy Resin (MLO 7779) . . . . .	68
26	Mean Wear Scar Diameter as a Function of Load . . . . .	90
27	Oil Insoluble Iron per Unit Area as a Function of Load . .	91
28	Oil Insoluble Organic Iron as a Function of Temperature in the Slow-Sliding Tests (MLO 7789A) . . . . .	92
29	Junction Temperatures as a Function of Load . . . . .	93
30	Iron Particles as a Function of Load . . . . .	94
31	Mean Wear Scar Diameter as a Function of Speed . . . . .	96
32	Iron Particles as a Function of Speed . . . . .	97
33	Oil Insoluble Iron per Unit Area as a Function of Speed . .	98
34	Iron Particles per Unit Area as a Function of Speed . . . .	99
35	Junction Temperatures as a Function of Speed . . . . .	100
36	Organometallic Iron Formation as a Function of Octadecyl Alcohol Concentration . . . . .	103
37	Wear as a Function of Octadecyl Alcohol Concentration . . .	104
38	Wear as a Function of Stearic Acid Concentration . . . .	108
39	Effect of Aromatic Components on Wear . . . . .	110
40	Wear as a Function of the Various Additive Concentrations .	112
41	The Effect of the Functional Groups on the Formation of the Oil Soluble Organometallic Iron . . . . .	113
42	The Effect of the Functional Groups on the Formation of the Oil Insoluble Organometallic Iron . . . . .	114
43	Effect of Zinc Dihexyldithiophosphate Concentration on Wear Products . . . . .	116
44	Effect of Dilauryl Acid Phosphate Concentration on Wear Products . . . . .	118

LIST OF ILLUSTRATIONS (Concluded)

<u>Figure</u>		<u>Page</u>
45	Effect of Tributyl Phosphite Concentration on Wear Products	120
46	Effect of Fluid Purity and Tricresyl Phosphate Concentration on Wear	122
47	Lubrication Mechanism of Dialkyl Phosphites as Proposed by Forbes and Battersby	125
48	Effect of Temperature on Wear, 1.0% Tributyl Phosphite at Slow Speed	128
49	Effect of Temperature on Wear Product Distribution, 1.0% Wt. % Tributyl Phosphite at Slow Sliding	129
50	Effect of Speed on Wear, 1.0% Tributyl Phosphite	131
51	Effect of Speed on Wear Product Formation, 1.0% Tributyl Phosphite	132
52	Effect of Load on Wear, 1.0% Tributyl Phosphite	134
53	Effect of Load on Wear Product Formation, 1.0% Tributyl Phosphite	135
A1	Metallic Wear Products as a Function of Time	153
A2	Metallic Wear Products as a Function of Time	154

LIST OF TABLES

<u>Table</u>		<u>Page</u>
1	Characteristics of Cellulose Filters . . . . .	30
2	Fluid Flow Study Using an Oxidized Base Fluid . . . . .	39
3	Physical Properties of Standardization Fluids . . . . .	41
4	Physical Properties of Additives . . . . .	42
5	Fluid Flow Study Using Dimer Acid (PRL 3697) . . . . .	43
6	Fluid Flow Study Using n-Octyl Polymethacrylate-25 . . . . .	45
7	Fluid Flow Study Using n-Octyl Polymethacrylate-55 . . . . .	46
8	Fluid Flow Study Using Oleic Acid . . . . .	49
9	Fluid Flow Study Using Barium Sulfonated Hydrocarbon (PRL 3530) . . . . .	53
10	Fluid Flow Study Using a Heavy Resin (MLO 7779) . . . . .	56
11	Fluid Flow Study Using a Partially Hydrogenated Resin (MLO 7760) . . . . .	57
12	Fluid Flow Study Using a Hydrogenated Resin (LH 136, 137)	58
13	Fluid Flow Study Using a Polar Base Stock . . . . .	64
14	Fluid Flow Study Using a Barium Sulfonated Hydrocarbon (PRL 3530) and a Heavy Resin (MLO 7779) . . . . .	65
15	Fluid Flow Study Using Various Additives in KG-80 . . . . .	67
16	Fluid Flow Study with Metal Filters . . . . .	69
17	Wear Product Analysis as a Function of Load . . . . .	89
18	Wear Product Analysis as a Function of Speed . . . . .	95
19	Wear Product Composition of MLO 7789A in the Shell Four-Ball Wear Tester . . . . .	101
20	The Effect of Octadecyl Alcohol Concentration on Wear Product Composition . . . . .	102
21	The Effect of Base Fluid Purity on Additive Response . . . . .	105
22	The Effect of Octadecyl Bromide Concentration on Wear . . . . .	106
23	The Effect of Stearic Acid Concentration on Wear . . . . .	107

LIST OF TABLES (Concluded)

<u>Table</u>		<u>Page</u>
24	Effect of Fluid Type on Wear . . . . .	109
25	Effect of Aromatic Component on Wear . . . . .	111
26	Effect of Zinc Dihexyldithiophosphate on Wear and Its Products . . . . .	115
27	Effect of Dilauryl Acid Phosphate (DAP) on Wear and Its Products . . . . .	117
28	Effect of Tributyl Phosphite (TBP) on Wear and Its Products . . . . .	119
29	Effect of Fluid Purity and Its Response to Tricresyl Phosphate (TCP) Concentration on Wear and Its Products . . .	121
30	Effect of Bulk Fluid Temperature and Atmosphere on Wear . .	123
31	Effect of Bulk Fluid Temperature and Atmosphere on Wear . .	124
32	Wear Product Analysis of Tributyl Phosphite in MLO 7789A . . . . .	126
33	Effect of Temperature on Wear Product Distribution at Slow Speed . . . . .	127
34	Wear Product Distribution as a Function of Speed . . . . .	130
35	Wear Product Distribution as a Function of Load . . . . .	133
A1	Flow Plan for Separation of Wear Debris . . . . .	148
A2	Effect of Atmosphere on Wear Products . . . . .	149
A3	Wear Debris Formed by Several Inhibited Fluids . . . . .	150
A4	Wear Products from First Hour Run in the Four-Ball Wear Tester . . . . .	151
A5	Wear Products from a Second Hour Test Using "Run-In" Bearing System . . . . .	152

SECTION I  
FLUID AND LUBRICANT STUDIES

1. SUMMARY

Studies have been continued to understand better the interaction of lubricants and working fluids and the environment in which these materials must function. A new microtest for the evaluation of the oxidative and thermal degradation of fluids and lubricants has been developed. This test, in conjunction with gel permeation chromatography, promises to provide a means for the rapid determination of the extent of oxidative and additive degradation. A PRL small capillary viscometer has been developed to study the apparent existence of a film near the bearing surface with viscosity properties considerably different from those of the bulk lubricant. Studies discussed in Annual Report AFML-TR-74-201, Part II, relative to an improved understanding of the lubrication mechanism in the concentrated contact area have been continued and expanded.

AD A03162

It has always been imperative to develop laboratory procedures and methods that would simulate actual conditions to which different materials are exposed in operative conditions. The development of such tests not only has obvious economical advantages since laboratory tests, typically, are cheap and fast, but also provides a better understanding of the different phenomena that occur while the materials are being used. A better understanding is achieved because such tests provide a means for strict control of all variables that could affect their performance. In general, these laboratory tests can be easily reproduced with consistent results, but often the results are difficult to interpret.

In the case of the oxidative deterioration of lubricating fluids, the difficulty of interpretation is a direct consequence of the presence of gas-liquid and solid-liquid interfaces. Variations in the size and properties of these interfaces at different stages of deterioration complicate the analysis of the effect of different variables. Comparisons between various fluids are also of dubious value when the constancy of properties of these interfaces cannot be guaranteed.

An additional but not less significant limitation to the understanding of the problem is that numerous chemical reactions have been postulated or proven to occur during the deteriorative process. Also, many factors such as catalysts, temperature, inhibitors, natural inhibitors, oxidation products and volatile compounds have been shown to modify the oxidative resistance of lubricants.

In order to overcome the first difficulty, a new oxidative test in which large and standardized gas-liquid and solid-liquid surfaces are provided has

been developed. An attempt will be made in future studies to by-pass the second complication by means of a phenomenological model (a simplified reaction scheme) where few homogeneous, irreversible and first order reactions are postulated. The model's validity will then be analyzed.

Synthetic esters were used in this study not only because specific knowledge in the area was needed, but also because they are a pure chemical species. The qualitative and quantitative analyses were greatly simplified. Gel permeation chromatography has proved to be flexible and accurate, and neither limitations nor unreliabilities in this technique were evident during the course of this work.

Current boundary lubrication theory indicates that the effectiveness of lubricity additives may be related to their ability to form thick, viscous films at the bearing metal surfaces. Boundary lubrication data cannot be used to predict the properties of these films because of the complexities of the theoretical equations. The economic importance of boundary lubrication led to this study of the flow characteristics of various lubrication additive formulations in micropore filters. The effects of base fluid viscosity, mean pore diameter, and additive concentration are examined.

The flow characteristics of the additive solutions were determined by measuring the efflux time through cellulose filters with a mean pore diameter of 0.2 to 1.2 microns. The apparatus used was similar to an Ostwald-Fenske viscometer with a cellulose filter replacing the calibrated capillary tube. Variations of the filter pore diameter are small with 99 percent of the pores having a diameter within seven percent of the mean pore diameter. Porosity variations were taken into account by calibration of the apparatus with a nonpolar base stock of super-refined mineral oil. These experiments were performed in a constant-temperature water bath at 100 degrees Fahrenheit.

A variety of lubrication additives have been examined in this apparatus including organic acids, resin fractions of paraffinic crude oil, a barium sulfonate, an organic phosphate, and Acryloids.

The cellulose filters were modeled as uniform cylindrical pores. In addition to the relative uniformity of the pore structure, flow in the filter was found to obey Darcey's law for the nonpolar base fluids. The additives reduced the flow rate through the filter by an amount greater than that accountable by bulk viscosity effects. This reduction in flow rate was modeled as a rigid adsorbed film on the capillary surface. This effective film thickness was found to remain constant or increase with increasing mean pore diameter depending upon the additive type. Additive concentration and base oil viscosity have only secondary effects on the film thickness.

The films of constant thickness are of the same order of magnitude as monolayer coverage. Dimer acid, a dibasic dimer of oleic acid, and n-octyl polymethacrylates exhibit constant film thicknesses. Dimer acid forms a film approximately 15 Angstroms thick. The n-octyl polymethacrylates form films of 40 and 75 Angstroms; film thickness increasing with increasing molecular weight of the polymer.

Oleic acid, the resins and barium sulfonate exhibit effective film thicknesses that increase with increasing mean pore diameter and are essentially independent of additive concentration and base fluid viscosity. The effective thickness varies from less than a monolayer to greater than two monolayers.

The organic phosphate exhibits a large effective film thickness and possibly belongs to this second group of additives. Stearic acid and the Acryloids also form thick films effectively stopping flow in the filters.

Findings from boundary lubrication data indicate the possibility of interference with combinations of additives in lubricants. Results of this study of the flow in thin films supports this theory. Additionally polar base stocks and the presence of oxidation products in the base stock interfere with the formation of surface films. Combinations of additives apparently reduce the viscosity or thickness of the viscous sublayer. On the other hand, calibration of the filter with a polar base stock or a base stock containing oxidation products appears to yield an erroneous calibration time so that either the increase in efflux time is not apparent or the film formation is prevented on the filter surfaces.

In addition, a series of experiments was conducted with metal filters. The results of this study are similar to those observed for the cellulose filters. However, the irregularity and large diameter of the pores in the metal filters makes them a less desirable porous media to use in studying the fluid flow in thin films.

Techniques have been developed which allow the accurate determination of wear debris developed using the four-ball wear tester. These techniques and some nonadditive fluid studies are discussed in Annual Report AFML-TR-74-20, Part II. This work has been continued using additive-containing lubricants.

The effect of the operating parameters and the functional groups of an alcohol, a bromide, and an acid was examined. Preferential and competitive adsorption of polar species on the metal surface and the subsequent reactions were shown to be the key process in boundary lubrication. Additive competition showed that one additive could completely nullify another. Pure aromatics and alcohol functional group seemed to provide the source of the oil-soluble organo-metallic compounds (iron compounds) formed. Chemically active groups like acids or halides appeared to give rise to oil-insoluble organo-metallic iron formation.

Phosphorus-containing commercial antiwear additives such as zinc dialkyl-dithiophosphate (ZDP) and tricresyl phosphate (TCP) were investigated using the experimental technique developed in this study. By comparing the reaction product distribution from the wear debris analysis of ZDP and TCP with a phosphite and an acid phosphate, physical evidence was obtained supporting the notion that the acid phosphate impurities in ZDP and TCP probably were the antiwear agents. Detailed study of tributyl phosphite wear product distribution as a function of temperatures suggested a hydrolytic reaction mechanism.

Surface temperature has been demonstrated in this study to be the key parameter in boundary surface interactions both physically and chemically. The importance of the chemical interactions in boundary conditions is shown.

## 2. DEVELOPMENT OF A 40 MICROLITER OXIDATION TEST

A small scale, rapid oxidation test capable of providing a quantitative or semiquantitative evaluation of the stable life as well as the degree of degradation of base stocks and fluid formulations for aircraft gas turbine lubricants. This type of information can be obtained in test times ranging from one minute to two hours as opposed to test times of three days to a month required using modified Spec. MIL-L-7808 type oxidation and corrosion tests.

a. Test Apparatus. Oxidation and evaporation tests are performed using the glass tube shown at full scale on Figure 1. It is essentially a glass vial having a flat bottom upon which a catalytic specimen can be placed.

In order to provide isothermal conditions on the catalytic surface during the experiments, this glass vial is submerged in a constant temperature bath to the level indicated in the above mentioned figure. The bath comprised an electrically heated, aluminum block with 12 holes in which the oxidation tubes could be placed. The holes were filled with a low melting point Cerrobase alloy. Wiring and construction details have been described in previous reports.

The detachable test tube cover contributes to the maintenance of constant operating conditions by means of a rigorous standardization of the gas flow patterns inside the glass vial. In all quantitative experiments, a constant gas flow of 20 cc per minute is circulated through the system. A gas exit tube is also provided in the same cover. The lower part of the cap and the upper section of the glass vial are constructed with the two elements of a 24/40 ground glass joint. The whole glass apparatus is held in the Cerrobase bath with the aid of a "transite" holder. The holder is built in two separate pieces that are held together with screws.

Catalytic specimens are constructed from a 3/4-inch cold-rolled steel bar. Details of their shape and dimensions are included in Figure 1. The upper part of these pieces have a flat depression where lubricating liquids would remain during the tests. This small "container", if evenly covered with 40 microliters of lubricant, would have a film thickness of 150 microns. Continuous film thicknesses were never generated during the experiments, since capillary effects caused greater thicknesses of lubricant to occur near the perimeter of the catalytic specimen. Because of this capillary effect, it is actually impossible to estimate the average height of the liquid film. It will be seen later that the capillary rise does not affect the interpretation of the results, since no concentration profiles of reactants are generated under experimental conditions.

In any case, the curved intersection between the vertical and horizontal walls of the depression helped to maintain a constant thickness in regions where capillary rise would have caused greater depths of lubricant. The shape of this intersection also makes it possible to reuse the catalytic specimens several times, since the machining procedure after each use did not change the size of the active catalytic surface. The only modification that occurs to the metallic pieces after each new machining is a slight reduction in height.

b. Test Procedures. After careful washing and successive rinsings (four times) of all internal surfaces of the tube and cap, the glass system is dried in a conventional laboratory oven for at least ten minutes.

When a catalyst is used, the surface in contact with the lubricant during the oxidative test is machined in advance according to details shown in Figure 1, and stored in pure benzene (thiophene-free quality). Previous work has indicated the need for using catalysts within 24 hours of the final polishing of their active surface. During the course of this work it has been noticed that no significant change of the catalytic material surface properties occurs even though metallic specimens are stored for periods of as long as ten days.

Catalytic specimens were handled with metallic tweezers after machining since secretions from the skin have been reported to cause corrosion of the metal surface. When needed for an experiment, a stored catalyst is washed and rinsed with acetone. After this operation the excess acetone is quickly dried by exposing the specimen to a stream of dry air. When dryness was assured, the catalyst was placed in the glass tube and the whole system submerged in the Cerrobase bath.

The time needed for the equipment to reach an essentially constant temperature was measured. The complicated geometry and the existence of solid-solid contacts between different parts of the system made any theoretical evaluation impossible. Measurements were performed by soldering a small thermocouple to the catalytic surface of the metallic specimen. The time required for the active surface to reach undetectable temperature variations with the instrumentation used was found to be approximately 25 minutes after immersion in the hot bath. As an additional precaution, all experiments were performed 45 minutes after the system was placed in the constant-temperature bath.

These surface temperature measurements also proved that within the range of temperatures at which these experiments were carried out (230°C to 255°C) the steady state temperature of the catalytic surface was 5.3°C lower than the temperature of the molten Cerrobase alloy.

After the steady state temperature was reached, the system is considered to be ready for the injection of the lubricant. For this purpose a 100 micro-liter syringe is used, coupled with a 230 millimeter long detachable needle type "LT". Special care must be taken in cleaning the needle and syringe prior to use. They are washed several times with tetrahydrofuran (THF) and the internal surfaces finally dried by means of a stream of air.

Before use, the syringe and needle are rinsed twice with the lubricant solution to be used in the experiment to assure that there was no trace of THF left in the injection system. This last step is considered essential since small amounts of polar compounds have been reported to have a significant effect on the rate of the oxidative deterioration of lubricating fluids. The same kind of influence has been suggested in AFML-TR-74-201, Part I, which indicates that traces of volatile nonreactive compounds affect oxygen solubility.

After the final rinsing, the syringe is completely filled with lubricant. The needle is placed in the proper position, and a small amount of fluid is allowed to wet the syringe-needle joint in order to create a wet joint, which performs better than a dry one. The desired amount of lubricant is then measured into the syringe and the excess fluid removed from the needle with a paper towel.

Since the needle is relatively long, requiring high pressure for injection, there is a probability of leaks occurring while injecting, due to the high viscosity of the lubricant at room temperature. This risk was avoided by preheating the needle for four or five seconds inside the hot glass system. This preheating period has no measurable effect on the determination of the oxidation time. During this interval, the liquid is exposed to relatively low temperature thermal degradation, rather than oxidation. The extent of the reactions during this injection process has proved to be negligible in other experiments of this study. An additional advantage of this procedure is the shorter time needed for the fluid to reach the steady state temperature of the experiment.

After preheating, the lubricant is quickly injected. At this point the measurement of time begins. The air supply hose is then connected to the vertical glass tube.

Fifteen seconds before the end of the chosen oxidation period the procedure for finishing the experiment has to be started. After some practice, the operator is able to stop the reaction within  $\pm$  3 seconds. This procedure involves the following consecutive steps:

- 1) Removing the air supply hose from the glass tubing,
- 2) Removing the glass system from the constant-temperature bath,
- 3) Separating the cap from the glass tube,
- 4) Placing the glass tube in a water bath, and
- 5) Quenching the fluid and the steel catalyst by injecting approximately 2 cc of THF.

Since THF has a relatively low boiling point (65°C), it boils vigorously after its injection into the hot system. This boiling has been considered to be responsible for some losses of lubricant from the system because of the projection of small droplets of lubricant in THF solution out of the tube. Distillation losses of the oxidized material are negligible during this boiling. Proof of this statement is that the vapor pressure of the ester in the boiling THF-Lubricant solution is estimated to be lower than  $4 \times 10^{-6}$  mm Hg.

It should be mentioned that the losses due to the boiling of the lubricant-THF solution can be reduced by cooling the glass tube in the water bath for four or five seconds before adding the two-milliliter quantity of THF. When this is done, the boiling solution extracts less heat from the system, since the glass walls are significantly cooler. This provides more moderate boiling and therefore a smaller loss of solution in the form of small droplets. For the case of relatively long oxidation tests, this short cooling time (as a function of reaction time) introduces a small and insignificant error in the analysis of results.

c. Preparation of Analytical Solutions. Once the glass tube and the catalyst reaches room temperature, the lubricant-THF solution is extracted with a syringe from the oxidation reactor and placed in a graduated cylinder. The same syringe is used afterwards to wash with pure THF, the catalyst, and tube walls of traces of the remaining solution of lubricant. The system is rinsed several times using approximately 0.5 cc of pure solvent each time. The washing liquid is collected in the graduate cylinder, to avoid any loss of oxidized material.

When the tube walls are rinsed to prepare analytical solutions, only the lower part of the tube was actually cleaned. It is done this way because the upper part of the vial and the glass cap, being cooler than the rest of the system, serves as a condenser for lubricant vapors during oxidative tests. Therefore it is considered that the material found above the hot section does not undergo catalytic deterioration.

The relevance of this evaporation was also studied by preparing analytical solutions with THF used in the rinsing of the inner surfaces of the upper part of the tube and cap. Evaporative losses are difficult to measure because the presence of lubricant in the upper part of the vial is also caused by the already mentioned projection of droplets during the quenching procedure. Since two phenomena cause the same measurable effect, it is difficult to evaluate the relative extent of each of them.

In any case the evaporative losses are not significant. In oxidative exposures within the stable lifetime of the lubricant-inhibitor solutions used, typical evaporative losses were not greater than six percent of the total volume of the injected ester. Some consideration will be given later to the extent of these losses in more severe deteriorations.

Almost all of the samples investigated in this work were diluted to six milliliters with THF to prepare the analytical solutions even though a volume of three milliliters had been considered to be sufficient to obtain reliable results. This three milliliter value is mentioned since two milliliters of solution is necessary to completely fill the sampling loop of the Gel Permeation Chromatography unit and one milliliter was assumed to be required to flush the injection system and to account for spilling losses while handling.

A six milliliter volume of solution was chosen rather than three milliliters because volumetric errors accounted for a significant part of the error of the results of this work. This can easily be noticed when considering that the smallest division of the graduated cylinder used in preparing the solutions was 0.1 milliliter. This value introduces a relative error of  $\pm 1.66$  percent when a three milliliter solution is prepared and  $\pm 0.83$  percent when the sample is diluted to six milliliters.

Since the smallest division of the microsyringe used was one microliter, the amount of lubricant considered in a typical test can be written as 40  $\pm$  0.5 microliter. This adds 1.25 percent of error to the value of concentration of the solution.

From these results it appears that the total error in the value of the concentration when preparing a six milliliter solution is  $\pm$  2.08 percent compared with 2.91 percent for the three milliliter dilution. Therefore, it can be seen that if three milliliter solutions had been prepared, a 50 percent additional error would have been introduced. This evaluation also considers the experimental fact that the sensitivities of the concentration detectors of the analytical unit are not modified by a further dilution to six milliliters.

As a consequence of these calculations, it is obvious that since the sole volumetric error is  $\pm$  2.08 percent, differences in concentration between equivalent runs as large as four percent had to be expected. If more accurate values are needed in future work, the error introduced by the graduated cylinder could be eliminated by preparing weighed solutions. In such a case the total error in concentration would only be the one introduced by the microsyringe ( $\pm$  1.25%).

d. Gel Permeation Chromatography (GPC) Analysis. Gel permeation chromatography is a separative technique which essentially involves steric permeation of a solute through an inert gel. The qualification of the gel as inert emphasizes the fact that the separation achieved may be regarded as a consequence of the geometrical features of the different molecules.

Since geometrical properties of molecules depend strongly upon the molecular weight of the chemical species, it is often stated that gel permeation chromatography resolves a complex sample into different fractions according to the molecular weight of the solutes. Even though this assertion is quite correct it is not general, as shown for example, by Benoit et al. (1). In this reference it was proved that a series of polystyrene samples having the same molecular weight but different structures eluted at different times from a GPC column.

It is more proper to state, as clarified by Grubisic et al. (2) that the elution volume of the various fractions depends on the "hydrodynamic volume" of the species. A measure of this parameter can be obtained from Einstein's viscosity law:

$$[\eta] M = K V$$

where:

M = molecular weight of the sample

V = hydrodynamic volume

K = constant

$[\eta]$  = intrinsic viscosity, defined by the equation:

$$[\eta] = \lim_{C \rightarrow 0} \frac{\ln \frac{[\eta/\eta_0]}{C}}{C}$$

Where  $\eta$  is the dynamic viscosity of a solution (obtained from the time of flow of a known fixed volume of solution in a capillary viscometer),  $\eta_0$  is the dynamic viscosity of the solution and C is the concentration of solute in the solution. By plotting the product versus the experimental elution volume, these authors have obtained an excellent fit for all types of molecules. This kind of correlation was not verified when M alone, instead of the above mentioned product was used.

This behavior can be justified if it is considered that the displacement of molecules within the chromatographic column resembles that found in the viscometric experiment. The velocity gradients generated in the capillary test are equivalent to those caused by the flow of solvent through the pores of the chromatographic column. Therefore, in general, GPC results should be seen as a combination of molecular weight and viscosity properties.

(1) Solvent-Solute Interactions. Even though the pores of the gel can be considered to be mainly responsible for the separation, other factors different from the steric have been indicated as affecting the elution volume of the solutes.

Solvent effects in GPC have been reported frequently. These secondary interactions can be caused by:

- 1) Alteration of the porosity of the pore network due to different swelling effects on the gels,
- 2) Modification of the molar volume of the solute due to the formation of solvated species; and
- 3) Self-association of the solute species because of the low solubility of the solute in the solvent.

Some details of the theoretical relevance and of the experimental evidence of these solvent-solute interactions have been reported by Haley (3), Freeman (4), Cazes and Gaskill (5), and Cogswell et al. (6).

(2) Gel-Solute Interactions. The influence of the chemical composition of the gel on the elution volume of the solute has been mentioned and analyzed by Freeman (4) and Freeman et al. (7). This interaction has been reported also to be affected by the structure of the eluting solvent.

Therefore, the molecular size alone might not define the elution volume of the species when secondary effects are present. The analyst must then be careful when assigning specific molecular sizes to the eluting fractions of samples if there is not a clear understanding of the chemical structure of the solutes. The existence of these secondary factors is particularly frequent with low molecular weight solutes.

(3) Analytical Unit. Analytical and preparative work were performed by using a Waters' Model 502 Gel Permeation Chromatography/Liquid Phase Chromatography Unit. This instrument had Differential Refractive Index (RI) and Ultraviolet Light Absorption (UV) detectors.

This duality in the detection system synergized the resolutive capabilities of the columns used. This was evident when a pair of species having the same elution volume was resolved quantitatively because one of them absorbed UV light. An additional advantage of the UV detection system is its extreme sensitivity to compounds having UV-resonating chemical bonds. As an example of its outstanding performance it should be mentioned that during the course of this work, it was possible to measure quantitatively amounts of phenothiazine as small as  $1 \times 10^{-6}$  gram.

Care has to be taken with respect to the temperature of the room where the unit is placed. It is convenient to work in a constant-temperature room since the Differential Refractive Index detector shows a significant change in analytical results with changing temperature.

e. Interpretation of Results. The full line tracing on Figure 2 shows the RI (Differential Refractive Index) and UV (Ultraviolet Light Absorption) chromatograms of an unoxidized sample of 0.1 percent phenothiazine in trimethylolpropane triheptanoate. The RI detector registers one sharp peak with a slight tailing which corresponds to the elution of the ester. It can also be noticed that there is no measurable response to phenothiazine by this detector.

The RI chromatogram of the severely oxidized sample (c), shows a significant reduction in the height of the ester peak and the presence of higher molecular weight products. It was found that the response of the RI detector was proportional to the mass concentration of the eluting species, and was independent of the molecular weight of the different fractions obtained as products of the oxidation. Since the abscissa of the chromatograms represents a constant flow rate of analytical solution, this is equivalent to stating that the area of the RI chromatograms remained essentially unchanged through the different stages of the oxidation when samples having the same weight were analyzed.

This was verified by comparing the area of the RI chromatogram of a 40-microliter sample of pure ester with the chromatographic area of an equivalent sample of the same substance after a severe oxidative test. Oxidation caused the conversion of approximately 90 percent of the ester, and the synthesis of products having molecular weights as high as 60,000. The area of the chromatogram of the oxidation products of this reaction represented 52.8 percent of that of the original ester. The ester evaporated from the sample during the oxidation, which condensed in the upper (cooler) part of the system, was found to be equivalent to 28.7 percent of the amount initially injected in the system. The increase in the weight of the catalyst, due to the formation of insoluble sludge, was found to be equal to 7.4 mg, or 18.6 percent of the originally injected ester.

The three amounts found in different parts of the system totaled 100 percent of the initial sample. Therefore, the response of the RI detector to the mass concentration of the different molecular weight species, in the analysis of the soluble material found on the surface of the metallic catalyst (52.8 percent of the 40 microliter sample), can be considered to be independent of the molecular size of the oxidation products.

These results are in agreement with those obtained by Hazell et al. (8), who reported that the response of the RI detector was proportional to the weight concentration and independent of the molecular size of the samples, for the case of polystyrene standard solutions having molecular weights ranging from 5000 to 3,500,000.

The UV chromatogram of an unoxidized sample of 0.1% phenothiazine in trimethylolpropane triheptanoate presented in Figure 2 shows a sharp peak at an elution time corresponding to a calibration molecular weight of 170, which is due to the presence of phenothiazine in the sample. There is also a trace of impurity with a molecular size close to that of the ester, which has been registered by this detector. This impurity was considered such, and not the response of the UV detector to the elution of the ester, because there was not a measurable reading in the same area of the UV chromatogram when a phenothiazine - di-2-ethylhexyl sebacate solution was analyzed.

The linearity of the GPC unit to both inhibitor and ester concentrations can be periodically verified by analyzing solutions with different concentrations of these materials. The heights of these peaks are found to be proportional to the concentration of the species. This can be expected since the concentration of the analytical solution was only 0.66 percent of ester in THF, and therefore interference due to solute concentration was not likely to occur during the chromatographic elution.

The UV chromatogram of sample (b) in Figure 2 shows the typical characteristics found in the analysis of oxidized, inhibited ester solutions. The differences with respect to the original sample of the same material are:

- 1) A significant reduction in the concentration of phenothiazine,
- 2) An increase in the level of UV absorption in the 450 calibration molecular weight fraction, and
- 3) The presence of a UV absorbing chemical species, having a molecular size equivalent to a calibration molecular weight of 240.

It was considered that no UV absorbing species with a molecular size close to that of phenothiazine were produced during the oxidative deterioration of the ester-inhibitor solution. This assumption was verified by analyzing the UV chromatogram of a severely oxidized solution of phenothiazine in trimethylolpropane triheptanoate (sample (c), Figure 2). The phenothiazine initially present in this sample had been destroyed long before the end of the oxidative experiment and no UV absorbing material having a size similar to that of the inhibitor molecule was found in the analysis. The small signal

registered at a calibration molecular weight of 170 was considered to be the tailing of the material which eluted at 240 calibration molecular weight.

When quantitative analysis of phenothiazine concentration is required, this tailing might interfere in the interpretation of the results, namely when small amounts of phenothiazine are present in the sample. Therefore, this tailing signal is subtracted from measurements of heights of phenothiazine peaks. From values of relative sizes of tailings in ester and phenothiazine peaks, it was decided that a compound with a calibration molecular size of 240 should have a tailing with a height equal to 10 percent of its maximum response at the calibration molecular weight of 170. This means that reported concentrations of phenothiazine are measurements of the size of the peak at the calibration molecular weight of 170 minus 10 percent of the height of the signal present in the 240 molecular weight region of the chromatogram.

Because some UV absorbing impurities having a calibration molecular weight of 450 were initially present in the trimethylolpropane triheptanoate, the increase of the UV response in this area of the chromatogram with longer oxidation times is reported here with respect to its original value. Therefore for this ester, the unoxidized UV trace in the 450 calibration molecular weight area was considered to be the baseline from where measurements of heights of peaks were made. It is obvious that this kind of correction was not needed for the case of di-2-ethylhexyl sebacate, since no trace of UV absorbing impurity was found in the analysis of this fluid.

In all cases UV readings were expressed in arbitrary units of concentration. For these purposes a UV absorbing compound was reported to be present at a 100 percent concentration when it gave a signal as large as that provided by the initial concentration of phenothiazine (0.1 percent).

It is apparent from this preliminary work that the 40-microliter oxidation and corrosion test can be used to determine the interrelation of additive-depletion and fluid degradation to form high molecular weight products. In the use of aircraft gas turbine lubricants, the principle degradative changes comprise a loss of additives as well as the degradation of the ester base fluid. The degradation of the base fluid in a typical operational system begins before the inhibitor-type additives have been completely removed by the oxidative and thermal degradative processes. Typical specification oxidation tests for aircraft gas turbine lubricants are designed to measure the stable life of the additive system rather than the degradation of the ester base stock. The use of a dual detector (refractive index and ultraviolet spectrometer) GPC unit for the analysis of the degraded aircraft gas turbine lubricants allows for the separate observation of the additive behavior (UV) and the base stock behavior (RI). The general differences in molecular weight of the additive package and the ester base stock make this plan for separate observation and analysis particularly effective. In addition, the strong response of oxidation inhibitors to UV makes the analysis of the small quantities particularly effective. At low temperatures, e.g. 350°F, the formation of high molecular weight products does not constitute a significant fraction of the products until the oxidation inhibitor has been completely depleted. At high temperatures, e.g. 500°F, both inhibitor depletion and sludge formation proceed concurrently.

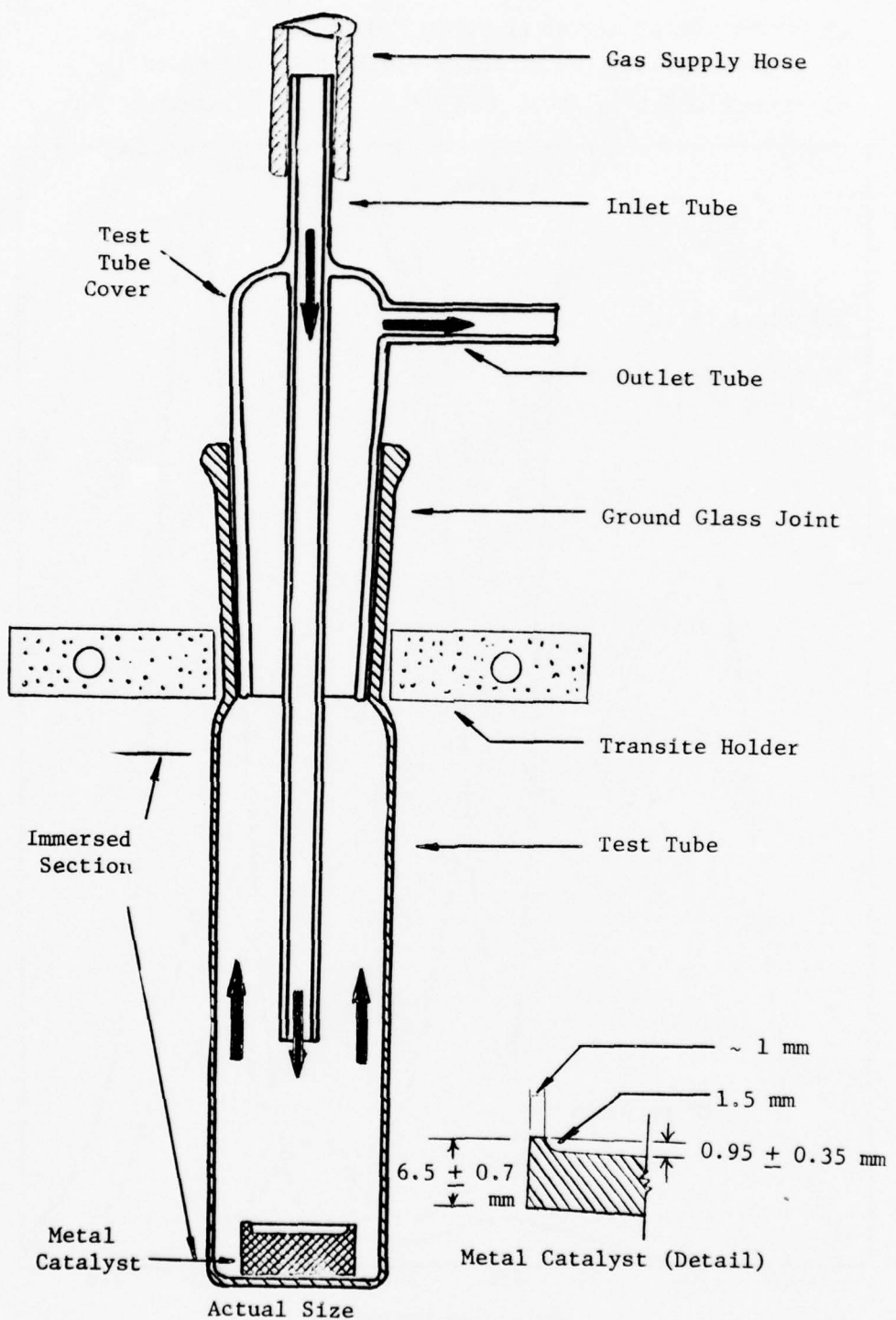


Figure 1. APPARATUS FOR OXIDATION TESTS

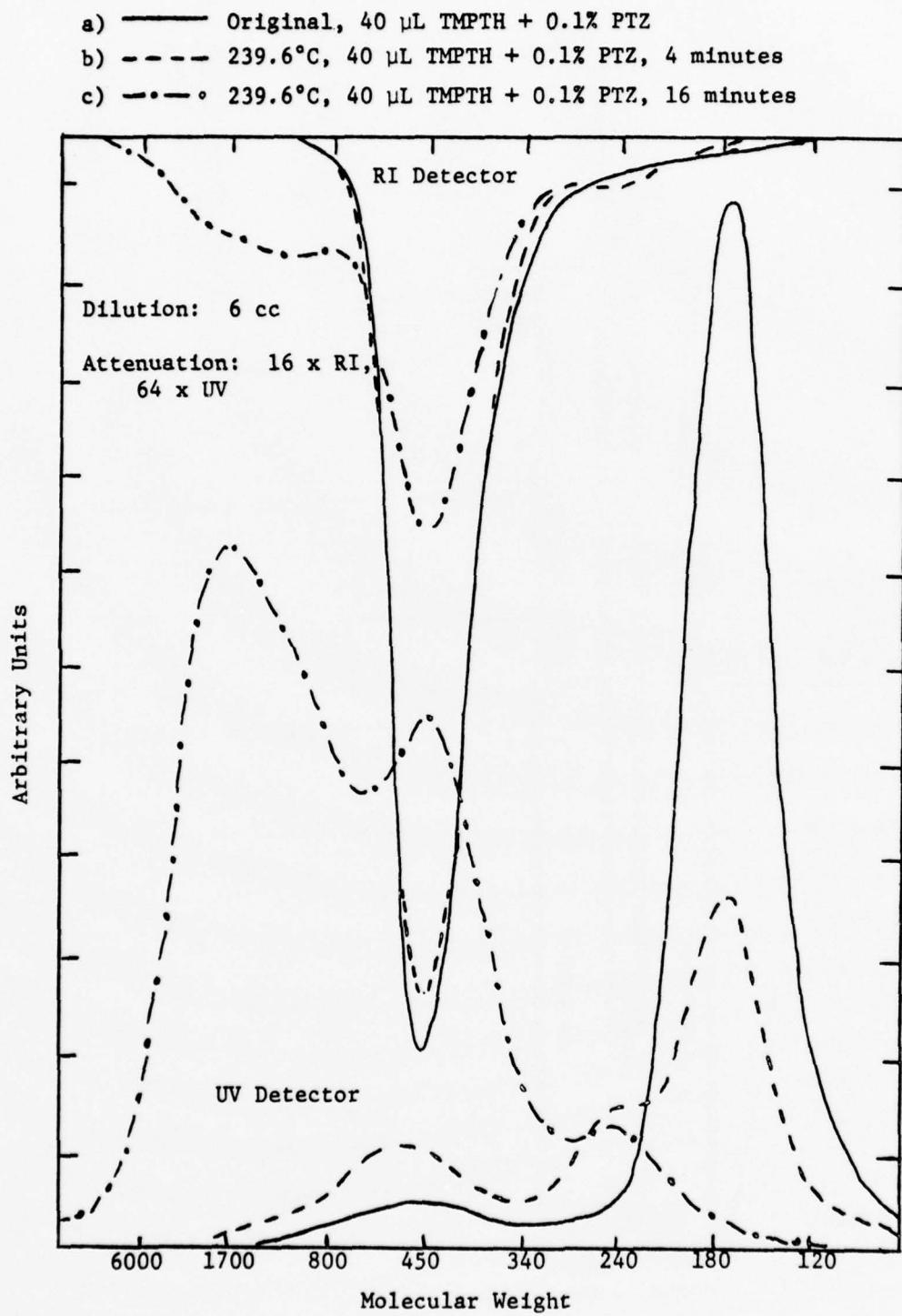


Figure 2. CHROMATOGRAMS OF THE OXIDATION PRODUCTS OF ESTER-INHIBITOR SOLUTIONS

### 3. EFFECT OF LUBRICATION ADDITIVES ON FLOW IN THIN FILMS

A PRL small capillary viscometer has been developed. This instrument has been developed to study the apparent existence of a film near the bearing surface with viscosity properties considerably different from those of the bulk lubricant. These films result from the concentration of polar components from the fluid or from the lubricant-system interaction in concentrated contacts. The establishment of the concept that these films exist and an understanding of the formation of these films is directly applicable to the gear and bearing lubrication characteristics of gas turbine lubricants.

a. Modeling of Porous Media. The methods of modeling of porous media are essentially limited to nonintersecting cylinders [Dullien and Batra (9)]. The complexities of most porous media eliminate virtually all other model considerations. As the cellulose filters used in this work (see Table 1) have pores that are nearly circular in cross-section and have a small variation in pore size, these filters were modeled as a bundle of nonintersecting cylinders of uniform length and diameter.

For each cylinder, the shear stress under laminar flow may be written mathematically as

$$\tau = \frac{\Delta P r}{2L} \quad (1)$$

where:

$\tau$  = shear stress

$\Delta P$  = total pressure drop over the length  $L$ , and

$r$  = radial distance.

The shear stress is related to shear rate by:

$$\tau = -\mu \frac{dv}{dr} \quad (2)$$

where:

$\mu$  = fluid viscosity, and

$\frac{dv}{dr}$  = shear rate.

For a Newtonian fluid, the fluid viscosity is constant. That is, the viscosity is independent of shear stress and time. Thus, the shear rate can be written as

$$\frac{dv}{dr} = \frac{\Delta P r}{2\mu L} \quad (3)$$

Equation 3 is integrated to yield the velocity profile

$$v = \frac{\Delta P}{4\mu L} \left[ 1 - \left( \frac{r}{R_o} \right)^2 \right] \quad (4)$$

where:

$R_o$  = radius of the capillary.

Integrating equation (4) over the cross-section of the capillary yields the volume rate of flow of:

$$q = \frac{\pi \Delta P R_o^4}{8\mu L} \quad (5)$$

Inherent in this derivation are the following assumptions:

- 1) The fluid is incompressible,
- 2) End effects are negligible,
- 3) The fluid is a continuum, and
- 4) There is no slip at the wall.

These assumptions are in addition to the previous assumptions that the flow is laminar and the fluid is Newtonian.

For the  $N$  capillaries which compose the model of the porous medium, the total volume rate of flow,  $Q$ , is

$$Q = Nq = \frac{N \pi \Delta P R_o^4}{8\mu L} \quad (6)$$

The apparatus used in this work is similar in operation to an Ostwald-Fenske viscometer. The volume of liquid that flows through the porous medium is a constant. Thus, the efflux time,  $t$ , for a filter is

$$t \propto \frac{\mu}{\Delta P R_o^4} \quad (7)$$

If two Newtonian fluids are run through the same filter apparatus, then  $N$ ,  $\Delta P$ , and  $R_o$  are constant, and the viscosity corrected efflux time ratio,  $Z'$ , which may be written as

$$Z' = \frac{t_2 \mu_1}{t_1 \mu_2} \quad (8)$$

where:

subscript 1 refers to the calibration fluid,  
subscript 2 refers to the test fluid,

must be unity.

If this ratio,  $Z'$ , is greater than unity, the increase may be theorized to be due to adsorption of a rigid film on the capillary walls as shown in Figure 3 (a). Combining equations (7) and (8) yields

$$Z' = \frac{R_o^4}{R_1^4} \quad (9)$$

If the thickness of this film is  $A$ , then

$$A = R_o - R_1 = R_o \left(1 - \frac{1}{Z'}\right)^{\frac{1}{2}} \quad (10)$$

A strongly adsorbed rigid layer would be independent of pressure drop and pore diameter. Such a layer was apparently observed by Zorin, Sovolev, and Churaev (10). In addition, if this film or layer consisted primarily of the additive, the film thickness would not be a function of the bulk fluid viscosity.

However, this layer might not be a rigid layer. The works of Karasev and Deryagin (11) and Deryagin et al. (12) suggest that the film near the liquid-solid interface may exhibit a constant viscosity that is greater than that found in the bulk. The mathematical expression for this case may be derived by assuming two-phase flow with no slippage at the liquid-liquid interface. This possibility is identical to that pictured in Figure 3 (b) with a layer of thickness,  $h$ , that is not rigid but has a viscosity,  $\mu_2'$ , greater than that of the bulk. Equation (3) must be integrated over the two phases separately to yield the following equations for the fluid velocity,

$$v_2 = K_1 \frac{(R_o^2 - r^2)}{2\mu_2'} \quad (11)$$

and

$$v_1 = K_1 \left[ \frac{-r^2}{2\mu_1'} + K_2 \right] \quad (12)$$

where:

$$K_1 = \frac{\Delta P}{2L} \quad (13)$$

and

$$K_2 = \frac{R_o^2}{\mu_2'} - \frac{(R_o - h)^2}{\mu_2'} + \frac{(R_o h)^2}{\mu_1'} \quad (14)$$

Equation (11) is valid for  $R_o - h \leq r \leq R_o$  and equation (12) is valid with  $0 \leq r \leq R_o - h$ . Integration of these equations over the cross-sectional area of the capillary yields the expression for the volume rate of flow

$$q = \frac{\pi \Delta P}{8L} \left[ \frac{(R_o - h)^4}{\mu'_1} + \frac{R_o^4}{2\mu'_2} - \frac{(R_o - h)^4}{2\mu'_2} \right] \quad (15)$$

This model predicts an effective film thickness that is a function of pore diameter but not of pressure drop. This is combining equations (7), (8), and (15)

$$z' = \frac{R_o^4 / 2\mu'_2}{\frac{(R_o - h)^4}{\mu'_1} + \frac{R_o^4}{2\mu'_2} - \frac{(R_o - h)^4}{2\mu'_2}} \quad (16)$$

where:

$\mu_2$  = atmospheric viscosity as determined in Ostwald-Fenske viscometer,  
 $\mu'_1$  = bulk viscosity in the pore, and  
 $\mu'_2$  = film viscosity.

The flow rate is also related to the viscosity of the film. If the viscosity of the sublayer,  $\mu'_2$ , is a multiple of the bulk viscosity,  $\mu'_1$ , the effective film thickness, A, will not be a function of the bulk viscosity. This, of course, means that the film consists of both additive and bulk fluid. On the other hand, the film may be predominantly additive, in which case, A would be a function of the fluid viscosity.

The variables discussed - mean pore diameter, pressure drop and fluid viscosity - are combined in the equations for shear stress and shear rate (equations (1) and (3)). Since the pressure drop was relatively constant, a plot of the effective film thickness, A, versus shear stress,  $\tau$ , or shear rate,  $(dv/dr)$ , should be linear if the fluid films are either rigid films or have a constant viscosity greater than that of the bulk fluid. The exact relationship will depend upon the composition of these films. The values of  $\tau$  and  $(dv/dr)$  were calculated from equations (1) and (3), respectively. The entire pressure drop,  $\Delta P$ , was assumed to be across the filter. The manufacturer's listed mean pore diameter and filter thickness were used as the capillary diameter and length.

b. Apparatus and Procedure. The test apparatus used in this work is similar in design and operation to an Ostwald-Fenske viscometer. However, instead of using a calibrated capillary as a means of measuring relative viscosity, a filter was used.

(1) Apparatus. As seen from Figure 4, the unit consisted of a double bulb, a filter assembly, and a vented flask. During the experiments,

this whole unit was lowered into a constant-temperature water bath maintained at 100 degrees Fahrenheit. To prevent water from leaking into the assembly, Teflon ferrules were used to seal the connection between the glass tube and the filter assembly. The ground glass joint was sealed using the calibration fluid rather than a silicone grease to avoid contamination of the filter. Spring clamps prevented separation of this joint. The lower portion of the filter assembly fitted into a rubber stopper which in turn fit into an Erlenmeyer flask. The flask could be either vented to the atmosphere or attached to a vacuum assembly.

The entire run assembly is shown schematically in Figure 5. The Erlenmeyer flask was normally vented to the atmosphere. However, a vacuum could be applied to the flask to increase the pressure drop across the filter. Two one-cubic foot tanks were placed in parallel with the Erlenmeyer flask to serve as a reservoir. This maintained a constant, relative pressure below the filter.

Two different filter assemblies were used in the work. The first assembly (Figure 6) was purchased from Millipore Filter Corporation (Part No. XX66-025-50). This assembly takes a one-inch filter and has a filter area of 0.6 square inch. The filter is placed upon a metal support screen. Two Teflon rings, one above the filter and one below the screen, prevent flow around the filter and hold it in place. Teflon tape, applied to the threads, prevents water from leaking into the assembly and blinding the filter.

The second type of filter assembly (see Figure 7) was designed to handle 1/8-inch thick sintered metal filters. Since these filters were the same diameter as that of the cellulose filters, the design is similar to the Millipore assembly. Thus, some cellulose filter runs were made using this assembly with, as expected, no discernible differences from the runs using the Millipore assembly.

These assemblies were machined from 316 stainless steel. The sintered metal filters were held in position by Teflon rings which, as in the Millipore assemblies, prevented oil bypassing of the filter. An O-ring seal prevented water from leaking onto the filter. The O-ring provided a much better seal than simply wrapping the threads with Teflon tape as was necessary with the Millipore assembly.

(2) Procedure. The test apparatus was operated in a manner similar to the procedure used with an Ostwald-Fenske viscometer.

The filter apparatus was filled with the pure calibration oil as the filter was assembled. This procedure eliminated problems with air entrapment. After completely assembling the apparatus as shown in Figure 4, the lower bulb was filled with oil to a level above the upper etched line (see Figure 8). The Tygon tubing was clamped shut and then the apparatus was hung in the constant-temperature water bath. After coming to thermal equilibrium, the

run was initiated. The time for the lower bulb to empty - upper etched line to lower etched line - was recorded. After repeat runs of the calibration fluid reached a steady efflux time, the unit was drained to a low level. However, the meniscus was kept visible so that air would not become trapped in the metal filter assembly. A hypodermic syringe with a long needle was used to refill the apparatus with the oil plus additive. The tip of the needle was kept just below the meniscus, again to avoid air bubble entrapment. After thoroughly rinsing the assembly by refilling and draining the lower bulb, it was filled and left to equilibrate. After this oil reached a constant run time, apparatus was drained, disassembled and cleaned with naphtha and acetone. The apparatus was then thoroughly dried at 250 degrees Fahrenheit before being used again.

To obtain accurate data with this apparatus, the filter must be handled carefully to avoid contamination. Differences in the filter porosity, however, are accounted for by calibrating each filter during the run. Generally, this calibration was performed by the same oil that contained the additive. This procedure minimized viscosity corrections and potential interference of the base oils.

After each run the filter was closely examined for water, dust, and other contaminants. Water appeared as droplets and actually blinded the filter media. Dust laid on top of the filter but did not blind the filter. Filter contamination included crystallization of certain additives on the filter. Some additives darkened the filter. This darkening was taken as an indication of additive adsorption and not of blinding of the filter. If, upon examination of the filter, water or crystals were found, the run was discarded. The run was considered valid if constant efflux times were obtained for both calibration and additive fluids even if a few dust particles or filter discoloration was observed.

All fluids used in this study were prefiltered in the apparatus shown in Figure 9. Unfiltered oil is placed in the funnel. From there it passed through a 5.0 micron filter and a 0.1 micron filter in series. From the lower filter assembly, the oil passed into a Erlenmeyer flask. The filtration was assisted by applying a vacuum to the flask. The Erlenmeyer flask and other glassware were thoroughly rinsed with the filtered oil before the oil was collected or stored in them.

The oils run with a vacuum applied downstream of the filter were stored under vacuum at a constant temperature of 110 degrees Fahrenheit. This eliminated degassing of the oil within the filter and minimized the time required to reach thermal equilibrium.

The additives were added to prefiltered base oil. The weight percentages were accurate to three significant figures. After thorough mixing, the samples were refiltered.

Several of the base oils were contaminated. These oils were slightly yellow in color and exhibited a gradually increasing efflux time. The contamination appeared to be oxidation products. Therefore, these oils were mixed with alumina and prefiltered. This removed the contaminants and produced constant efflux times. However, reoxidation of the base oils was

extremely rapid. A few days after the alumina treatment, the oils began to exhibit gradually increasing efflux times again. This was true if the oils were stored under a vacuum (less than one centimeter absolute pressure). Addition of 50 parts per million of an antioxidant, Parabar 441, was necessary to prevent reoxidation. The presence of the Parabar 441 did not appear to affect the results of these experiments.

c. Experimental Error. The major source of measurement error in this work was due to the inability to determine accurately the run time. Additional possible sources were the bath temperature, the pressure drop over the filter, liquid viscosities, and additive concentration.

The determination of the run time proved to be the largest source of error. The diameter of the glass tubing (see Figure 8) was limited by the dimensions of the hypodermic tubing used to refill the bulb, while the bulb volume was varied according to the expected flow rate. Thus, for a viscous fluid with a relatively slow flow rate, the volume of fluid in the glass tubing becomes a significant portion of the total volume to be timed. Thus, the meniscus may take fifteen seconds to move past the etched line. However, experience with the unit combined with a long run time, and repeated calibration runs yielded a difference between successive runs of less than 0.2 percent.

The bath temperature was controlled within a maximum error of 0.1 degree Fahrenheit. As the control scheme is identical to that used in the constant-temperature viscosity baths and all runs are relative to the calibration fluid, the effect of temperature upon viscosity is negligible.

The pressure drop over the filters consisted of the liquid head plus, in some cases, an applied pressure drop. Since the calculations of the relative efflux times are relative to a calibration fluid, only the applied pressure drop is a source of error in the measurement of the efflux times. The vacuum applied to the Erlenmeyer flask was measured relative to atmospheric pressure by a mercury manometer. The height was measured to within 0.05 centimeter. Thus, the maximum percent error for the vacuum assisted runs was 0.2 percent. However, the increased flow rate of the vacuum assisted runs reduced the error in timing the run. Thus, the variation of repeat runs did not increase over the runs without the application of a vacuum.

The value of the pressure drop is necessary for the calculation of shear stress and shear rate. The liquid head was calculated by measuring the distance between the etched lines and the filter. The average of the distances between the upper etched line and the filter, and between the lower etched line and the filter was used to calculate the pressure drop over the filter. The error of the individual measurements was 0.01 centimeter out of approximately 10 centimeters. For the vacuum assisted runs, the error was approximately 0.2 percent. The pressure drop in this case consisted of that measured on the manometer plus the pressure drop due to the liquid head.

Liquid viscosities were used to calculate the relative efflux times, and in turn, the effective film thickness. All viscosities were measured in Ostwald-Fenske viscometers. Since the same viscometers were used to measure the viscosities of both the calibration fluid and the additive fluid, the errors of the relative viscosities were negligible. In addition, the Ostwald-Fenske viscometers and the filter have similar shear rates. Thus, the possibility of a non-Newtonian bulk viscosity is minimized.

The additive concentration was found not to be a significant variable in this study. The additive concentration was measured within 0.01 gram. The error in concentration was less than one percent.

The primary measurement error in this work was that of determining the efflux time. Other sources of measurement error were negligible.

In addition to measurement errors, several other sources of error were recognized during the course of this work. These errors are: the possibility that any flow is non-Newtonian in these fine capillaries; blinding the filters by dirt, water, or oil contaminants; degassing of the fluids during vacuum assisted runs; and crushing of the filter during vacuum assisted runs.

While the test apparatus has a maximum shear rate similar to an Ostwald-Fenske viscometer, the narrow capillaries may produce non-Newtonian flow in normally Newtonian fluids. If the fluid behavior remains Newtonian, the flow time will be directly proportional to fluid viscosity as measured with an Ostwald-Fenske viscometer. Two pure nonpolar mineral oils, MLO 7021 and MLO 7755, were selected for this test. Their viscosities are 3.03 and 13.14 centistokes, respectively, at 100 degrees Fahrenheit. In addition to these two fluids, three mixtures of these fluids with viscosities of 5.33, 7.75, and 10.5 centistokes were also run in the same experimental setup. For this test a 0.45 micron Millipore filter was used in the experimental setup as shown in Figure 4 using the procedure previously outlined. The results (see Figure 10) show a definite linear dependence of efflux time with viscosity. A slight increase in efflux time was noted for a check run with MLO 7021. This slight increase was probably due to dust which unavoidably entered the apparatus during refilling operations. As the study lasted five days and almost a liter of fluid was run through the filter, this slight increase was not felt to be significant. Additionally, these oils were prefiltered with a 0.45 micron filter and not the 0.1 micron filter which was standard for all other runs. Tests generally lasted only eight to twenty-four hours and less than two hundred milliliters of fluid was filtered.

The second source of error is inadvertent blinding of the filters. Three things were found to cause gradual, continuously increasing run times - dirt, water, and contamination of the oil.

All oils used in this run were prefiltered using a 0.1 micron Millipore filter. Pure oils were initially filtered. Additives were then added to prefiltered oil. The mix was then refiltered with a 0.1 micron Millipore filter. In check runs with oleic acid in MLO 7021, this prefiltering step did not change the concentration of the acid significantly.

Water blinding of the filters was a recurring problem. Water blinded the filter apparently by entering through the threads of the Millipore filter assembly (Figure 6). This water leakage was essentially eliminated by applying Teflon tape to these threads. The presence of water was easily detected by relatively large, continuous increases in run time. Examination of the filter showed white areas where the water had blinded the filter. This is in contrast to the oil wetted areas which tended to be opaque. Often drops of water were also present, further confirming water blinding.

Unlike pure, uncontaminated mineral oils, those containing oxidation products did not quickly approach a constant run time but exhibited a gradual increase in run time. These oils also exhibited a slight darkening as compared with the water white color of a super-refined mineral oil. When an essentially constant run time was obtained, the oxidation products appeared to behave similarly to oleic acid and effectively masked the increase in run time normally observed with this additive. As seen from Table 2, the oil (MLO 7685) containing oxidation products yielded a viscosity corrected efflux time ratio of approximately one. Treatment with activated alumina removed these oxidation products. The oil now exhibited run time behavior identical to uncontaminated oils. To maintain this behavior 50 ppm of Parabar 441, an antioxidant, was added to the oil. The antioxidant did not affect the flow behavior of this oil in the cellulose filters.

The apparatus used in these experiments permitted only a small range of pressure drops over the filter. Applying pressure to the upstream side of the filter to increase shear stress would necessitate construction of a pressure shell. To avoid the necessity of this construction, a vacuum was applied to the downstream side of the filter. This presented two additional problems. First, oil, when passing through the filter, became degassed. Secondly, the applied pressure drop might crush the filter.

The released gas formed numerous fine bubbles. To avoid errors that might be caused by this degassing within the filter, degassed oils were used for all runs made under vacuum assist. These oils were degassed for at least twenty-four hours at less than one centimeter of mercury absolute pressure. During a run, the maximum vacuum applied was less than 50 centimeters of mercury. The oils were maintained at slightly above run temperature during this degassing and subsequent storage during the run. Preheating minimized the time required for the sample to reach the equilibrium run temperature of 100 degrees Fahrenheit. During this time the oil was exposed to normal air pressure. Minimizing this exposure was necessary to prevent significant amounts of air from redissolving into the oils and subsequent degassing within the filter.

A high pressure drop over the filter resulted in crushing the filter. To determine the mechanical strength of these filters, a series of runs was performed at various pressure depths. A 0.2 micron filter was used for this experiment. As shown in Figure 11, the structure of the cellulose filter begins to break down at approximately 40 centimeters of mercury. This crushing of the filter was permanent and could not be reversed by reduction of the pressure drop. As a result of this experiment, pressure drops higher

than 40 centimeters of mercury were not applied to the cellulose filters in this work. While all measurements in this work were relative to the calibration oil or pure mineral oil and thus, the relative efflux time ratio would not be affected by this permanent crushing of the filter, the filter pore size and thickness might be altered making comparison of crushed filter runs with normal filter runs impossible.

d. Experimental Results. As previously mentioned, many theories of elastohydrodynamic lubrication are based upon adsorption of the surface active additives at the liquid-solid interface. Their presence here assures their availability for further reaction with the metal surfaces, protecting them and reducing wear. While a pure monolayer is sufficient to reduce wear, a single layer will not provide lasting protection. However, monolayer coverage would be expected to occur at the liquid-solid interface. An organic acid, for example, oleic acid, would chemisorb on the metal providing monolayer coverage.

This monolayer should be detectable in fluid flow studies using narrow capillaries. If the capillary has a diameter of 0.2 micron, a monolayer of oleic acid approximately 22 Angstroms thick should decrease the fluid flow rate by approximately four percent.

The apparatus in this study used a filter with a uniform pore size to detect the presence of adsorbed molecules via a reduction in the fluid flow rate. Calibration of the filter using a fluid of similar viscosity was necessary to account for variations in the filter porosity.

(1) Results with Cellulose Filters. Four oils and twelve additives were used in this study. The properties of these oils and additives are shown in Tables 3 and 4. The oils were primarily super-refined mineral oils. These oils contained negligible amounts of polar impurities. Any polar impurities must be removed to prevent interference with these tests.

The types of additives tested consist of two acids, three resins (two partially hydrogenerated), dimer acid, a barium sulfonated hydrocarbon, an organic phosphate, two Acryloids, and two polymers (n-octyl polymethacrylates). In general, the following variables were studied with each additive - mineral oil viscosity, filter pore diameter, and additive concentration. The data generally show a viscosity corrected efflux time ratio ( $Z'$ ) of greater than one where

$$Z' = \frac{t_1 \mu_2}{t_2 \mu_1} \quad (17)$$

This ratio,  $Z'$ , was used to calculate the effective film thickness,  $A$ , by equation (10). That is

$$A = R_o \left( 1 - \frac{1}{Z'} \right)^{\frac{1}{4}} \quad (18)$$

where  $R_0$  is the mean pore radius. The effective film thickness,  $A$ , was then plotted versus shear rate (see equation (3)) or shear stress (see equation (1)). As the change in pressure drop was small, the shear stress is essentially proportional to pore diameter, and shear rate is proportional to pore diameter and inversely proportional to fluid viscosity.

These plots are separated into two distinct groups. In the first group, the effective film thickness,  $A$ , was independent of shear rate. For the second group,  $A$  was an increasing function of either shear rate or shear stress.

The additives that formed the first type of plot appeared to form rigid films. Dimer acid, n-octyl polymethacrylate-25 and n-octyl polymethacrylate-55 formed relatively thin, stable films.

In the second case, the oleic acid, the resins and the barium sulfonate form films that increase in thickness as a function of pore diameter. The value of  $A$  is generally larger with respect to the size of the additive molecule than those formed by the second group of additives. The large effective film thickness observed for the Acryloids, stearic acid, and the organic phosphonate places them in this category.

Dimer acid formed a thin film of constant thickness (see Table 5 and Figure 12). Over the range of mean pore diameters and additive concentrations studied, this acid formed a film approximately 15 Angstroms thick. Dimer acid is a dibasic acid, the dimer of oleic acid. Dibasic acids are believed to adsorb parallel to the surface, which indeed appears to be the case on the cellulose filters.

Two n-octyl polymethacrylates were studied (see Tables 6 and 7). The first (No. 25) has a molecular weight of about 8,000; the second (No. 55) about 11,500. As seen from Figures 13 and 14, these additives form stable rigid films of approximately 40 and 75 Angstroms, respectively. Over the limited concentration range studied, the effective film thickness does not depend on concentration. The lower molecular weight molecule appears to have a slight dependence of  $A$  on shear rate. This is not the case for n-octyl polymethacrylate-55, which shows no dependence of  $A$  on  $(dv/dr)$ . Generally, the film for n-octyl polymethacrylates appears to be essentially a rigid film with no dependence upon pore diameter or viscosity.

The observed values of  $A$  for the dimer acid, n-octyl polymethacrylate-25 and n-octyl polymethacrylate-55 are relatively small. The film formed by these additives appears to be an adsorbed monolayer with no interference with the bulk fluid flow.

The monobasic acids, the resins, the barium sulfonate and apparently the Acryloids and the organic phosphate, behave in a completely different manner. The values of  $A$  are much larger than those obtained for the rigid films and generally increase with increasing pore diameter.

While oleic acid was the most extensively studied, the data also show the most variation. In part, this variation may be attributed to the small increase in the viscosity corrected efflux time ratio,  $Z'$ , (see Table 8). Additionally, many of the oleic acid runs were made before the water contamination problem was recognized. Thus, some of the runs with the naphthenic white oil, MLO 7021, may exhibit an effective film thickness greater than the thickness actually present.

However, the following conclusions can be drawn for oleic acid (see Figures 15 and 16). The effect of concentration appears negligible in the range studied - 0.1 to 2.5 weight percent. The base fluid viscosity does not affect the effective film thickness,  $A$ , over the viscosity range of 3 to 77 centistokes. The  $A$  increases as the pore diameter increases as seen in Figure 15. The effect of pressure appears small (see Figure 16). However, the scatter in the data masks any small effect. The two points with a shear stress of  $92 \times 10^{-5}$  pound per square inch absolute are not significantly different from those with a shear stress of  $1 \times 10^{-5}$  pound per square inch absolute (see Table 8). These points have an average value of  $A$  of 10, while the average value of  $A$  from Figure 15 is also approximately 10 for the 0.2 micron filters. The maximum value of  $A$  observed was over 50 Angstroms, equivalent to approximately two rigid monolayers. The behavior of  $A$  with respect to pore diameter, pressure drop, and bulk fluid indicates that the decrease in flow rate is a result of a fluid sublayer existing at the liquid-solid interface consisting of both acid and base stock extending some distance into the fluid.

The second acid investigated was stearic acid. High concentrations of acid (2.5 weight percent) in the base fluid solidified at room temperature. Lower concentrations (0.5 weight percent) apparently formed a normal solution appearing clear, water white at room temperature. Viscosity measurements in the Ostwald-Fenske viscometer also appeared normal. However, the solution would not pass through the 0.1 micron filter at room temperature. Therefore, prefiltration was carried out with the aid of a heat lamp. During the actual run, the flow through the 0.46 micron filter stopped completely. The effect of the filter apparently oriented the molecules and crystallized the acid. The higher temperature in the prefiltration step prevented solidification of the acid. Stearic acid melts at about 160 degrees Fahrenheit. This was approximately the temperature during prefiltrations, thus, permitting the stearic acid solution to pass through the filter.

The barium sulfonate behaves slightly different (see Table 9 and Figures 17 and 18). The lower concentration of the sulfonate is not sufficient to form a thick film. The high concentration (5 weight percent) shows a linear relationship with shear stress (see Figure 17) and possibly with shear rate (see Figure 18). As the pressure drop over the filter was essentially constant for this series of runs,  $A$  is a function of both pore diameter and the base fluid viscosity. This behavior again indicates the presence of a relatively thick viscous sublayer. Since the effect of bulk viscosity appears to be small, this layer probably consists of both the base stock and barium sulfonate with a concentration different from that in the bulk fluid.

Three resins were examined, a heavy resin (MLO 7779), a super-refined resin (MLO 7760), and a hydrogenated resin (LH 136, 137). Tables 10, 11, and 12 and Figures 19, 20, 21, 22, and 23 are the results of these experiments. As the plots of effective film thickness versus shear stress show (Figures 20, 21, and 23), A for the heavy resin is about twice that for the super-refined resin, which in turn is about five times that of the hydrogenerated resin. Over the concentration range of one to five weight percent the amount of additive did not affect the film thickness. The effective film thickness increases with increasing pore diameter but not with fluid viscosity. The change in the pressure drop was negligible for this series. As a result of these observations, the flow appears to be retarded by a thick, viscous sub-layer consisting of both the resins and the base stock.

Ortholeum 162, an organic phosphate, provided a very thick film. At five weight percent in a naphthenic white oil (MLO 7021), the effective film thickness was 140 Angstroms with a shear rate of 480 per second. This run was made with a 0.45 micron filter and a calibration time of 316 seconds.

Two Acryloids were studied during this run (Ac 333 and Ac 966). During prefiltration these additives continually plugged the 0.1 micron filter. After prefiltration the Acryloids still plugged the 0.45 micron filters.

The organic acids, resins, barium sulfonate, organic phosphate, and Acryloids appear to form thick, viscous films. The effective film thickness, A, is much greater than can be explained by monolayer adsorption. However, the viscous layer model proposed previously accounts for this effect. This theory will be discussed in more detail in the following pages.

Lubrication studies have indicated the possibility that the combinations of additives found in lubricating oils may interfere with their effectiveness. This is verified by several examples in this study. The results of studies with an oxidized base stock, a polar base stock, and combinations of additives show a decreased effective film thickness.

The effect of an oxidized base stock was seen in a previous section. Briefly, an oxidized base stock effectively masked the expected increase in efflux times for oleic acid (see Table 2).

Table 13 shows the effect of a polar base stock. For these experiments, di-2-ethylhexyl sebacate (MLO 7710) was used as a base stock with 2.5 weight percent oleic acid. The base fluid essentially masks the effectiveness of the oleic acid. However, comparing the acid to a nonpolar hydrocarbon base stock, the effective film thickness is essentially the same as those obtained with oleic acid in a nonpolar base stock.

Thus, the oxidized base stock and the polar base stock interfere with the effect of oleic acid. In both cases, it appears that the polar molecules increase the calibration time so that the viscosity corrected efflux time ratio, Z', is in error. This is verified by the fact that Z' for di-2-ethylhexyl sebacate (MLO 7710) relative to the nonpolar mineral oil (MLO 7755) is not unity. In fact, it is two percent greater (see Table 13).

$$Z' = \frac{1.0267}{1.0066} = 1.02$$

Table 14 and Figure 24 are the results of a study with a combination of two additives - barium sulfonated hydrocarbon (PRL 3530), and a heavy resin (MLO 7779). These additives have also been run separately (see Figures 17 and 19). The results of the combined run are nearly identical to those of the heavy resin alone. This resin effectively masks the rigid film formed by the barium sulfonated hydrocarbons, forming a relatively thick shear sensitive film. However, the barium sulfonated hydrocarbon does appear to interfere slightly with the behavior of the resin.

Table 15 is the result of a study of additives in KG-80. For these runs the isopropyl oleate is the most effective additive. However, the concentrations of the oleic and dimer acids are small and the AO-702 causes considerable interference.

The interference of combinations of additives can be clearly seen from these previous studies. While the magnitude of the interference varies, it was present in each of these four studies.

(a) Modeling Fluid Flow The models proposed in the previous section appear to adequately handle the type of flow restrictions observed for the additives in the cellulose filters. For the rigid film model, A is independent of pore diameter, pressure drop and liquid viscosity. For the second model, A is a function of pore diameter and possibly liquid viscosity, but is independent of pressure drop. These behaviors are similar to those observed for the additives in this work.

These are not the only possible models, however. The surface film might not be rigid. The surface layer might consist of a rigid film plus a viscous, Newtonian sublayer. Additionally, the viscous layer or sublayer might be non-Newtonian.

The surface film might not be rigid. In fact, it probably is flexible, especially under the extremely high shear stresses found in boundary lubrication. However, during this study, the surface film was subject to very low shear stresses. In addition, the range of shear stress was small, from 1 to  $10 \times 10^{-5}$  pound per square inch absolute. If the film was flexible, A should decrease as  $\tau$  increases. This does not occur for any of the additives in this work over the limited range of shear examined.

The surface film might consist of a rigid, adsorbed layer plus a viscous film near the surface. For a surface film of this type, a plot of A versus pore diameter will be an increasing curve. The curve will approach some minimum value as a limit - the rigid layer thickness. In general, the data are not accurate enough or of a large enough range to confirm a non-linear curve. However, the minimum effective film thickness, the rigid portion, would be expected to be relatively large, at least a monolayer. For oleic acid with a molecular length of 22 Angstroms, the minimum A observed is 15

Angstroms. The heavy resin, which would be expected to have an effective molecular length several times that of oleic acid, has a minimum A of 25 Angstroms, while the super-refined resin has an A of 15. The hydrogenerated resin has an A of two. These data tend to reject this type of sublayer.

The surface layer may be non-Newtonian. Non-Newtonian behavior could be caused by the diminishing effect of the solid surface with distance from the surface or by an additive concentration gradient near the surface. As with the two film models previously mentioned, this would result in a nonlinear plot of A versus pore diameter. Figure 25 is a plot of data from the study with the heavy resin (see Table 10). This data appears to be the most self consistent (see Figure 20). However, when plotted on linear coordinates, the scatter is extensive permitting virtually any curve to be drawn through these points with equal validity. A more extensive study is necessary to rule out the possibility of a non-Newtonian sublayer.

(2) Studies with Metal Filters. In addition to the studies with the cellulose filters, several experiments were undertaken using 316L stainless steel sintered metal filters. These filters have a pore diameter of approximately five microns. While the pore size varies more than that of the cellulose filters and there is considerable interconnection, the same assumptions were made regarding fluid flow in this study.

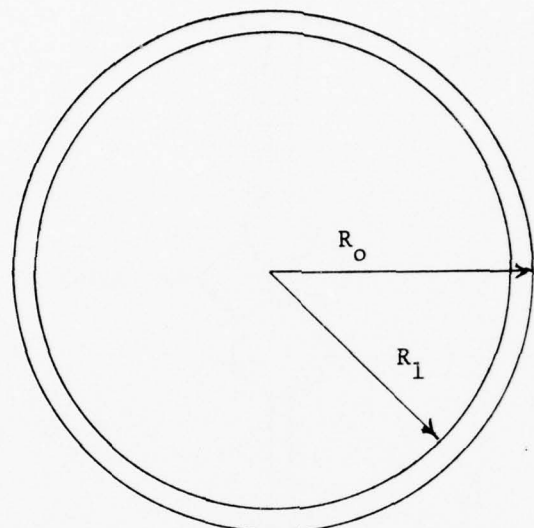
The data and calculated effective film thicknesses are presented in Table 16. Because of the difference in structure and surface properties, these data cannot be directly compared to the cellulose filter runs. With the exception of the five percent heavy resin (MLO 7779) plus five percent barium sulfonate (PRL 3530) in MLO 7789, a paraffinic mineral oil, the general trends are identical to those shown by these additives in the cellulose filter experiments. The small viscosity-corrected increase in run time for these additives, however, produced considerable variation in A.

The metal filters proved non-reusable. As with the cellulose filters, rinsing the metal filter with pure mineral oil would not remove the additive film. After cleaning with solvents, the calibration time decreased indicating a change in the flow characteristics of the filter.

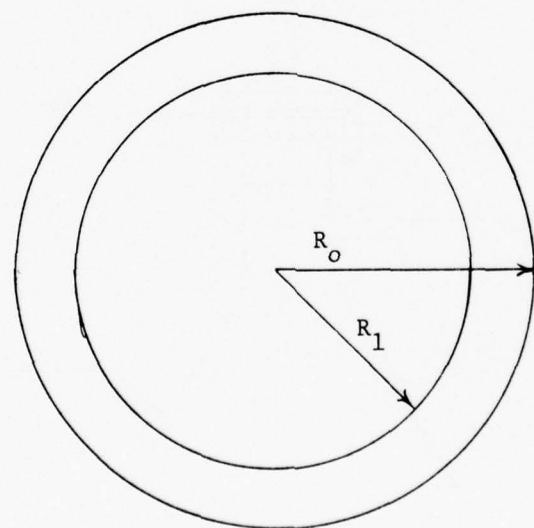
In addition, prewashing the metal filters with methanol prevented formation of a film with barium sulfonate (PRL 3530). The methanol apparently chemisorbed on the metal surface. This adsorption could not be reversed by heating at 250 degrees Fahrenheit for twelve hours. As a result of this interference, the filters must be kept clean. If cleaning is necessary, fitting the metal filters might be preferable to chemical cleaning.

Table 1  
CHARACTERISTICS OF CELLULOSE FILTERS

Mean Pore Size, Micron	Pore Size Variation, Micron	Thickness, Micron	Water Flow Rate, ml/sq cm-min, 77°F, 13.5 psi	Material of Construction and Manufacturer
0.10	0.008	130 $\pm$ 10	3.0	Esters of Cellulose-Millipore
0.20	0.02	150 $\pm$ 10	22.	Alpha Cellulose-Gelman
0.45	0.3	150 $\pm$ 10	65.	Esters of Cellulose-Millipore
1.2		150 $\pm$ 10	400.	Esters of Cellulose-Millipore



(a) Rigid Layer



(b) Viscous Sublayer

Figure 3. SCHEMATIC OF RESTRICTED PORE

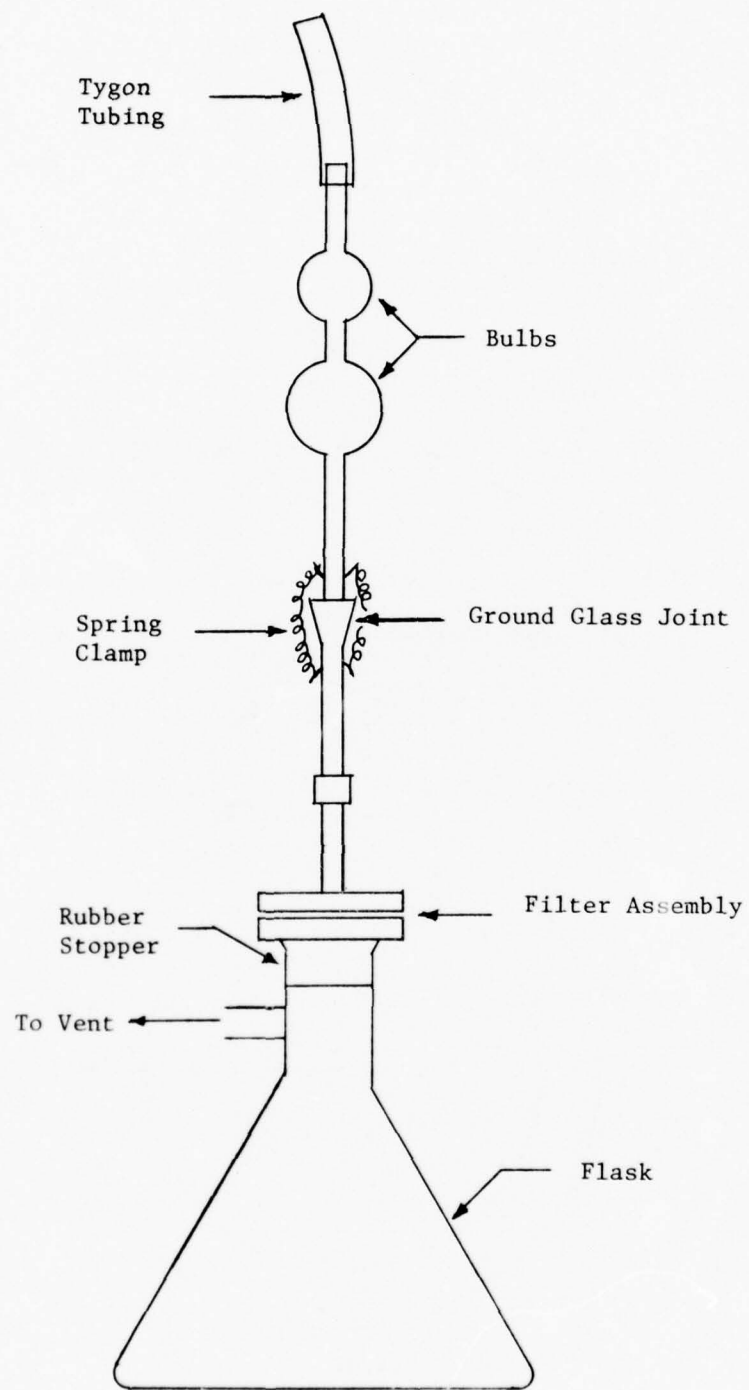


Figure 4. TEST APPARATUS

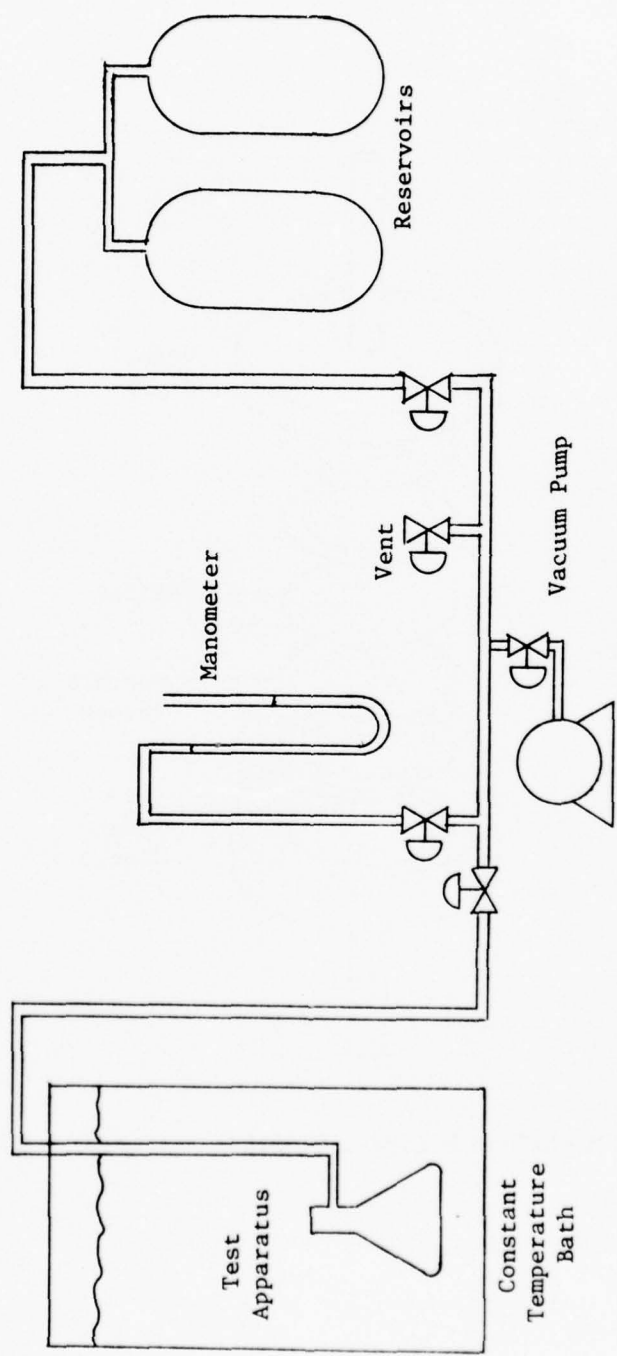


Figure 5. SCHEMATIC OF TEST ASSEMBLY

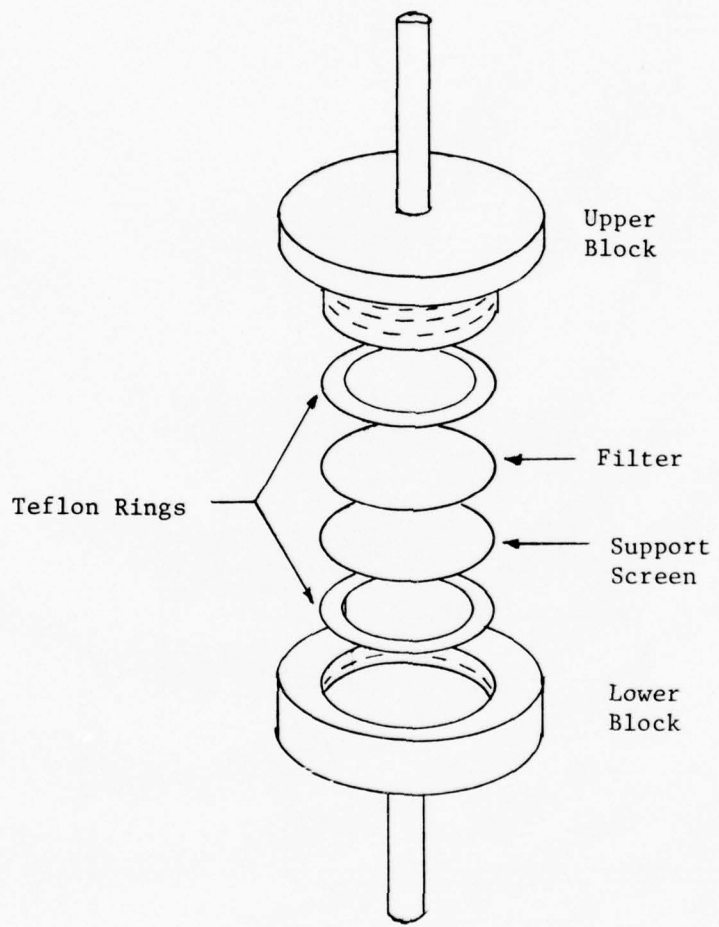


Figure 6. MILLIPORE FILTER ASSEMBLY

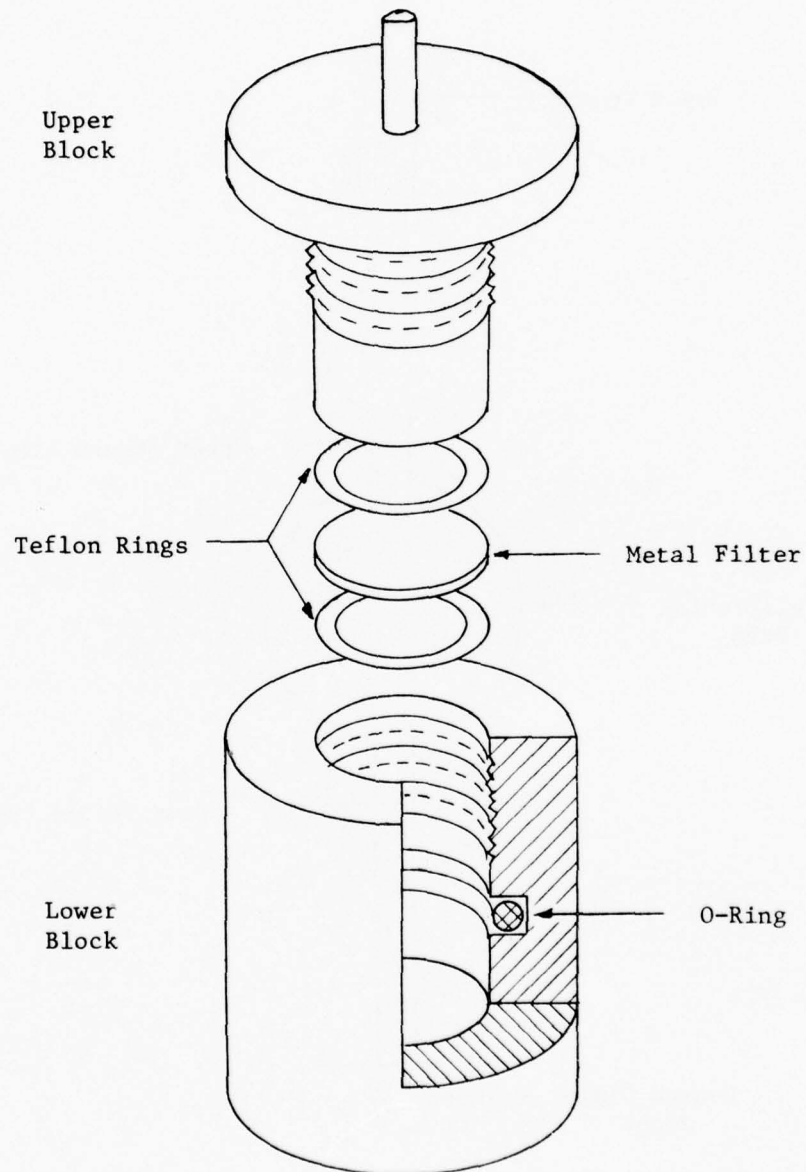


Figure 7. METAL FILTER ASSEMBLY

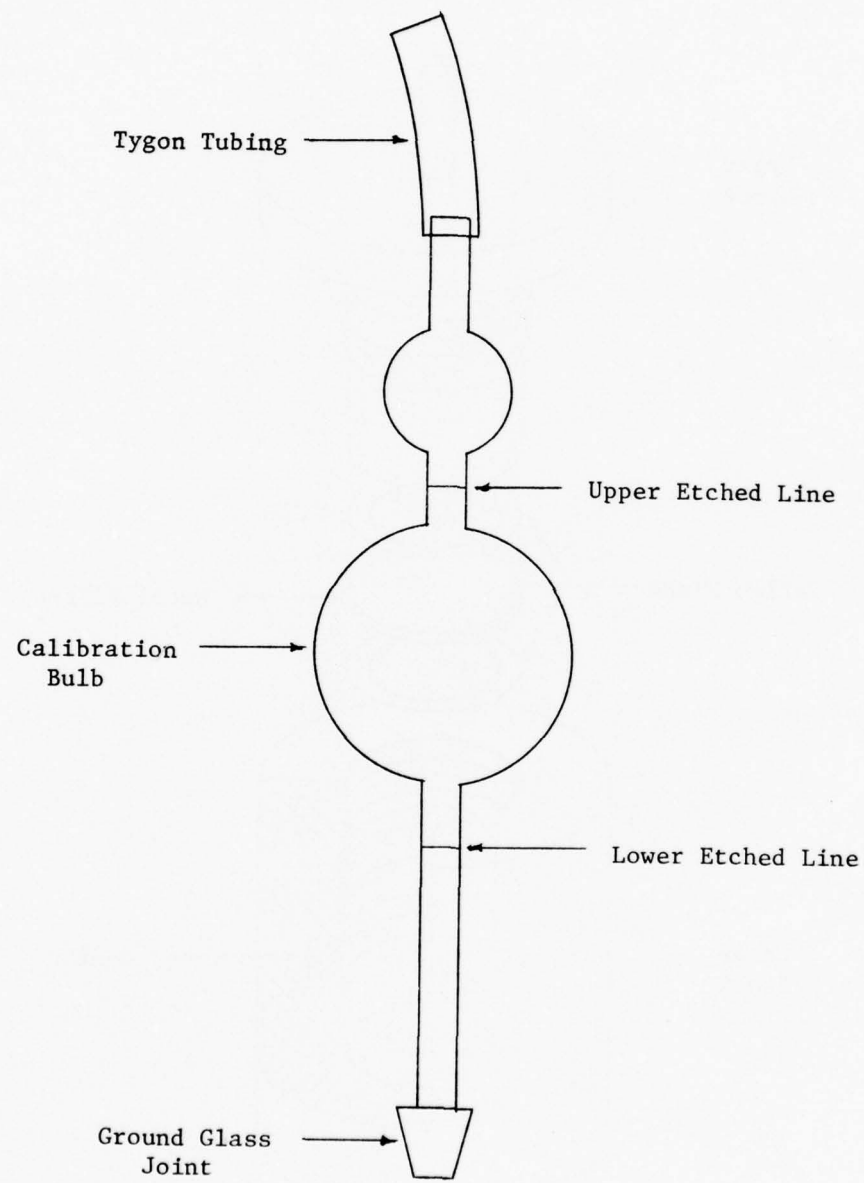


Figure 8. MEASURING BULB ASSEMBLY

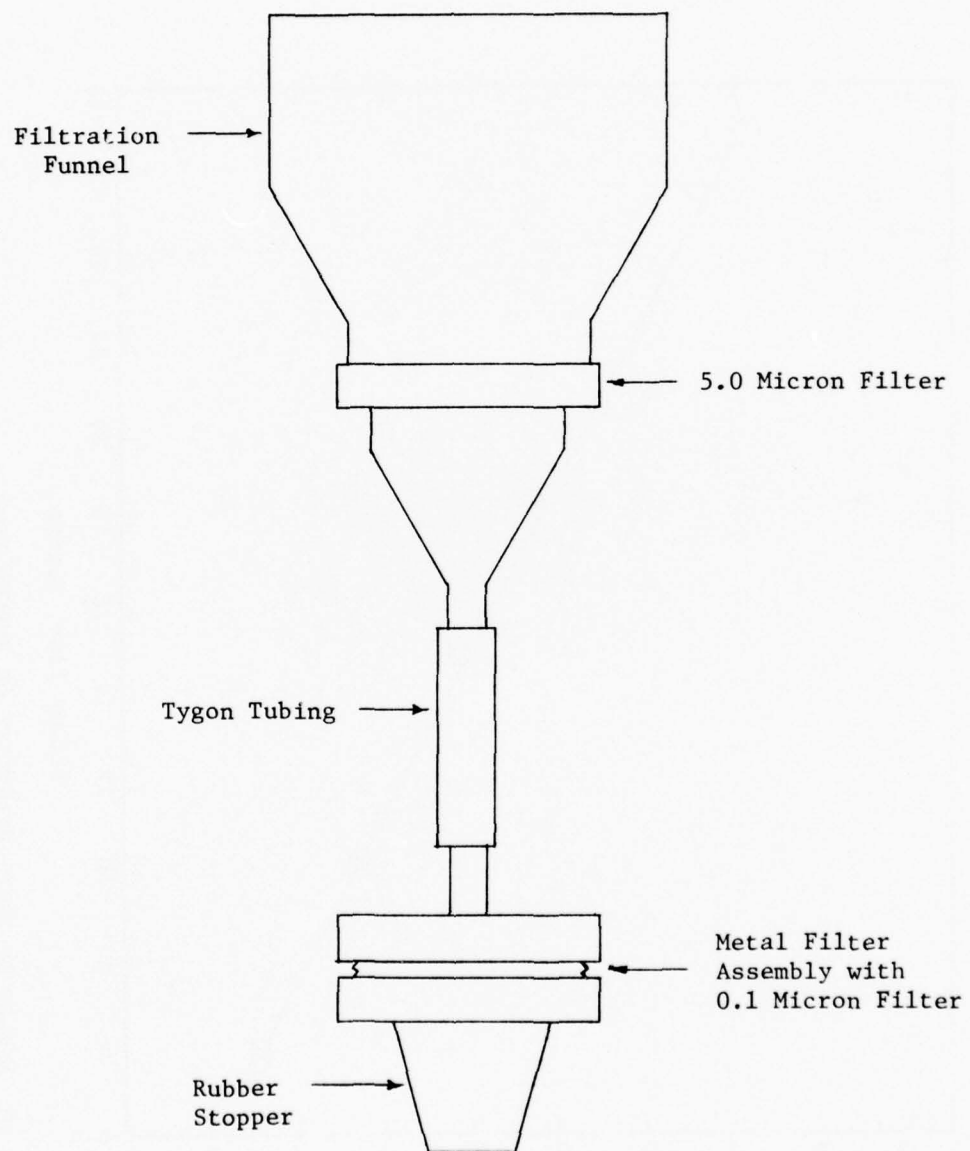


Figure 9. PREFILTRATION APPARATUS

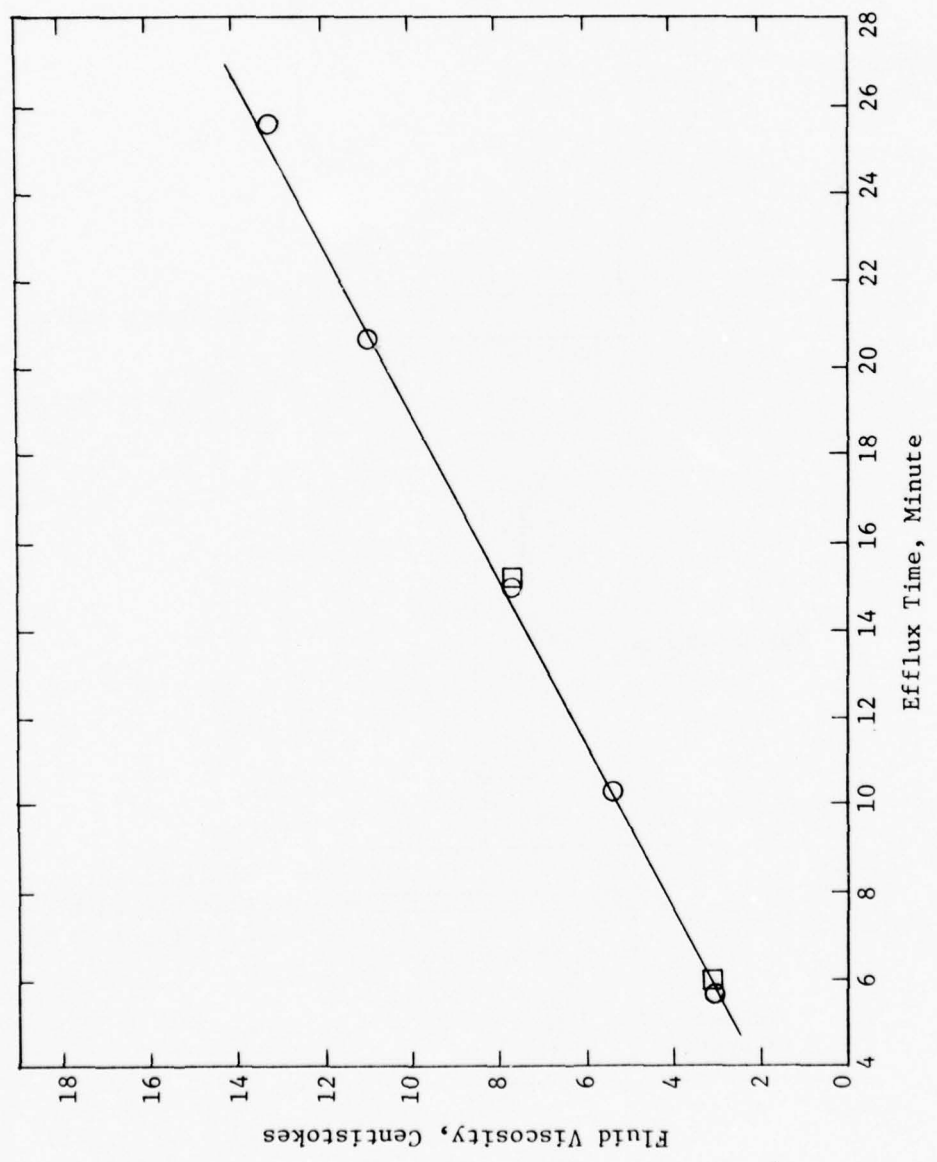


Figure 10. EFFECT OF FLUID VISCOSITY ON EFFLUX TIME

Table 2  
FLUID FLOW STUDY USING AN OXIDIZED BASE FLUID

Concentration of Oleic Acid, Wt. Percent	Base Fluid	Atmospheric Viscosity, Centistokes at 100°F	Filter Pore Diameter, Micron	Time of Calibration Run, Seconds	Viscosity Corrected Efflux Time Ratio, Z'	Apparent Film Thickness, A, Angstrom	Shear Stress, $\tau$ , PSIA $\times 10^5$	Shear Rate, $\frac{dv}{dr}$ , sec $^{-1}$
1.0	ML0 7685	3.342	0.2	351.8	1.0179	4	1.00	242.9
			0.2	358.7	1.0046	1	1.00	242.9
			0.2	332.6	1.0029	0.5	1.00	242.9
			0.2	345.1	.9884	-	1.00	242.9
			0.2	361.6	.9910	-	1.00	242.9
			0.2	404.7	.9925	-	1.00	242.9
			0.2	413.0	1.0076	2	1.00	242.9

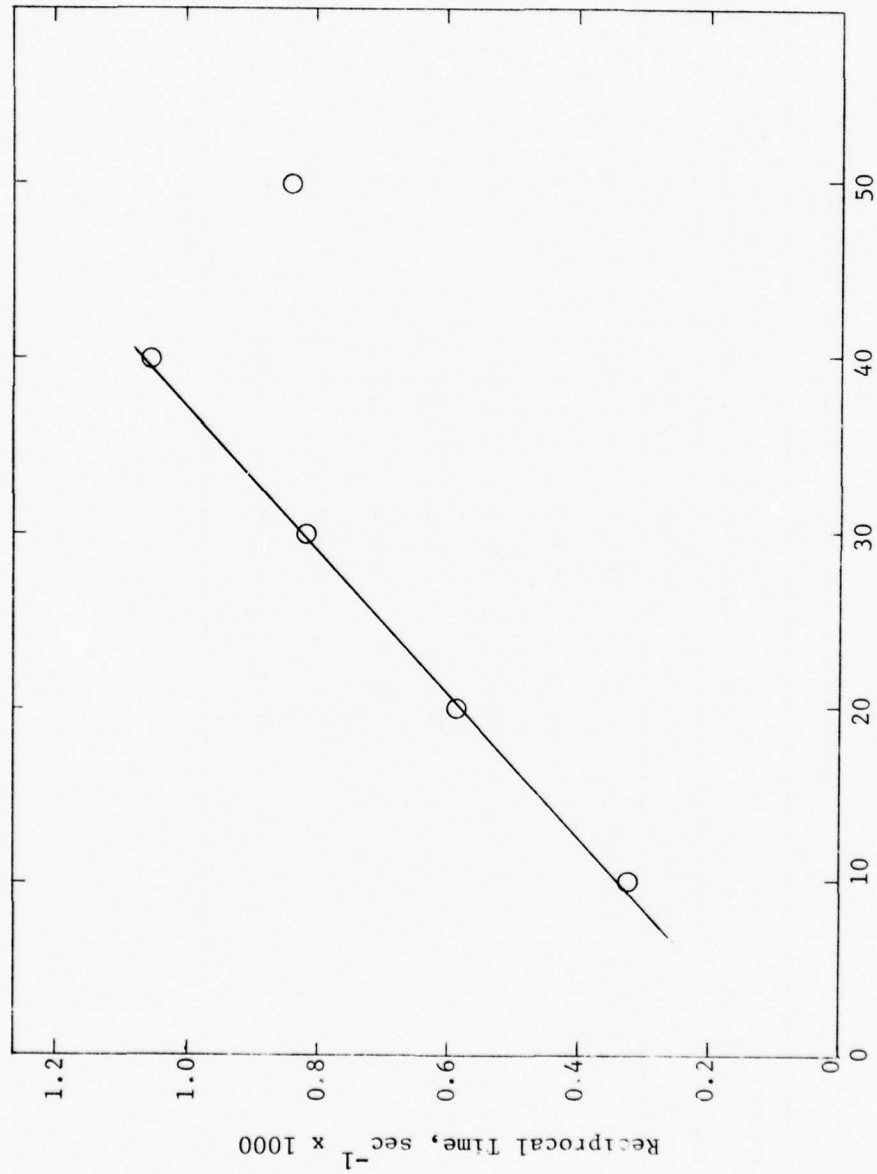


Figure 11. EFFECT OF APPLIED PRESSURE DROP ON EFFLUX TIME

Table 3  
PHYSICAL PROPERTIES OF STANDARDIZATION FLUIDS

MLO Number	Physical Description	Atmospheric Viscosity, Centistokes at 100°F
---	Cetane	3.054
7021	Naphthenic White Oil	3.035
7685	Naphthenic Mineral Oil	3.223
7755	White Oil	13.14
7789	Paraffinic Mineral Oil	13.31
7625	White Oil	76.9
7710	Di-2-Ethylhexyl Sebacate	12.6
KG-80		164.7

Table 4  
PHYSICAL PROPERTIES OF ADDITIVES

Designation	Description	Approximate Molecular Weight
--	Oleic Acid	282
--	Stearic Acid	284
PRL 3697	Dimer Acid of Oleic Acid Empol 1022	565
PRL 3530	Barium Sulfonated Hydrocarbons	
PRL 3170	Ortholeum 162-Organic Phosphate, Dilaural Acid Phosphate and Diacid Lauroyl Phosphate	
--	AC 333 Acryloid	
--	AC 966 Acryloid	
MLO 7779	Kendall Resin-Heavy Resin	
MLO 7760	Kendall Resin-Partially Hydrogenated, Super Refined Heavy Resin	2000-3000
LH-136, 137	Kendall Resin-Hydrogenated PRL 7779	
	n-Octyl Polymethacrylate-25	8000
	n-Octyl Polymethacrylate-55	11,500

Table 5  
FLUID FLOW STUDY USING DIMER ACID (PRL 3697)

Concentration of Additive, Wt. Percent	Base Fluid	Atmospheric Viscosity, Centistokes at 100°F	Filter Pore Diameter, Micron	Time of Calibration Run, Seconds	Viscosity Efflux Ratio, Z	Apparent Film Thickness, A, Angstrom	Shear Stress, $\tau$ , $\text{PSIA} \times 10^5$	Shear Rate, $\frac{dv}{dr}$ , sec $^{-1}$
0.1	ML0 7021	3.02	0.2	306.2	1.0358	9	0.97	268.8
			0.45	305.9	1.0250	14	1.92	532.0
0.1	ML0 7755	13.08	0.2	1368.1	1.0378	9	1.01	62.1
			0.45	429.0	1.0232	13	2.04	125.7
			1.2	242.2	1.0091	14	5.87	521.6
0.5	ML0 7021	3.08	0.2	328.8	1.0669	16	0.97	263.6
			0.45	325.4	1.0438	24	1.92	521.6
0.5	ML0 7755	13.4	0.2	1368.1	1.0669	16	1.01	60.6
			0.45	429.0	1.0416	23	2.04	122.7
			1.2	242.2	1.0074	11	5.87	353.2

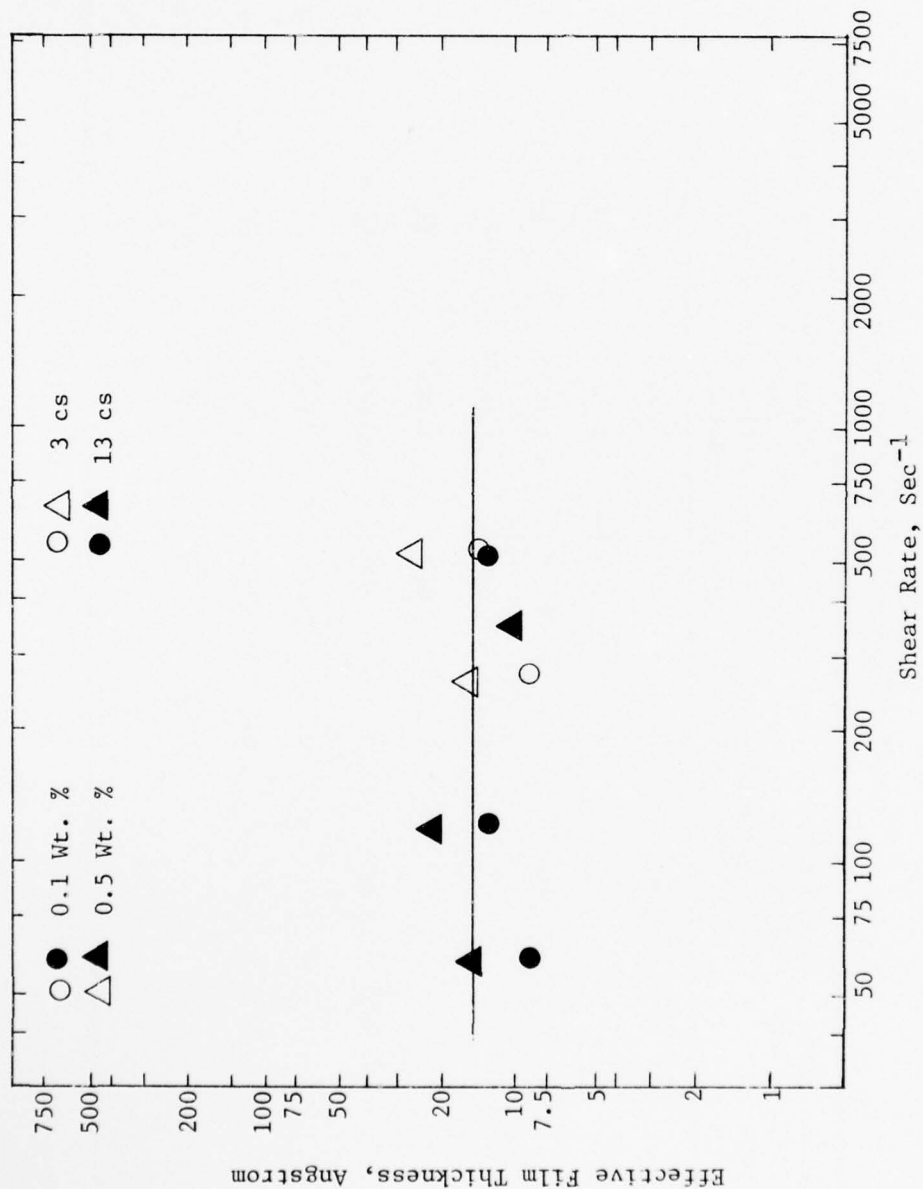


Figure 12. EFFECTIVE FILM THICKNESS OF DIMER ACID (PRL 3697)

Table 6  
FLUID FLOW STUDY USING N-OCTYL POLYMETHACRYLATE-25

Concentration of Additive, Wt. Percent	Base Fluid	Atmospheric Viscosity, Centistokes at 100°F	Filter Pore Diameter, Micron	Time of Calibration Run, Seconds	Viscosity Corrected Efflux Time Ratio, Z'	Apparent Film Thickness, A, Angstrom	Shear Stress, $\tau$ , PSIA $\times 10^5$	Shear Rate, $\frac{dv}{dr}$ , sec $^{-1}$
0.46	MLO 7021	3.28	0.45	373.6	1.1059	56	1.92	489.8
0.46	MLO 7755	13.56	0.2	1781.5	1.2152	48	1.01	59.7
			0.45	703.1	1.0274	15	1.27	75.8
			1.2	300.5	1.0448	66	5.31	315.9
0.92	MLO 7021	3.51	0.2	841.0	1.2081	46	1.42	339.0
			0.45	373.4	1.1260	66	1.92	457.7
			1.2	275.9	1.0130	19	5.31	299.0

Table 7  
FLUID FLOW STUDY USING N-OCTYL POLYMETHACRYLATE-55

Concentration of Additive, Wt. Percent	Base Fluid	Atmospheric Viscosity, Centistokes at 100°F	Filter Pore Diameter, Micron	Time of Calibration Run, Seconds	Viscosity Corrected Efflux Time Ratio, Z'	Apparent Film Thickness, A, Angstrom	Shear Stress, PSIA $\times 10^5$	Shear Rate, $\frac{dv}{dr}$ , sec $^{-1}$
0.46	ML0 7021	3.37	0.2	875.5	1.3086	65	1.42	353.1
			0.45	384.1	1.1673	85	1.92	476.7
0.46	ML0 7755	13.93	0.2	1029.1	1.2941	62	1.50	86.8
			0.2	1031.1	1.3237	68	1.50	86.8
0.45			642.8	1.1745	89	1.27	73.8	
			1.2	305.1	1.0362	53	5.31	307.6
0.92	ML0 7021	3.71	0.2	926.9	1.4370	87	1.42	320.8
			0.45	344.8	1.1759	89	1.92	433.0
0.92	ML0 7755	14.96	0.2	1134.0	2.1564	681	1.01	54.3
			0.45	572.3	1.1630	83	2.00	107.4

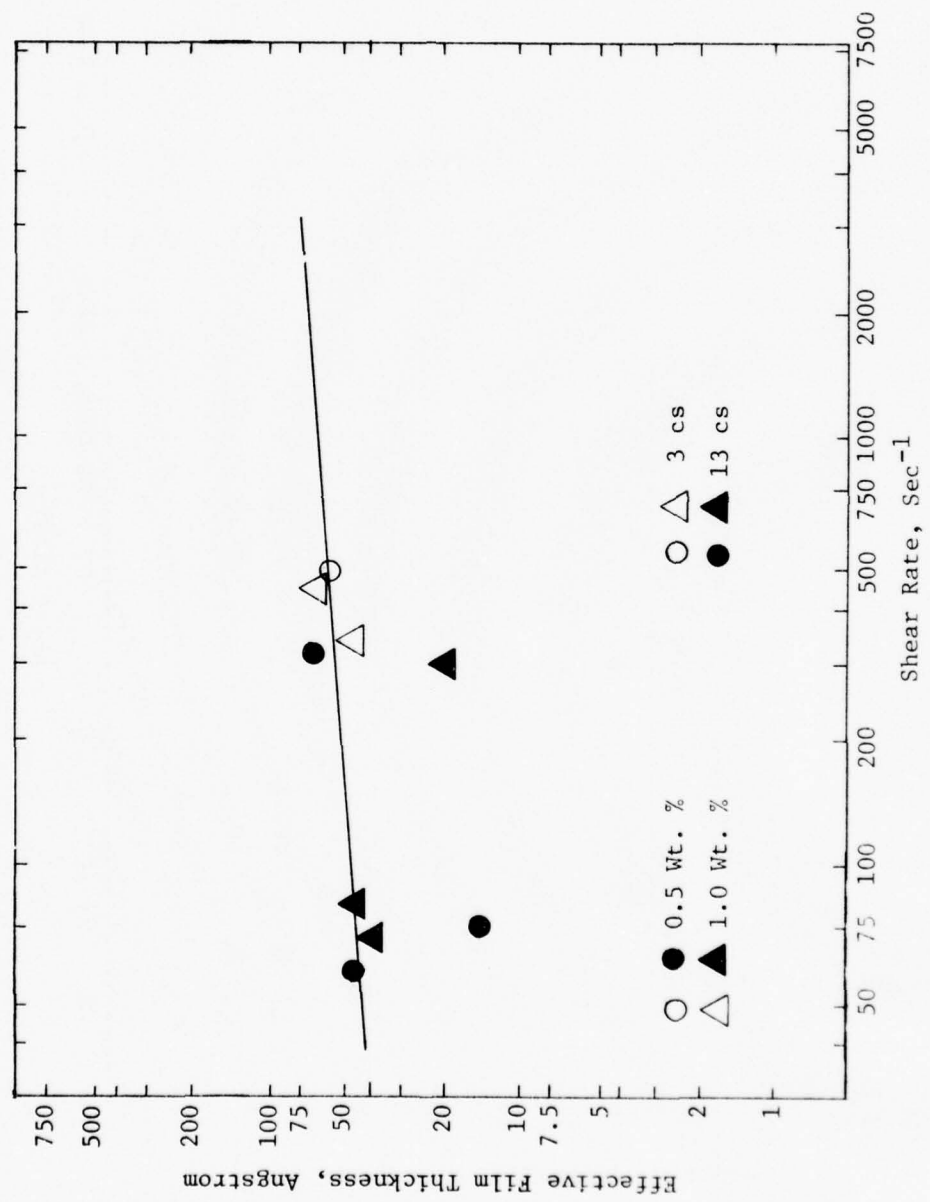


Figure 13. EFFECTIVE FILM THICKNESS OF N-OCTYL POLYMETHACRYLATE-5

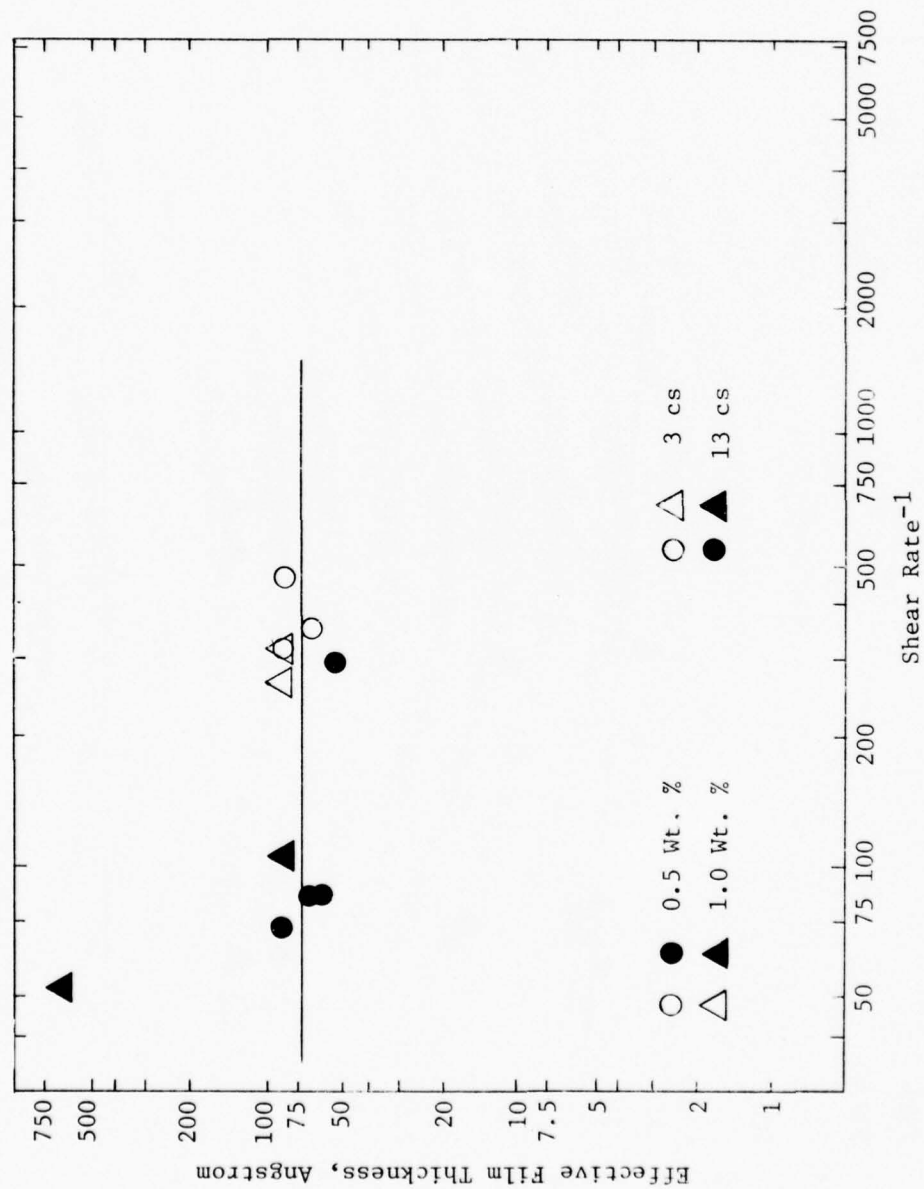


Figure 14. EFFECTIVE FILM THICKNESS OF N-OCTYL POLYMETHACRYLATE-55

Table 8

## FLUID FLOW STUDY USING OLEIC ACID

Concentration of Additive, Wt. Percent	Base Fluid	Atmospheric Viscosity, Centistokes at 100°F	Filter Pore Diameter, Micron	Time of Calibration Run, Seconds	Viscosity Corrected Efflux Time Ratio, Z'	Apparent Film Thickness, Angstrom	Shear Stress, $\tau$ , PSIA $\times 10^5$	Shear Rate, $\frac{dv}{dr}$ , sec $^{-1}$
0.1	MLO 7021	3.055	0.2	317.2	1.0058	1	0.97	265.7
			0.2	300.9	1.0234	6	0.97	265.7
			0.45	332.6	1.1333	70	1.96	538.1
0.5	Cetane	3.07	0.45	548.3	1.0207	12	1.87	535.5
			0.2	826.8	1.1542	35	1.42	386.4
0.5	MLO 7021	3.08	0.2	441.9	1.0922	22	0.60	164.7
			0.2	219.7	1.0172	10	3.93	1067.5
			0.45	108.7	0.998	--	--	--
0.5	MLO 7755	13.06	1.2	127.6	1.0345	50	8.08	2199.7
			0.2	945.5	1.0387	10	1.50	92.6
			0.45	507.6	1.0466	26	2.04	125.9
1.0	MLO 7021	3.135	1.2	397.1	1.0382	56	5.32	328.0
			0.2	356.5	1.0278	7	0.97	258.9
			0.2	329.6	0.994	--	0.97	258.9
1.0	MLO 7755	13.67	0.2	335.5	1.0115	3	0.97	258.9
			0.45	282.5	1.0035	2	2.12	566.1
			0.45	1313.8	1.0124	3	1.00	59.4
			0.45	461.0	.9645	--	2.04	120.2

Table 8 (Concluded)

Concentration of Additive, Wt. Percent	Base Fluid	Atmospheric Viscosity, Centistokes at 100°F	Filter Pore Diameter, Micron	Time of Calibration Run, Seconds	Viscosity Corrected Efflux Time Ratio, Z	Apparent Film Thickness, A, Angstrom	Shear Stress, $\tau$ , PSIA $\times 10^5$	Shear Rate, $\frac{dv}{dr}$ , sec $^{-1}$
2.5	MLO 7021	3.20	0.45	419.6	1.0124	7	2.04	59.4
				1.2	243.3	1.0500	73	5.87
2.5	MLO 7685	3.342	0.2	804.7	1.1807	40	1.45	377.6
				0.45	357.8	1.2188	109	502.1
2.5	MLO 7755	13.22	0.2	462.2	1.0748	18	1.00	242.9
				0.2	433.8	1.0534	13	1.00
2.5	MLO 7789	13.39	0.45	222.7	1.0850	20	8.18	1982.3
				0.2	55.37	1.0587	14	92.14
2.5	MLO 7625	72.07	0.2	956.5	1.0445	11	1.50	91.4
				0.45	583.2	1.0730	39	1.27
2.5	MLO 7789	13.39	0.45	1.2	119.3	1.0173	26	3.40
				0.2	288.6	1.0171	10	2.04
2.5	MLO 7625	487.0	0.2	173.6	•9993	--	55.73	122.8
				0.2	487.0	1.0292	7	92.19
								990.5

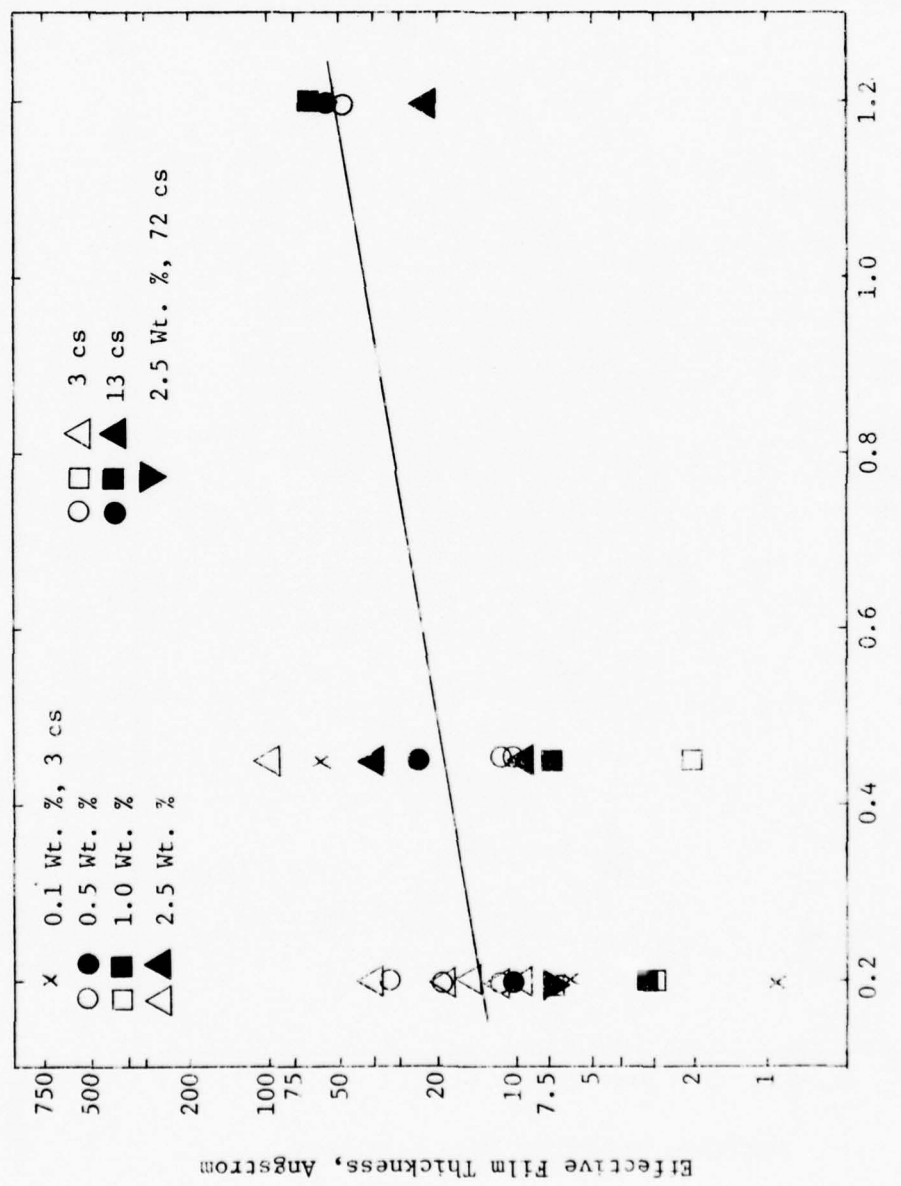


Figure 15. EFFECTIVE FILM THICKNESS AS A FUNCTION OF PORE DIAMETER FOR OLEIC ACID

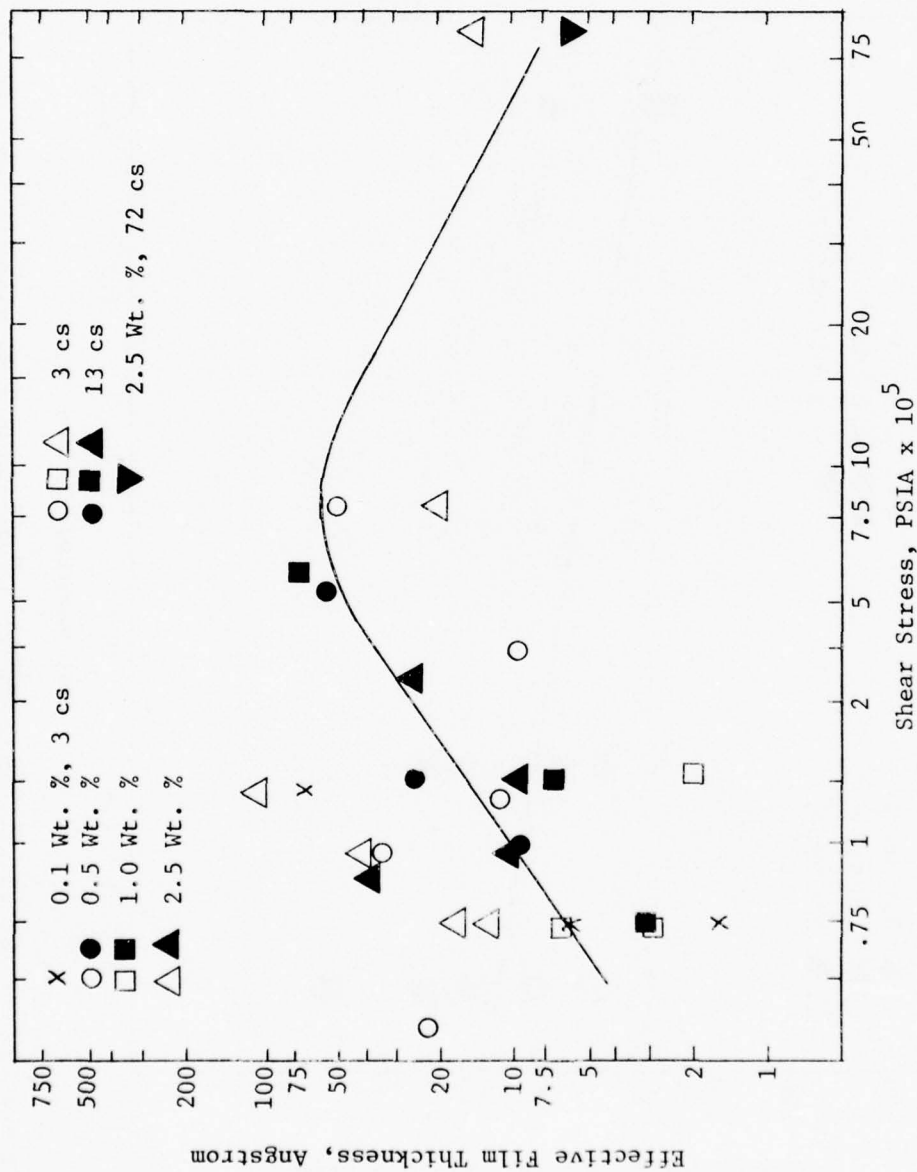


Figure 16. EFFECT OF SHEAR STRESS ON THE EFFECTIVE FILM THICKNESS OF OLEIC ACID

Table 9  
FLUID FLOW STUDY USING BARIUM SULFONATED HYDROCARBON (PRL 3530)

Concentration of Additive, Wt. Percent	Base Fluid	Atmospheric Viscosity, Centistokes at 100°F	Filter Pore Diameter, Micron	Time of Calibration Run, Seconds	Viscosity Corrected Efflux Time Ratio, Z	Apparent Film Thickness, A, Angstrom	Shear Stress, $\tau$ , PSIA $\times 10^5$	Shear Rate, $\frac{dv}{dr}$ , sec $^{-1}$
0.5	ML0 7021	3.08	0.2	327.4	1.0313	8	0.97	263.6
			0.45	341.7	1.0172	10	1.92	521.6
5.0	ML0 7021	3.075	0.2	341.6	1.1053	25	0.97	264.0
			0.45	327.6	1.0802	43	1.92	522.5
5.0	ML0 7755	12.82	0.2	1858.1	1.0821	20	1.01	63.3
			0.45	657.8	1.1361	70	1.27	80.1
			1.2	291.4	1.0427	63	5.31	334.2

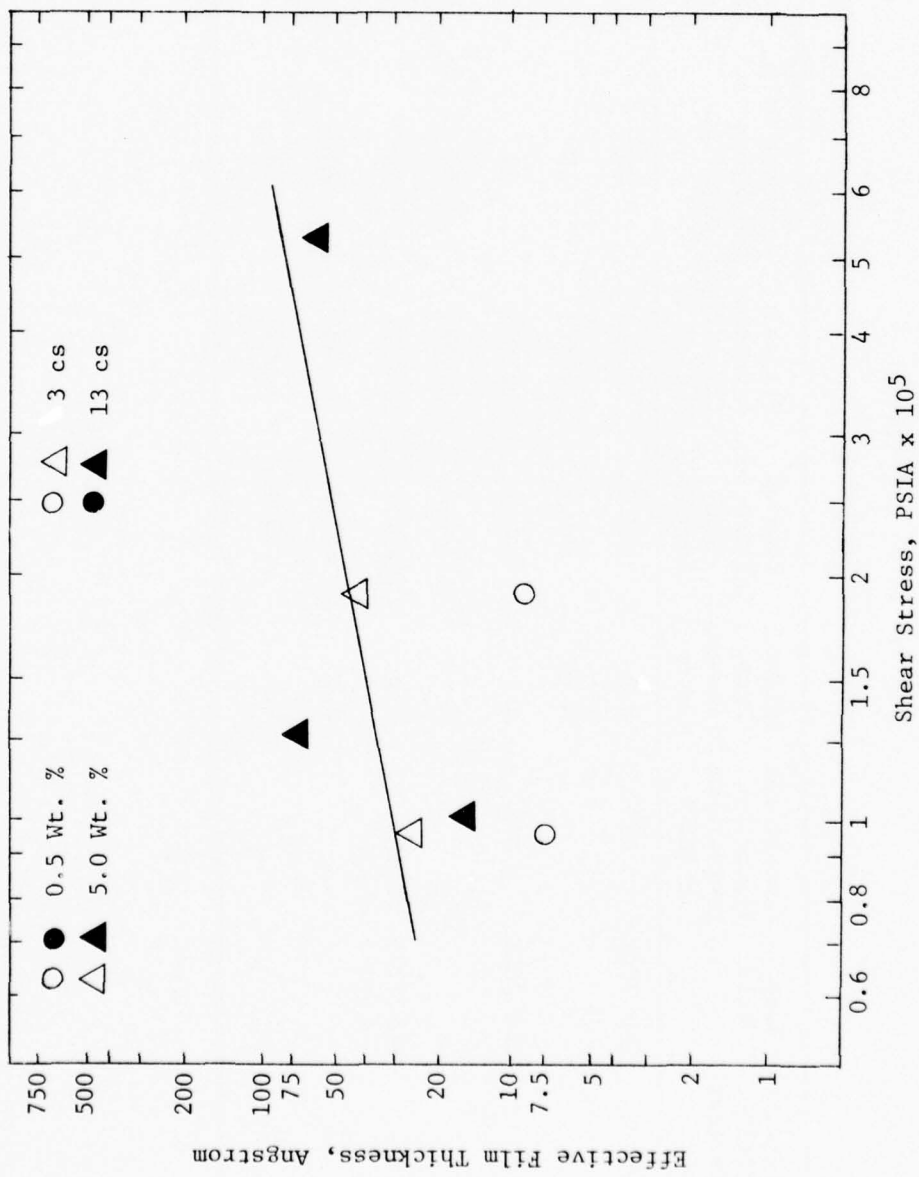


Figure 17. EFFECT OF SHEAR STRESS ON THE EFFECTIVE FILM THICKNESS OF A BARIUM SULFONATED HYDROCARBON (PRL 3530)

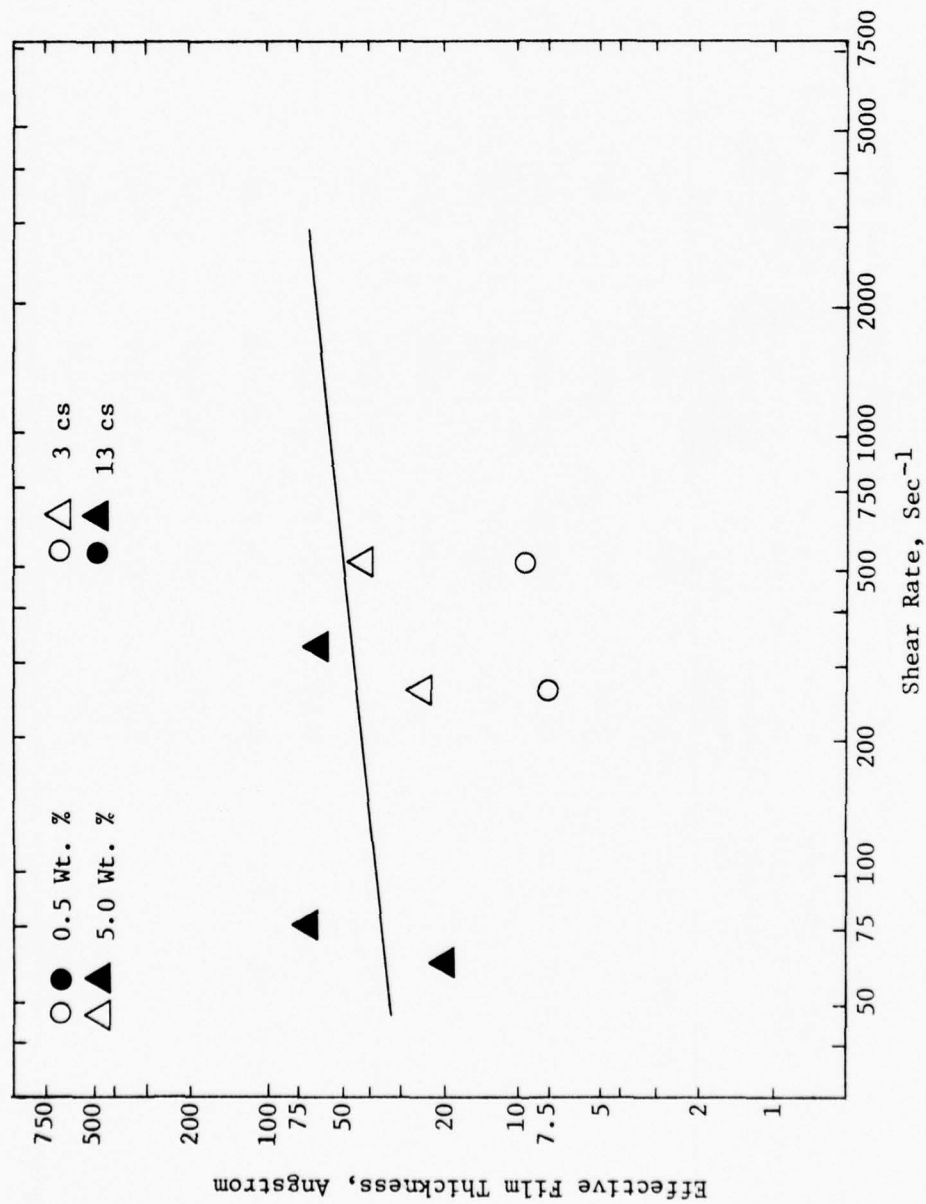


Figure 18, EFFECTIVE FILM THICKNESS FOR A BARIUM SULFONATED HYDROCARBON (PRL 3530)

Table 10  
FLUID FLOW STUDY USING A HEAVY RESIN (MLO 7779)

Concentration of Additive, Wt. Percent	Base Fluid	Atmospheric Viscosity, Centistokes at 100°F	Filter Pore Diameter, Micron	Time of Calibration Run, Seconds	Corrected Efflux Time	Apparent Film Thickness, A, Angstrom	Shear Stress, $\tau$ , PSIA $\times 10^5$	Shear Rate, $\frac{dv}{dr}$ , sec $^{-1}$
1.0	MLO 7021	3.23	0.2	298.9	1.1288	30	0.97	251.3
				0.45	352.5	1.1556	78	1.92
1.0	MLO 7755	14.20	0.2	1406.4	1.0806	19	1.00	497.4
				0.45	431.2	1.0901	48	57.2
5.0	MLO 7021	4.07	0.2	233.4	1.0954	135	2.04	115.8
				1.2	313.8	1.1238	29	5.87
5.0	MLO 7755	16.81	0.2	351.0	1.1463	75	0.97	333.3
				0.45	1454.5	1.1419	33	199.5
5.0	MLO 7755	16.81	0.2	491.3	1.1311	68	1.92	394.7
				1.2	233.4	1.1173	164	48.3
5.0	MLO 7755	16.81	0.2	238.0	1.1157	112	5.87	95.6
				1.2	238.0	1.1157	5.87	281.5

Table 11  
FLUID FLOW STUDY USING A PARTIALLY HYDROGENATED RESIN (MLO 7760)

Concentration of Additive, Wt. Percent	Base Fluid	Atmospheric Viscosity, Centistokes at 100°F	Filter Pore Diameter, Micron	Time of Calibration Run, Seconds	Viscosity Corrected Efflux Time Ratio, Z'	Apparent Film Thickness, A, Angstrom	Shear Stress, $\tau$ , PSIA $\times 10^5$	Shear Rate, $\frac{dv}{dr}$ , sec <sup>-1</sup>
1.0	MLO 7021	3.23	0.2	339.8	0.9881	--	6.97	241.6
			0.45	355.9	1.0182	10	1.92	478.1
1.0	MLO 7755	13.7	0.2	1352.0	1.0220	5	1.01	59.3
			1.2	239.8	1.0572	83	5.87	345.4
5.0	MLO 7021	4.025	0.2	300.1	1.1346	31	0.97	201.7
			0.45	358.7	0.9836	--	1.92	399.1
6.0	MLO 7755	17.13	0.2	1414.4	0.9748	--	1.01	47.4
			0.45	451.0	0.9894	--	2.04	96.0
			1.2	239.8	1.0543	79	5.87	276.3

Table 12

## FLUID FLOW STUDY USING A HYDROGENATED RESIN (LH 136, 137)

Concentration of Additive, Wt. Percent	Base Fluid	Atmospheric Viscosity, Centistokes at 100° F	Filter Pore Diameter, Micron	Time of Calibration Run, Seconds	Viscosity Efflux Time	Corrected Thickness, A, Angstrom Ratio, Z	Apparent Film Stress, $\tau$ , PSIA $\times 10^5$	Shear Rate, $\frac{dv}{dr}$ , sec <sup>-1</sup>
1.0	MLO 7021	3.21	0.2	295.5	1.0076	2	0.97	252.9
			0.45	394.9	1.0161	9	1.92	500.5
1.0	MLO 7755	13.67	0.2	1313.8	1.0122	3	1.01	59.4
			0.45	419.6	1.0122	7	2.04	120.3
			1.2	343.3	1.0498	73	5.87	346.2
5.0	MLO 7021	4.02	0.2	299.9	1.0064	2	0.97	201.9
			0.45	353.3	1.0034	2	1.92	399.6
5.0	MLO 7755	16.6	0.2	1313.8	0.9542	--	1.07	48.9
			0.45	419.6	1.0100	6	2.04	99.0
			1.2	243.3	1.0284	42	5.87	285.1

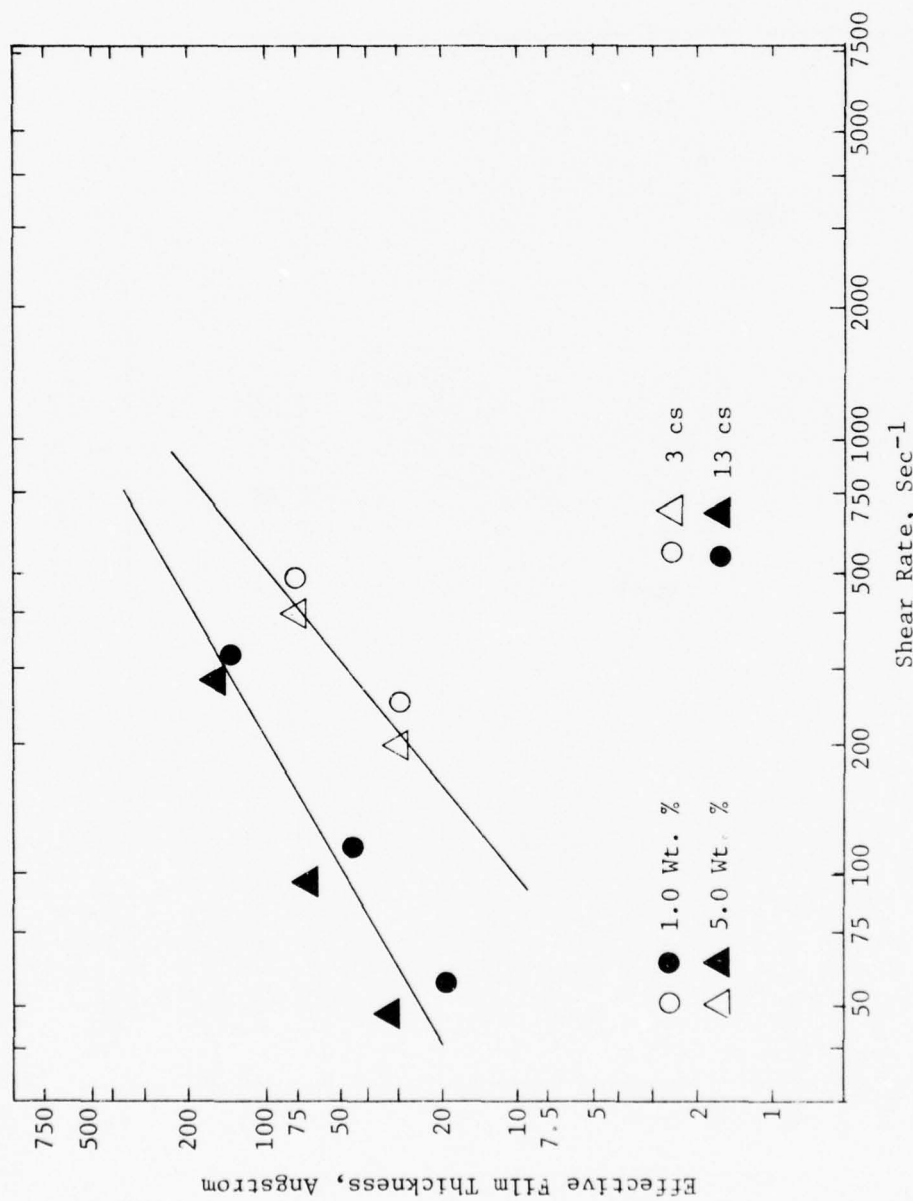


Figure 19. EFFECTIVE FILM THICKNESS OF A HEAVY RESIN (MLQ 7779)

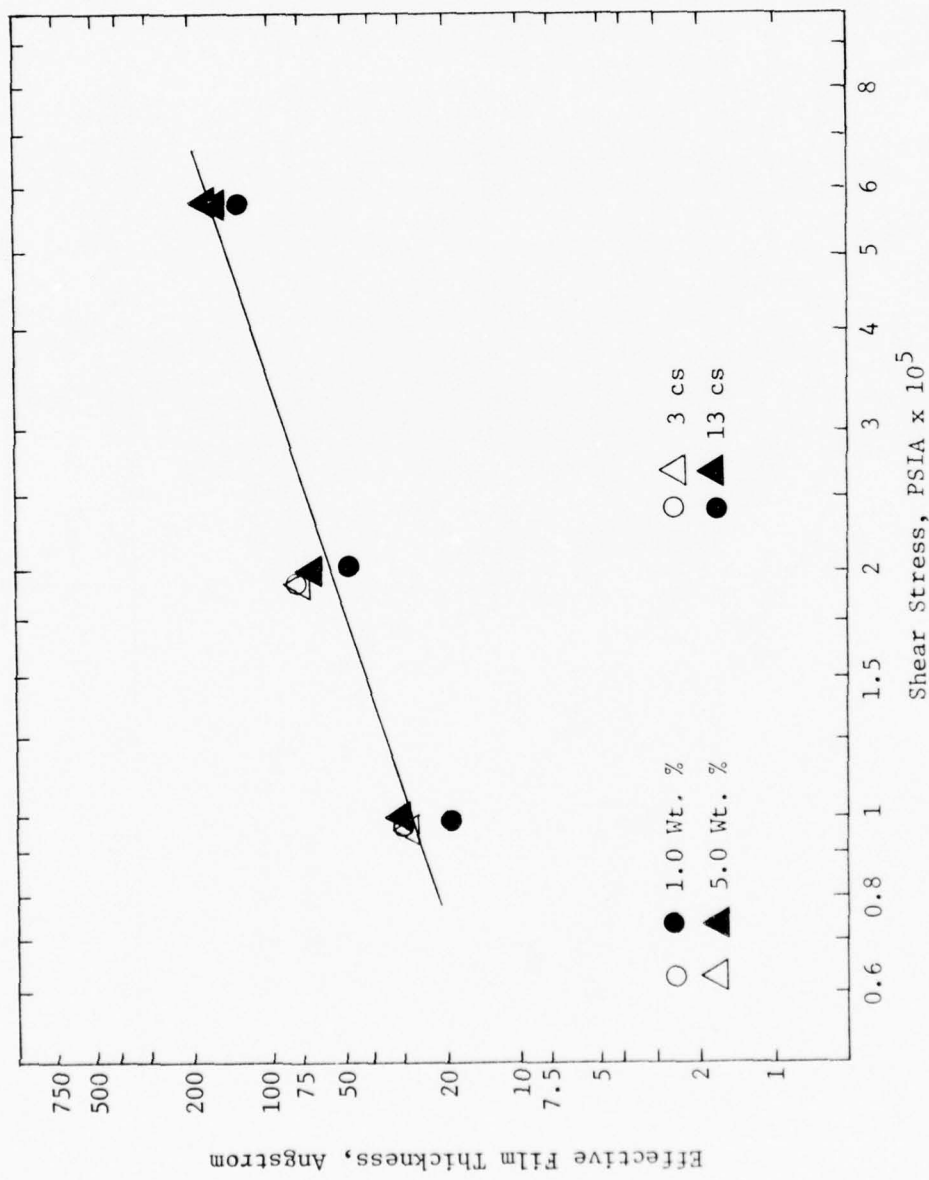


Figure 20. EFFECT OF SHEAR STRESS ON THE EFFECTIVE FILM THICKNESS OF A HEAVY RESIN (MLO 7779)

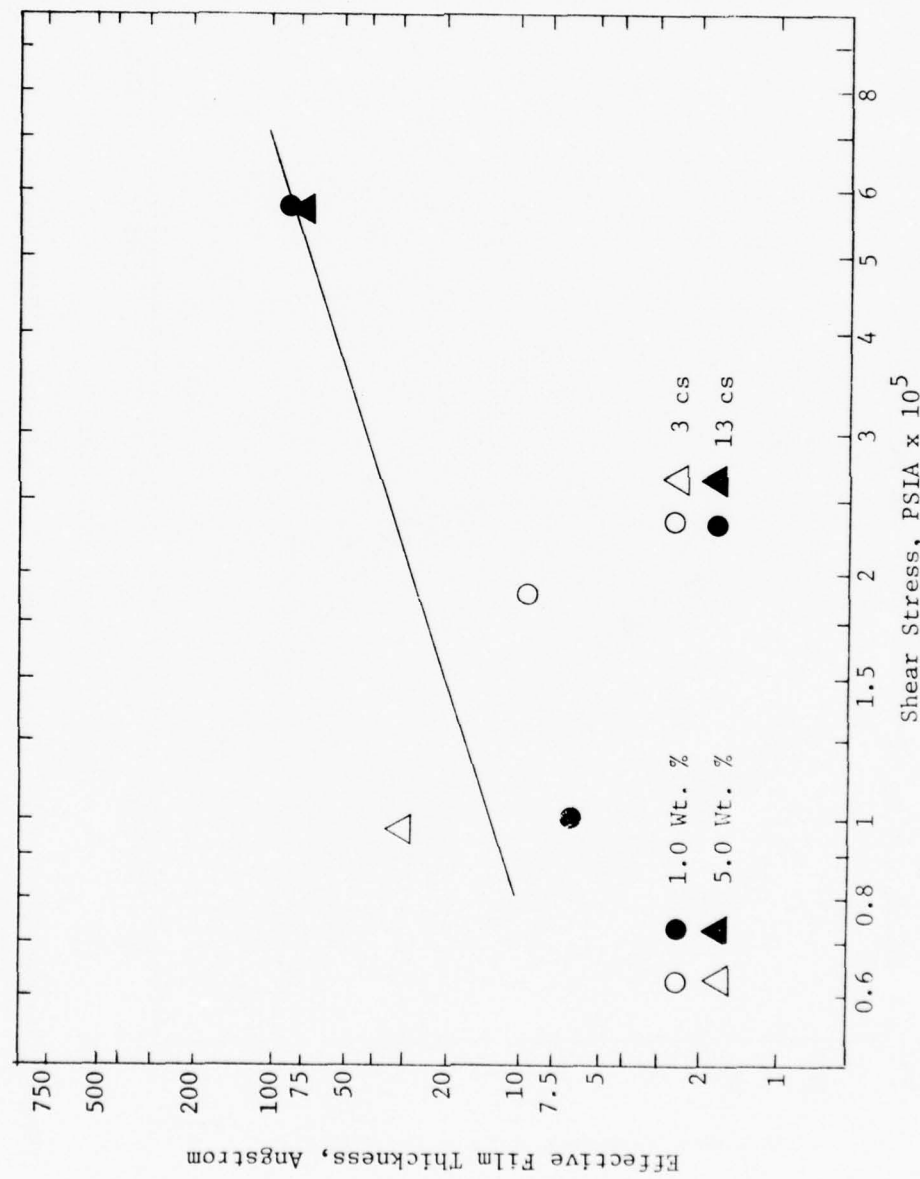


Figure 21. EFFECT OF SHEAR STRESS ON THE EFFECTIVE FILM THICKNESS OF A PARTIALLY HYDROGENATED RESIN (MLO 7760)

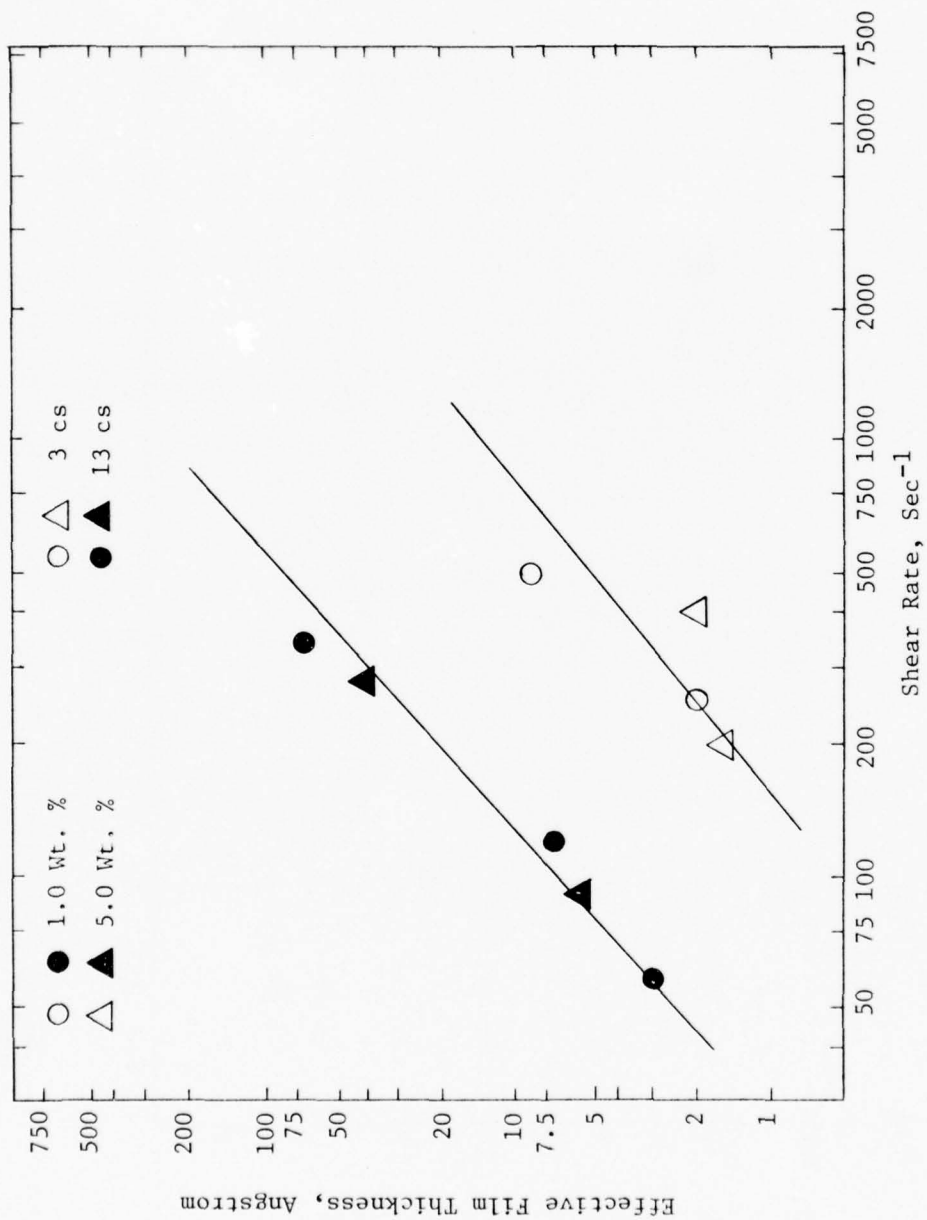


Figure 22. EFFECTIVE FILM THICKNESS FOR A HYDROGENATED RESIN (LH 136, 137)

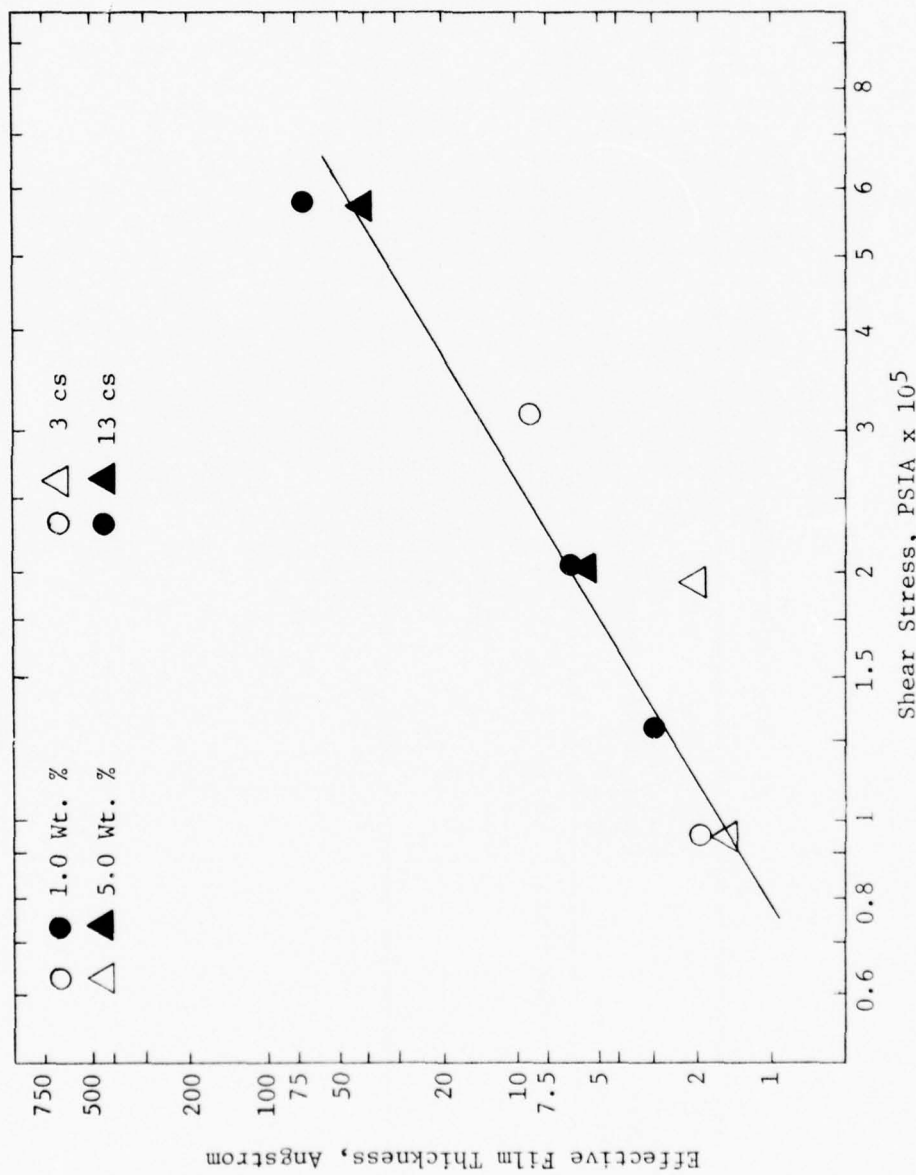


Figure 23. EFFECT OF SHEAR STRESS ON THE EFFECTIVE FILM THICKNESS FOR A HYDROGENATED RESIN (LH 136, 137)

Table 13  
FLUID FLOW STUDY USING A POLAR BASE STOCK

Concentration of Oleic Acid, Wt. Percent	Base Fluid	Atmospheric Viscosity Centistokes at 100° F	Filter Pore Diameter, Micron	Time of Calibration Run, Seconds	Viscosity Corrected Efflux Time Ratio, Z	Apparent Film Thickness, A, Angstrom	Calibration Fluid
0.5	MLO 7710	12.68	0.45	860.6	1.0066	4	MLO 7710
			0.45	879.9	1.0267	15	MLO 7775
			1.2	299.1	1.0533	77	MLO 7755

Table 14

FLUID FLOW STUDY USING A BARIUM SULFONATED HYDROCARBON  
(PRL 3530) AND A HEAVY RESIN (ML0 7779)

Base Fluid	Atmospheric Viscosity, Centistokes at 100°F	Filter Pore Diameter, Micron	Time of Calibration Run Seconds	Viscosity Corrected Efflux Time Ratio, Z	Apparent Film Thickness, Å, Angstrom	Shear Stress, $\tau$ , PSIA $\times 10^5$	Shear Rate, $\frac{dv}{dr}$ , sec $^{-1}$
ML0 7789	17.02	0.2	613.1	1.1275	30	1.01	47.7
	0.45	617.8	1.0762	41	2.04	96.6	
	1.2	116.9	1.0700	101	5.44	257.6	

Five Weight Percent of Each Additive

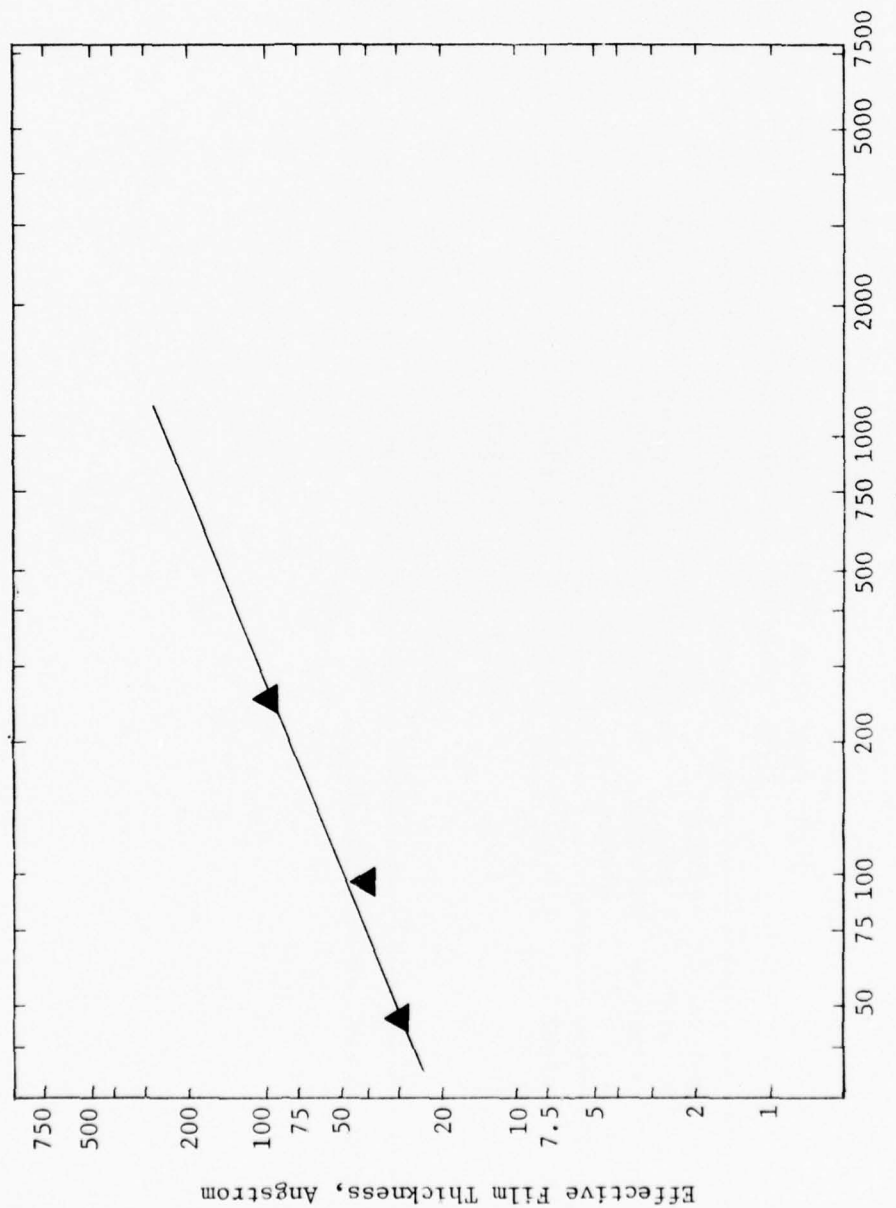


Figure 24. EFFECTIVE FILM THICKNESS OF A BARIUM SULFONATED HYDROCARBON (PRL 3530) AND A HEAVY RESIN (MLO 7779)

Table 15  
FLUID FLOW STUDY USING VARIOUS ADDITIVES IN KG-80

Designation	Additive	Weight Percent	Atmospheric Viscosity, Centistokes at 100°F	Apparent Film Thickness, A, Angstrom	Shear Stress, $\tau$ , PSIA $\times 10^5$	Shear Rate, $\frac{dv}{dr}$ , sec $^{-1}$
KG-80	---	---	164.7	39	1.18	6.68
KG-80(a)	AO-702 Kendall Antioxidant Isopropyl Oleate	0.5	142.6	1.0724		
KG-80(b)	AO-702 Kendall Antioxidant	0.5	168.8	1.0246	14	1.18
KG-80(c)	AO-702 Kendall Antioxidant Oleic Acid	0.5	167.5	1.0114	6	1.18
KG-80(d)	AO-702 Kendall Antioxidant	0.5	168.9	1.0090	5	1.18

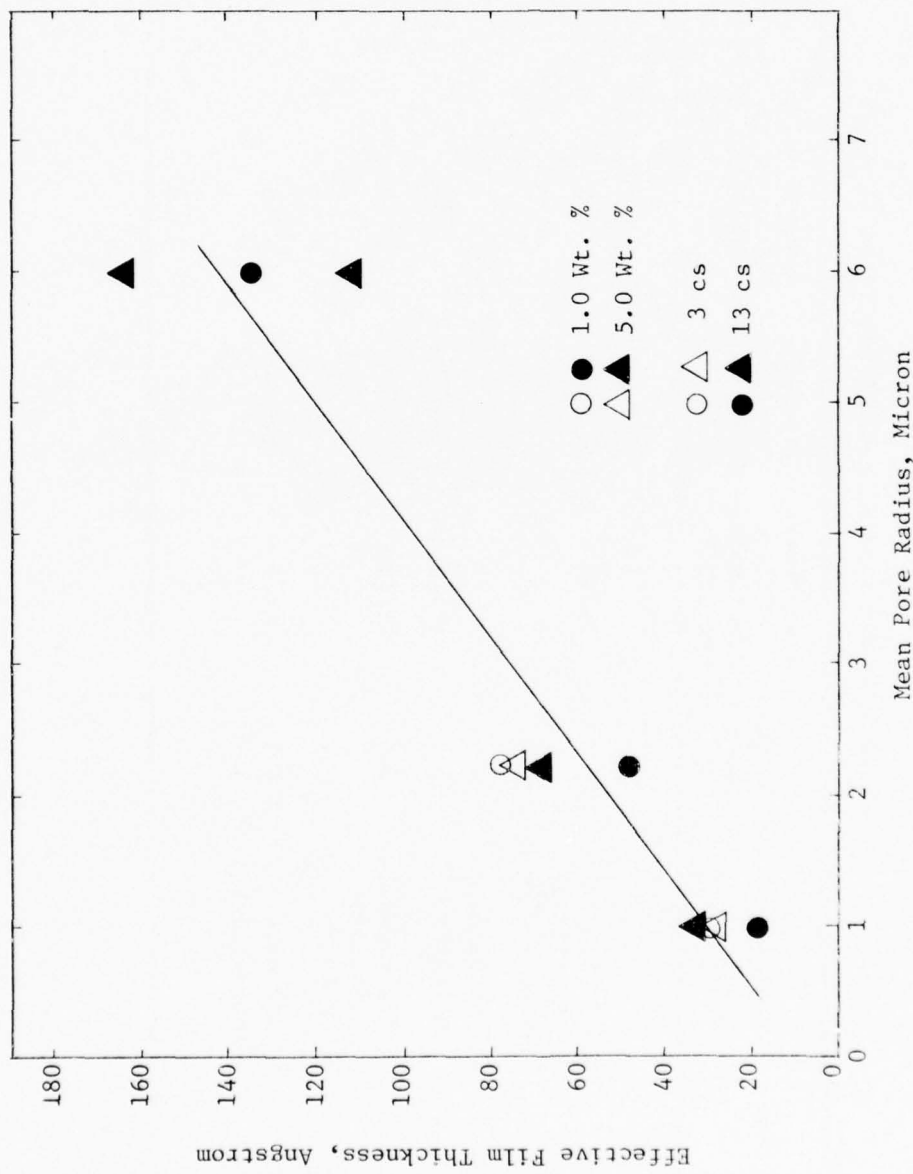


Figure 25. EFFECTIVE FILM THICKNESS AS A FUNCTION OF MEAN PORE RADIUS  
FOR A HEAVY RESIN (MLO 7779)

Table 16  
FLUID FLOW STUDY WITH METAL FILTERS

Concentration of Additive Wt. Percent	Base Fluid	Atmospheric Viscosity, Centistokes at 100°F	Time of Calibration Run, Seconds	Viscosity Corrected Run Time Ratio, Z'	Apparent Film Thickness, A, Angstrom	Shear Stress, $\tau$ , PSIA $\times 10^5$	Shear Rate, $\frac{dv}{dr}$ , sec $^{-1}$
2.5	Oleic	ML0 7625	72.1	660	1.0137	85	1.24
2.5	Oleic	ML0 7625	72.1	1829	1.0255	157	1.24
5.0	ML0 7779	ML0 7789	17.09	1263	1.0217	232	1.24
5.0	ML0 7779	ML0 7789	17.09	149	1.0428	261	96.1
5.0	ML0 7779	ML0 7789	17.02	714	.999	---	---
5.0	PRL 3530	ML0 7789	13.12	999	1.0124	77	1.24
5.0	PRL 3530	ML0 7789	13.12	638	1.0167	103	1.24

#### 4. THE EFFECTS OF CHEMICAL REACTIONS IN BOUNDARY LUBRICATION

Studies presented in Annual Report AFML-TR-74-201, Part II, discuss the techniques developed to study the mechanism of boundary lubrication. Wear debris is generated using a Shell four-ball wear tester designed to operate over a range of temperatures, speeds, and with a controlled atmosphere. Necessary techniques to separate the debris and to determine the nature of the chemical reaction occurring in the concentrated contacts are outlined in that report. Tests in the four-ball wear tester geometry with no load, at very low speeds, and at normal operating speeds have been used to vary the temperature effects at the wear surfaces. Standard and sequential type four-ball wear tests were used to provide data used to estimate reaction rates and temperatures. Techniques to estimate the junction temperature rise using a chemical conversion correlation between static and dynamic runs are discussed in the previous report. The junction temperature rise determined in this manner is shown to be substantially higher than the generally used Blok-Archard flash temperatures.

Work using the techniques developed in these previous studies has been continued. The present studies are concerned with the effects of additive materials in formulated fluids on the chemical reactions taking place at the bearing surfaces.

a. The Effects of Operating Parameters on Chemical Reactions. In boundary lubrication, the chemical system is defined by the chemical nature of the fluid and metal compositions. The reaction environment is decided by load, speed, atmosphere, bulk fluid temperature and the geometrical configuration of the rubbing surfaces. These parameters determine the reaction temperature and pressure. Mass and heat transfer are controlled by gas flow rate and the geometrical setup of the testing machine. In the following sections, some of these parameters are examined to ascertain their effects on the chemical reaction system.

(1) Effects of Load. The machine load defines the normal force at the contact junction. This normal force remains constant throughout the run and changes only if the machine load is altered. From geometric considerations, the normal force at each ball equals about 40.8 percent of the machine load. The mean specific pressure at the contact area is determined in addition to the normal force, by the contact area itself. The average contact pressure changes in a run as the wear area (the load supporting area) is constantly increasing from wear. The change in the mean specific pressure during a run could be as much as 25 times. From theoretical considerations, the normal force is elliptically distributed. Hence even though the mean pressure may vary greatly, the maximum pressure during a run could vary a lot less. This maximum pressure therefore is mainly a function of the machine load. Previous studies (AFML-TR-74-201, Part II) indicate that during a typical run, the average temperatures at the contact junction remain fairly constant. When one changes the load, the magnitude of the normal force is changed, and the mean specific pressure goes through a similar change. All of these point out that

during a run, the mean specific pressure change has little meaning and the key parameter is really the magnitude of the normal force which is determined by load alone.

In Table 17, the wear product analysis data as a function of machine loading are presented. The load was varied from 20 kg. (8165 gm normal force) to 120 kg. (48,960 gm normal force). As noted in Table 17, Run 68 has an abnormal friction curve indicating possible seizure and recovery. Run 70 has a rolling element in it. Therefore the data from these two runs were omitted in the figures where applicable. In Figure 26, the wear scar diameters are plotted against load on a log-log scale. The data suggest a transition region between 75 and 90 kg. load. After 90 kg. load, wear proceeds at a higher rate. In Figure 27, the oil insoluble iron data are plotted similarly. A straight-line relationship is obtained, indicating that the mean surface temperatures are proportional to the normal force. To examine this point further, theoretical estimation of the average junction temperatures using Bos' equation (13) and the friction measurement data is carried out. At the same time, using the oil insoluble organometallic iron conversion data, junction temperatures are estimated from Figure 28. These temperatures are plotted on the same graph as shown in Figure 29. The chemical conversion estimations are considerably higher than the theoretical average temperatures as before. The theoretical maximum temperatures when adjusted with Bos' experimental results come pretty close to the chemical conversion estimations. Lastly, the iron particles and iron oxides are plotted as a function of load in Figure 30. The iron particles increase linearly with load while the iron oxides decrease with load. This is reasonable as load increases, the normal force increases in magnitude forcing more asperity-asperity contact and generating higher temperatures in the process. As temperatures are raised, the chemical reactions which include the oil oxidation, degradation, surface metal-hydrocarbon reactions accelerate with speed. Since the initial oxidation products from the hydrocarbon oil are more active chemically, most of the oxygen available is preferentially used up by the oil which in turn generates polar products. The oxygen-bearing polar species from these reactions then adsorb onto the surface and subsequently react with the metal forming an active lubricating film. In this way, the surface metal has less oxygen to react with to form oxides or the iron particles generated during asperity-asperity contact find very little oxygen to react with in the high temperature zone.

Theoretically, the load has a much stronger influence on the junction temperature. In Figure 29, the theoretical equation predicts a much stronger dependence of temperature on load (slope =  $1.94^{\circ}\text{F/kg.}$ ); yet the chemical conversion data show much less dependence (slope =  $0.57^{\circ}\text{F/kg.}$ ), with the same functional form in both cases. One possible explanation to this is that the load is actually supported on a tiny fraction of the apparent wear area in the real case. The elliptical distribution of the normal force only aggravates the situation. The load supporting area therefore will be concentrated at the highest load and the temperatures in that small hot zone probably dominate the chemical reactions and the lubrication. Therefore from the high load to low load, the theory predicts a larger temperature spread while in reality, the difference in load for the region may not be as great as predicted.

(2) Effects of Speed. To assess the effects of speed on wear, a series of experiments were performed, in which the speed varied from 400 r.p.m. to 2,000 r.p.m. The results are presented in Table 18. As noted in the table, Runs 62 and 63 may have some problems and their reliability may not be as good as for the others. At 2,000 r.p.m. the lubricant failed and the run was terminated after only six minutes of running.

The mean wear scar diameters are plotted against the rotational speed in Figure 31. It can be seen that initially the wear increases with speed but beginning with the 800 r.p.m. datum, it takes an abrupt turn downward decreasing with increasing speed. At 2000 r.p.m., catastrophic wear occurs. The amount of iron generated is plotted in Figure 32 to demonstrate further that there is a maximum in wear as speed increases. Note that the gross amount of iron as iron oxides goes through a sharp maximum at 30 cm/sec. (800 r.p.m.) as does the total amount of metallic iron produced. The behavior of the oil insoluble iron-organics plotted in Figure 33 is equally puzzling. The high oil insoluble iron at 15 cm/sec. speed (400 r.p.m.) and its subsequent zigzag behavior can only be caused by either unusually large errors in the data or a real situation that has a very logical explanation. In the following sections, these two possibilities are explored.

Theoretically, as speed is increased, higher friction resulting from higher frequency of contact should generate more heat and higher surface/flash temperatures. High surface temperatures accelerate the chemical reaction rate and also the adsorption/desorption processes. Cameron (14,15) proposes a desorption failure mechanism in which, the lubricant fails due to high surface temperatures which hastens the desorption process. This may explain the increasing wear with increasing speed but fails to account for the decreasing wear with speed. It has been known for a long time that as speed is increased, the pumping rate of the lubricant through the contact junction is also raised. In a curvilinear contact in which the pressure is elliptically distributed, a liquid wedge may be generated according to the principles of fluid mechanics and enough internal pressure could be generated within the liquid film wedge that the hydrodynamic component in the lubrication mode is significantly raised to such an extent that the number and frequency of asperity-asperity contacts between the two surfaces are markedly reduced. This would result in lower wear, lower surface temperatures and fewer chemical reactions. The iron particles produced in this region due to low junction temperatures will be less likely to be oxidized. However, this process only works to a certain extent. As the speed is increased further, the oil film thickness increases. This means that the low thermal conductivity layer between the surfaces grows in thickness. The temperature gradient across the film also grows. Viscous dissipation of heat also increases. A higher mean surface temperature could result from these factors. As temperatures are steadily increased, the viscosity of the oil decreases and the hydrodynamic lubrication contribution lessens. Finally failure/seizure occurs when the temperature at the contact is too high for the base fluid to function. This could be what has been observed at 2,000 r.p.m. in this series. From these considerations, the production of iron particles per unit area is examined in Figure 34. It can be seen that the iron present as iron oxides increases initially with speed. At 30 cm/sec. (800 r.p.m.) the curve takes a turn about

and decreases with speed. The formation of iron particles initially decreases with speed and at the same transition point, begins to rise with speed and finally reaches catastrophic magnitudes. In Figure 35, the surface temperatures are calculated from experimental friction values and compared with the temperatures obtained from chemical conversion data. It can be seen that both curves have the same characteristics and shape. A lower temperature is shown at 38 cm/sec. which rises again at 57 cm/sec. These data lend credence to the above explanation.

The four-ball machine, from its design, suffers from the sensitivity to axis alignment. At different speeds, different dynamic balance and alignment may produce different vibrational characteristics. These vibrations may affect the wear behavior, and the drop in temperature may be the result of this. In view of the evidence considered, this author believes this observed phenomenon is not due to the vibrations. However, more experimental data are needed before this question can be resolved.

b. Effects of Functional Groups on the Formation of Organometallics as Related to Wear. From the study of the "pure" base fluid as presented in the previous studies (AFML-TR-74-201, Part II), one may conclude that the chemical reactions during lubrication are governed mainly by the polar species as a result of oxidation. Therefore, one logical extension of the study is to add a predetermined amount of active chemical having a particular functional end group to the base fluid and observe the response. Most of this functional additive study was made in the Shell Four-Ball Wear Tester which has a fixed speed of  $600 \pm 30$  r.p.m. To provide a meaningful comparison, the base fluid, PRL 7789A was first run on the same machine twice. The results are presented in Table 19. In the following sections, the effects of an alcohol, a halide and an acid with a C<sub>18</sub> alkyl backbone are examined.

Alcohol is one of the oxidation products. Long chain paraffinic alcohols are quite polar and surface active. Early adsorption studies indicated it could be used as a lubricant. At the same time, the polar hydroxyl group is chemically active and lower molecular weight alcohols have been used quite effectively to dissolve organic "sludge" in lubrication. For these reasons, octadecyl alcohol was used as an additive to the base fluid.

Table 20 summarizes the concentration effects of the C<sub>18</sub> alcohol. Figure 36 illustrates the effects the alcohol has on the formation of organometallic compounds. At a 0.01 percent by weight alcohol concentration, essentially no change was observed from the base state. From 0.1 to 1.0 percent alcohol, the amount of organic-iron compounds rises steadily approaching the base state, indicating that the solvency aspect of the alcohol may be acting as a detergent/inhibitor initially. As the concentration of alcohol is increased, the alcohol itself enters into the reaction scheme and "iron soap" may be formed in reducing the contacts at high temperature. At a concentration of five percent, the lubricant aspect of the alcohol manifests itself by increasing drastically the amount of organometallic iron compounds formed and at the same time, reducing gross wear area some 65 percent. Figure 37 illustrates this point graphically. As the fraction of organic

iron in wear debris increases, the average wear scar diameter decreases. At a five percent alcohol concentration, the sudden reduction in wear is accompanied by a sudden surge in organic-iron formation. As a boundary lubricant additive, octadecyl alcohol is not a good one. It illustrates, however, the importance of the polar functional group of a long-chain molecule. As one of the oxidation products, this indicates that unless extensive oxidation occurs, the net effect on the lubricant may be small. At high concentrations, the effects are quite dramatic. The oil-soluble organometallic iron's formation, can be deduced to result primarily from the oxidation products reacting with the iron. At the vicinity of the surface, the concentration of polar species must be significant to promote such reactions.

The effects of the base fluid purity on its responses to additive treatment is next examined for the alcohol case. The data at two alcohol concentration levels, 0.1 and 1.0 percent is compared in Table 21. In both cases, MLO 7789A, the purer fluid, shows better additive response and smaller wear scar diameters. The effect on organometallic formation is too small to see. This can be explained by the competition between the polar species in the oil (heteroatoms such as nitrogen, oxygen, sulfur, etc. in the oil are polar in nature) and the alcohol molecules. The alcohol molecules have less competition for surface adsorption when the polar impurities in the oil are removed by activated alumina percolation. Hence better response to additive treatment results. This is indicated by lower wear scar diameter and higher oil-soluble organic-iron levels. Alcohol when effective produces a lot of oil-soluble organic iron. In the untreated oil case, high wear scar diameters coupled with lower oil soluble organometallic compounds suggest the polar species in the oil itself is interfering with the alcohol additive.

Halides are often used as extreme pressure lubricant additives. These halide molecules, when incorporated into long chain hydrocarbon molecules, provide extremely reactive functional groups. Under extreme pressure lubrication conditions (high temperature and pressure), they react with the metal surface almost instantaneously, preventing scuffing/scoring/seizure. Under boundary lubrication conditions, they generally will not reduce wear but will increase the seizure load considerably.

In this study, the effects of octadecyl bromide on the formation of organometallic compounds was monitored. In the octadecyl alcohol case, the high concentration of the alcohol has been shown to increase the formation of oil soluble organic-iron compounds. Therefore, octadecyl bromide is used here to see whether increased reactivity of the end group will increase the formation of organometallic compounds. As shown in Table 22, the effects of octadecyl bromide concentration on wear and its products is examined. The bromide additive did not reduce gross wear. This was expected. In fact, wear increases with higher bromide concentration. The amount of oil soluble organic-iron remains fairly constant within the experimental error limit. This phenomenon differs from the alcohol which shows a large increase in oil-soluble iron. With bromide present, the oil insoluble iron is significantly higher than in the base fluid and increases with increasing bromide concentration.

This may suggest that the oil insoluble iron has a different formation mechanism. While both the alcohol and the bromide react with the iron surface, the reaction products of the alcohol-iron are probably metal soaps or complexes which are soluble in oil. The bromide, on the other hand, reacts with iron forming oil insoluble products. This would indicate that the reactivity of the functional group strongly affects the type and the nature of the reaction products.

Fatty acids are some of the earliest lubricants. They reduce friction and wear significantly. When used as an additive in oils, stearic acid has been extensively studied in terms of adsorption and orientation of molecules on metal surfaces. It has been found generally that carboxylic acids adsorb physically by forming carboxylate ions  $RC\begin{smallmatrix}O\\|\\O\end{smallmatrix}$ , and subsequently bond to the surface covalently  $RC\begin{smallmatrix}O\\|\\O-M\\|\\O-M\end{smallmatrix}$ .

The effects of stearic acid concentration on wear and its products are shown in Table 23. Wear decreases drastically with the addition of stearic acid. After 0.1 percent (wt.), further increasing of additive concentration does not further reduce wear. There is little oil soluble iron in the wear debris. The oil insoluble iron is below the base fluid level. Figure 38 also illustrates the effect of stearic acid concentration on wear. At 0.1 percent by weight acid level, 15 percent reduction of wear is obtained. High amounts of oil-soluble iron compounds are observed. At 0.1 percent and one percent acid, wear reduction reaches 39 percent and little oil-soluble iron is formed. The oil insoluble iron seems to increase linearly with the acid concentration. These observed data may be explained by the following hypothesis. At a very low acid level (0.01 percent), the boundary lubricant film is formed by a mixture of the stearic acid and hydrocarbon base fluid and there are apparent interactions between the acid and the paraffins. Under high temperature and pressure conditions, substantial oil-soluble iron compounds result from the reaction between the iron surfaces and the hydrocarbons. Some oil-insoluble iron complexes are formed which adhere strongly to the surface and provide the wear reduction. At higher acid concentrations, the stearic acid overwhelms the paraffinic base stock (or its polar impurities) and adsorbs preferentially on the surface. The subsequent covalent bonding between the acid and the iron provides a strong coherent (oriented) film thus effectively reducing friction and wear. Further addition of acid becomes excess material and does not affect the wear process. This hypothesis points to the importance of the physical properties of the reaction products between iron and the hydrocarbon. The fact that the stearic acid tends to orient itself in adsorption and provides a strong, coherent film probably explains its effectiveness as a boundary lubricant. In contrast to stearic acid, octadecyl bromide is chemically active; apparently the reaction products between iron and the bromide do not have the strength or orientation or chain length to act effectively as a lubricant. The reaction products are removed from the junction by shear stresses/cavitation/desorption fairly quickly. This results in corrosive attack on the iron.

Aromatic structures in lubricating oils have been viewed in the same class with the polar impurities in wear reduction and for increasing the load

carrying capacity of the oil. Unsaturated hydrocarbons like olefins and aromatics usually are chemically more active than saturated hydrocarbons such as paraffins and naphthenes. Correspondingly, the unsaturated hydrocarbons are more effective boundary lubricants. There are reports in the literature showing both synergism and antagonism when aromatics are mixed with paraffinics. Groszek (16) demonstrated that the mixture of oil is a poorer lubricant than either its aromatic or paraffinic fraction. In his work, he showed that the portions eluted with pentane (paraffins and naphthenes) or isopropanol (aromatics and polar impurities) from silica gel are a superior lubricant compared to the original oil. Appledoorn and Tao (17), on the other hand, using pure chemicals, demonstrated synergistic behavior, i.e., the mixture was the superior lubricant compared to either of its components, aromatics or paraffins. Beerbower (18) and Whitby (19) discussed the two results and concluded that the presence of polar aromatic sulfur compounds is responsible for the prowear effects in the natural-occurring oils. Pure aromatics are antiwear in nature. When both species are present, the sulfur compounds preferentially adsorb onto the surface hence blanketing the aromatics' effects.

In Table 24 and Figure 39, the wear data for dodecylbenzene, dodecyltoluene and triamylbenzene are presented. Comparing with the base fluid MLO 7789A, it can be seen that the pure aromatics have unquestionably better antiwear characteristics. Among the three, the monosubstituted aromatic has the best antiwear performance. Dodecyltoluene, because of its reactive tertiary hydrogens on the methyl group, is the most reactive species of the three, and has the highest wear among the three aromatics. Triamylbenzene has shorter alkyl groups and wear falls between the two aromatics. The amounts of organometallic compounds formed indicate the same trend. Dodecyltoluene produces the highest amount of organic-iron products in both the oil-soluble and insoluble phases. More than half of the wear debris collected is organic in nature (66 percent). Even dodecylbenzene, with the lowest wear, has far more organic-iron compounds than the super-refined paraffinic base oil, MLO 7789A.

The next step is to mix the paraffinic base oil with one of the aromatics. Dodecylbenzene was chosen for this purpose because of its good antiwear performance. The results are shown in Table 25. Wear decreases as the proportion of aromatics in the base oil increases. At about a 50:50 mixture, the wear rate is approaching that of the pure dodecylbenzene. However, no synergism nor antagonism is evident in terms of wear. Aromatics seem definitely a better antiwear agent than do paraffins.

The mixtures generally have a much higher amount of oil insoluble iron compared with either pure component. The proportions of organic-iron compounds in the wear debris are higher than in its components. Thus in terms of surface chemical activity, the aromatic species in the presence of paraffinic oils has a higher reactivity than pure aromatics or paraffins. This may suggest synergism under extreme-pressure lubrication conditions.

Aromatics by themselves are more thermally stable than paraffins. It takes about 900° to 1200°F to break up the ring structure. Reactivity of the aromatics, however, is high from the secondary and tertiary hydrogens undergoing substitution reactions. This would suggest that the alkylated aromatics

once reacted with the iron surface will tend to be thermally stable but highly active. This results in the high oil-insoluble iron in the case of the aromatics. When paraffins are present together with the aromatics, under the extreme temperature conditions, the paraffins break down and the resulting active species react with the aromatics which have adsorbed/reacted with the iron. The reaction products probably are more surface active and reactive than the pure components alone thus producing more oil insoluble organic-iron.

One interesting point between the results from aromatics and the aromatics-paraffins mixture is the amount of oil soluble organic iron generated. The pure aromatic has very high oil soluble iron levels, 26, 62, and 88  $\mu\text{g}$ . The mixture has hardly any oil soluble iron. If the pure aromatics are functioning as an antiwear additive, there should be a corresponding amount of oil soluble iron present in the mixture. This further indicates that there are interactions between the aromatics and the paraffins at the contact zone at high temperature, and that it is the reacted compound that is providing the antiwear activity rather than the pure aromatics.

The effects of the various functional groups on wear and on the chemical reactions have been examined individually. Figure 40 compares the three chemical species with regard to wear. Octadecyl bromide at levels of one percent and above has prowear characteristics indicative of its chemically corrosive nature. Alcohol is only effective at five percent (wt.) in reducing wear as its low reactivity/polarity would indicate. Stearic acid functions well at a low concentration of 0.1 percent (wt.) showing the effectiveness of the carboxylic acid end group in terms of reactivity and strong covalent bonding. Figure 41 examines the three chemicals in terms of oil soluble iron compound formation at various concentrations. They all seem to be concentration dependent. There is apparently an additive concentration that will produce a minimum amount of oil-soluble organic-iron compounds. For alcohol and stearic acid, this concentration is 0.1 percent. For bromide the concentration is one percent. Looking at Figure 40, wear versus concentration, these concentrations seem to correspond with the change in wear behavior of the various additives. For the alcohol and the stearic acid, it is the beginning of wear reduction by the additives. For the bromide, the concentration (1%) is the beginning of the prowear behavior. This suggests that at these concentrations, the effects of the additives on the wear processes are first observed. It may be further speculated that as a result of preferential adsorption of the additives on the solid surfaces and subsequent additive-metal surfaces, additive-base fluid interactions are such that the metal surfaces are well covered and protected. Minimum amounts of oil-soluble iron are formed. At higher additive concentrations, the polar impurities in the additives may exert a major influence and the base fluid-additives interactions may be replaced by additive-additive interactions at the metal surface. The nature of the additive-metal reactions then determines the amount of oil soluble-iron compounds to be formed.

The effects of the functional groups on the formation of the oil-insoluble organometallic iron are examined in Figure 42. As with the case with oil-soluble iron, there seems to be a minimum in the curves except for stearic acid which has a linear straight line. Octadecyl bromide being the most

active chemical species, has the highest organic-iron concentration at all levels. Stearic acid comes in second and the alcohol is closely third. This suggests that reactivity of the functional group plays a very important role in determining the amount of the oil-insoluble organic-iron to be formed during lubrication.

c. The Study of Phosphorus-Containing Additives. Thus far, this study has examined the base fluid, plus some polar compounds in terms of chemical reactions in boundary lubrication. While the study furnishes some basic information on the role of chemical reactions in lubrication, no commercial antiwear additive agent has been studied. Phosphorus-containing compounds, primarily alkyl and aryl phosphates and phosphites are the most important commercial antiwear agents today. In the following sections, some of these additives will be investigated using the four-ball wear tester and subsequent debris analysis.

The chief effect of phosphorus-type additives is a reduction in wear without much effect on the coefficient of friction. Beeck et al. (20,21) in 1940 first suggested that some phosphorus additives reacted with the metal surface to form metal phosphides. The phosphides were produced at the high points of contact under boundary conditions and subsequently low melting eutectics with the metal were formed. This eutectic then was wiped into the valleys by the rubbing action. This provided a much smoother surface. The suggestion was that phosphorus additives acted as a chemical polishing agent. This low melting eutectic was said to exist at a phosphorus concentration of about ten percent and had a melting point of 1020°C which was 515°C below the melting point of iron.

Davey (22) evaluated a series of alkyl and aryl phosphate and phosphite esters in mineral oils. All of the phosphate additives tested were found to have the same type of effect on wear reduction. Phosphites were found to be better than phosphates, and alkyl esters were found to be better than aryl esters for improved lubrication.

The chemical polishing theory advanced by Beeck et al. was later revised by subsequent studies. Low wear was not accompanied by gross smoothing of the bearing surface. Bieber and Klaus (23) using a combination of thin-layer chromatography and neutron activation analysis were able to determine that the chemical reaction product with the iron at the bearing surface is iron phosphate rather than an iron phosphide eutectic. These studies suggest that the iron phosphate results from a reaction between the iron and an acid phosphate.

Thermal stability of metal phosphorus compounds has been proposed by several researchers as an important parameter for determining the relative antiwear activities of these additives (24,25,26). However, no concensus can be reached as to whether high thermal stability or low stability is more beneficial due to non-uniform testing chemicals and equipment.

Zinc dialkyldithiophosphate (ZDP) is one of the most widely used antiwear agents. It is an excellent lubricity additive which also exhibits oxidation and corrosion inhibition. Although this compound has been studied extensively, the detailed mechanism by which it functions has not been completely understood.

Several investigators agree that the lubrication mechanism of ZDP involves chemical reaction(s) between the additive and the bearing metal (27,28,29). Both phosphorus and zinc have been identified in the reacted surface film. Other authors advance the theory that thermal decomposition of the ZDP molecule occurs prior to chemical reaction (29,30,31). The results of a study evaluating the antiscuff performance of ZDP in an engine show that the atomic ratio of Zn:S:P changed upon decomposition of the zinc additive (24). This seems to support the theory that the P to Zn linkage is broken when ZDP decomposes. Barton, Klaus et al. (32) used paper chromatography in conjunction with neutron activation analysis to analyze the polar lubricity additives in ZDP. Small but significant quantities of both phosphorus and zinc-containing polar impurities were found. Using various acid phosphates and phosphites in wear tests, it was hypothesized that the acid phosphates as impurities in ZDP were the effective antiwear agents. The following lubrication mechanism for ZDP was proposed:

- 1) Preferential adsorption of polar zinc- and phosphorus-containing impurities on the surface of the metal,
- 2) Asperity contact producing high local temperatures, and
- 3) Chemical reaction of the polar phosphorus-containing impurities, which are believed to be a partial acid ester and/or a thiacid ester of phosphorus, with the bearing metal to produce a metal phosphate surface film.

In this study, it has been shown that high local temperatures are indeed produced at the wear junction. The preferential adsorption characteristics of ZDP and its impurities are well documented (28,29,32).

In short, steps (1) and (2) of the proposed mechanism are verified. Step (3) is still to be studied. Due to the complexity of the chemical reactions and the numerous chemical species present in the system, absolute definition of the reaction products and mechanism probably will not be resolved in the near future. Some physical evidence of chemical reactions and their effect on wear probably are helpful at this stage.

Table 26 and Figure 43 present the data obtained in this study. ZDP is effective in reducing wear at 0.01 percent (wt.). Starting at 0.1 percent, the effective wear rate is controlled completely by ZDP. With a sharp drop in gross wear, the amount of iron oxide in the debris is reduced by 4-5 times. This suggests that the ZDP or its polar counterparts dominate the metal surface adsorption/reaction processes. Once the surface is saturated with Zn, P compounds, any further increase in the additive concentration will not affect the rate of wear. This is shown to be the case. The wear rates of 1.0 percent and 5 percent ZDP are essentially unchanged.

The amount of oil-soluble and insoluble organometallic compounds in this case exhibit similar concentration dependence to those of previous additives (functional group additives) i.e., a minimum and a gradual rise as concentration increases. This can probably be explained, at least in part, by impurity levels. At the minimum, the surface is saturated with polar molecules of the additives/impurities. As more additive is put into the system, more polar impurities are available and some of the polar impurities present in very small quantities are at a concentration level where they begin to influence the adsorbed layer(s) composition(s). Chemical interactions at the surface can also be affected. Depending on the chemical species present at the surface, e.g., acidic varieties, more organometallic compounds may be formed.

These data demonstrate that chemical reactions are present and the reaction products exhibit a concentration dependence on the additive level. This suggests that there are multiple impurities interaction/competition for adsorption sites. Base stock-additive interactions may also be indicated. The effectiveness of the lubricating film is illustrated by the dramatic reduction of iron oxides at effective additive concentrations.

In the previous studies (32), dilauryl acid phosphate (DAP) has been used for comparison studies with ZDP. Lubricity tests (4-ball and EP) indicated similar behavior for DAP and ZDP. Paper chromatograms of DAP also showed similarities with the polar impurities in ZDP. Therefore it was postulated that the polar impurities in ZDP are some kind of acid phosphates. Paper chromatography coupled with neutron activation analysis indicated that there were at least one percent (mole) impurities based on phosphorus present in ZDP. With the analytical methods developed in this study, a better comparison of DAP and ZDP can be made in terms of organometallic compounds, wear product distributions, etc.

The results of the wear study with DAP are presented in Table 27 and Figure 44. At 0.01 percent (wt.) of DAP, no wear reduction was observed. From 0.1 to five percent, constant wear level at 50 percent of that of the base fluid was achieved. After 0.1 percent, further addition of DAP did not change the wear level. As the wear is reduced, the amount of iron oxide formed diminishes rapidly (from 200  $\mu$ g to 11  $\mu$ g, a twenty times decrease). This phenomenon seems to be characteristic of most of the effective lubricity additives. It suggests that oxygen or oxycompounds compete with the lubricity additive for surface active sites. Without the additives, oxygen or oxygen-bearing compounds dominate the surface adsorption/reaction processes, hence high oxide formation. With the lubricity additive present at low concentrations, the resulting mixed species on the surface may exhibit synergism or antagonism. In most of the cases studied in this work, either adverse interaction or synergism has been observed. For example, at 0.01 percent (wt.) DAP, the wear level is higher than that of the base fluid. The organometallic compound levels are substantially higher than those of the base fluid or the fluid with effective DAP concentrations (55  $\mu$ g as compared with 14, 5, 8  $\mu$ gs). The oxide level also increases. This indicates that as a result of the possible mixed adsorption/interaction, a higher reaction rate or more reactions take place. The following hypothesis may be proposed to explain the observed

trends. In order for the boundary film to be effective, the species in the film must have approximately the same bonding strength with the surface. If specie A has a much weaker link with iron than does specie B, under the same shear stress/rubbing/cavitation conditions, A would be preferentially removed, leaving holes and gaps in the film. These discontinuities would tend to break up the rest of the film, and at the same time, expose the metal to oxygen attack.

Comparing ZDP and DAP wear product distribution at the most effective concentrations, i.e., 0.1 percent for DAP and one percent for ZDP, their product distributions are similar. Since the purity of both additives is unknown, direct comparison at equal active species concentration level cannot be made. Qualitatively, it can be said that DAP and ZDP probably have the same active species/same mechanism that would result in similar product distributions at two different concentration levels.

The early hypothesis of the ZDP working mechanism was that metal phosphides were formed (20,21). Later, the impurities in ZDP were the chief antiwear agents which were suspected to be either phosphates or phosphites. A comparison of ZDP with phosphate (DAP) has been made. In this section, the effects of tributyl phosphite (TBP) on wear are examined.

Table 28 and Figure 45 present the data obtained in this work. It can be seen that wear is strongly dependent on concentration. There seems to be a minimum in wear at one percent TBP. Further addition of the phosphite increases the wear rate significantly. This is in contrast to ZDP and DAP. The wear protection offered by TBP is also not as good, 0.6 mm for TBP versus 0.40-0.46 mm for DAP and ZDP in wear scar diameters.

Organometallic formation in this case also exhibits a different behavior pattern. Very little oil-soluble metal compounds are found but the oil-insoluble iron concentration rises almost exponentially with the additive concentration. This suggests that TBP is active chemically. At low concentrations, the TBP offers wear protection. But as the concentration is increased, reactivity also is increased probably due to the base fluid to TBP ratio change at the surface level. Instead of wear protection, a mild form of chemical corrosion sets in, increasing the wear level. Forbes and Battersby (33) studied the chemical mechanism of dialkyl phosphites. They postulated that the phosphites hydrolyzed to phosphonic acids which, being an acidic species, reacted with the iron readily. If this is true, then at increased additive concentration, the acid concentration is also increased. This mechanism also explains the large amount of oil-insoluble organic-iron being formed and their exponential increase with phosphite concentration.

The comparison between ZDP, DAP, and TBP wear products suggests that ZDP works similarly to DAP but phosphites exhibit different mechanisms.

Tricresyl phosphate (TCP) has been used widely as an antiwear additive for mineral oil and synthetic hydraulic fluids and lubricants in the last two decades. Studies on the mechanism of lubrication by TCP are many (21,23). The early hypothesis of an iron-iron phosphide eutectic of low melting point

(chemical polishing theory) has been shown inadequate. Recent studies at this laboratory show that the chemical reaction product with the iron at the bearing surface is some kind of iron phosphate. These studies suggest that the iron phosphate results from reaction(s) between the iron and acid phosphates. Studies using radioactive TCP<sup>32</sup> have shown that significant amounts (5-25 percent) of phosphorus containing polar impurities (probably acid phosphates) preferentially adsorb and subsequently react with the iron surface to form a protective film. Other studies indicate that the bulk tricresyl phosphate provides a starting material for the formation of acid-type polar species from oxidative, thermal, and hydrolytic reactions.

In the following sections, various aspects of TCP action in super-refined paraffinic mineral oil will be examined.

The effect of fluid purity on additive response is illustrated in Table 29 and Figure 46. MLO 7789A is the result of activated alumina percolation of MLO 7789. As shown by octadecyl alcohol previously, the purer fluid is more responsive to additive treatment. The wear levels are lower at all three concentrations. No difference in oil-soluble iron is noted. The oil-insoluble iron shows different behavior. For the untreated oil, there is no minimum in the oil-insoluble iron concentration. The percolated fluid shows a probable minimum at one percent (wt.) TCP. This can be explained by the competition of the polar impurities in the oil and the TCP for preferential adsorption at the surface. Percolation removed the impurities, and TCP without competition functions much better and also shows more sensitivity towards concentration.

TCP as an antiwear agent, is not very effective at high loads. Its effective range lies between 1 kg. to about 30 kg. in the 4-ball tester. At 40 kg. load, it takes five percent TCP to be effective. At 10 kg., only 0.05 percent TCP reduces the wear 50 percent. Comparing the product distribution of TCP and DAP (Dilauryl Acid Phosphate, Table 27), the 0.1 percent DAP results are similar to those obtained at five percent TCP. This supports the acid phosphate mechanism proposed by Bieber et al. (23).

The effects of bulk fluid temperature and atmosphere on wear are next examined with MLO 7789A plus five percent (wt.) TCP. The results are shown in Table 30. Neither the temperature or the atmosphere (O<sub>2</sub> concentration) seem to affect the TCP performance very much. At low temperature in air, wear is relatively high. As the temperature increases, wear level first decreases then increases slightly. At 300°F in air, there is a noticeable increase in the iron oxide formation. This suggests that the TCP is losing effectiveness in terms of surface adsorption demineralization. The helium atmosphere does not affect the organometallic compound formation. This indicates that oxygen is not critical in TCP's mechanism.

When TCP and octadecyl bromide are mixed together and tested, TCP dominates the wear process. This is shown in Table 31. Octadecyl bromide has been shown previously to produce high wear and large amounts of oil-insoluble iron under these operating conditions. The data suggest that TCP dominates the surface adsorption/reaction processes. Wear level is low and

oil-insoluble iron is also low. Helium atmosphere does not change much. This demonstrates the critical importance of relative polarity of different species in the base oil. The most polar species will be preferentially adsorbed and subsequently reacted in spite of large amounts of other less polar material present.

Additive studies are generally made with wear test equipment. Data interpretation, most of the time, is based on gross wear which is easily measured in terms of wear scar diameters. From the standpoint of chemistry and taking the view that the wearing conjunction is really a continuous chemical reactor, gross wear data do not offer any indication of the relative importance or extent of the chemical reactions. This is more critical in additive lubrication research. Additives, by definition, are chemically active/polar species such that a minimum concentration can alter the chemical system significantly. The debris analysis developed in this study when used in connection with wear data, offers an insight into the chemical changes that are taking place in the system. The dramatic reduction in the amount of iron oxide measured when effective additive concentrations are used and the high concentration of organometallic compounds resulting from chemical corrosion pin points the importance of chemical reaction in lubrication.

d. The Lubrication Mechanism of Tributyl Phosphite. Dialkyl and trialkyl phosphites have been used as load carrying additives in lubricants for many years. Davey (34) first studied a large variety of triaryl, trialkyl and tricyclo phosphates and phosphites, some containing Cl and some S groups. He found that generally phosphites were superior to phosphates. Recently, Eberhardt et al. (35,36) published some data on the load carrying characteristics of some tri-substituted phosphites. Forbes and Battersby (33) in studying the adsorption/reaction of some dialkyl phosphites suggested that:

- 1) Under antiwear conditions, an iron-organo-phosphite film was formed via partial hydrolysis of the phosphite; and
- 2) Under antiscuff conditions, further hydrolysis occurred so that mainly an iron-inorgano-phosphite film was formed.

This mechanism is illustrated in Figure 47. In arriving at this mechanism, the authors had to eliminate the oxidative/thermal degradation mechanisms. Hall pointed out in his discussion of the paper that no direct evidence was obtained supporting the fact that iron organo-phosphite film was formed in antiwear region.

The wear debris analysis developed in this study has been shown to be effective in analyzing organometallic compound(s) formation during antiwear region of additives. Therefore, it will be interesting to study the working mechanism of a phosphite using this technique. Tributyl phosphite, based on its high organometallic compound formation rate, was chosen for further scrutiny.

To establish a basis for comparison, one percent tributyl phosphite (TBP) in MLO 7789A (super-refined paraffinic white oil percolated through activated

alumina) was run in the GE/Brown modified wear tester at 600 r.p.m., 167°F and 40 kg. The results are shown in Table 32. Run 94 was made in helium atmosphere. In all runs with helium, the oil was first heated to 167°F and degassed. The ball pot assembly was flushed with high helium flow rate for two minutes before starting. It can be seen that oxygen and moisture seem to affect the wear rate and chemical reactions quite significantly.

The wear scars produced by tributyl phosphite are highly irregular with jagged outlines. A hypothetical rectangle is superimposed on the wear scars and the equivalent diameter calculated from the rectangular dimensions. This may affect the reproducibility of the results to some extent.

The large amount of organometallic iron compound found in the wear debris at the base state (Run BAP) supports the notion that chemical reactions are the dominant factor in TBP lubrication. The questions remaining are: whether these reactions are thermal degradation; oxidation; or hydrolysis. Therefore, the slow-sliding, externally temperature controlled wear tests were carried out as a function of temperature. If the reactions are thermally induced, then the amount of organic-iron should increase with temperature.

The results of this series of tests are shown in Table 33 and Figures 48 and 49. From 167° to 300°F, the total organic-iron increases by a factor of nine. Then from 300° to 400°F, the organic-iron drops as suddenly as it rises. In fact, both the oil-soluble and oil-insoluble iron exhibit similar behavior as illustrated in Figure 49. At temperatures of 400°F and above, a very even, fine, greyish white deposit was observed covering the ball pot and wear scars. It was further found that these powder-like deposits were insoluble in organic solvents but slightly soluble in water. Comparing the color and its physical characteristics, it was speculated that these may be  $P_2O_5$  or phosphorus oxides. Between 300° and 400°F, the reaction mechanism must have changed from organic-phosphorus-iron interaction to the formation of phosphorus oxides which are probably strong enough to provide lubrication either by organic-phosphorus compounds or inorganic compounds, the amounts of iron oxide are drastically reduced.

The gross wear as illustrated in Figure 48 appears not to be affected by the change in temperature and lubricating mechanism of the TBP. The fact that both iron oxides and iron particles begin to decrease after 300° to 400°F suggests that the inorganic phosphorus film is very effective in covering and protecting the bearing metal surface, especially in view of the high bulk temperatures. Bulk oil oxidation of hydrocarbons appears to have no effects on TBP. Considering the effect of octadecyl alcohol on the formation of organometallic compounds and the fact that large amounts of alcohols are produced according to the hydrolytic mechanism (33), the importance of preferential adsorption/reaction in the lubrication system becomes paramount.

Since the temperature at the junction is directly related to the sliding speed and friction level, the change of mechanism observed in the slow-sliding, externally controlled temperature series can be demonstrated by the change of

speed at normal loading. Table 34 presents such data. The wear rate seems to fluctuate about the result of the 800 r.p.m. run as illustrated in Figure 50. Very little oil-soluble organic-iron can be found. This is reasonable. In the slow-sliding runs, the bulk oil is subjected to a high temperature. A large amount of alcohol can form, which in turn can react with iron forming oil-soluble organic-iron. In this series, only a small amount of oil is subjected to high temperature in an oxygen-limited environment and very little alcohol or similar polar species is formed. Thus small amounts of oil-soluble organic-iron are found. The oil-insoluble iron, as illustrated in Figure 51, reaches a maximum at 600 r.p.m. After 600 r.p.m., the level of organic-iron falls to about 1/4 of the 600 r.p.m. level. At 2000 r.p.m., there appears to be an increase in the formation rate of the organic-iron.

The amount of iron particles exhibits a continuous increase with speed. This is different from the observed trend in the temperature dependent series. Iron oxides, on the other hand, do exhibit similar behavior with speed and with bulk temperature, i.e., decreasing amounts with speed after an initial increase.

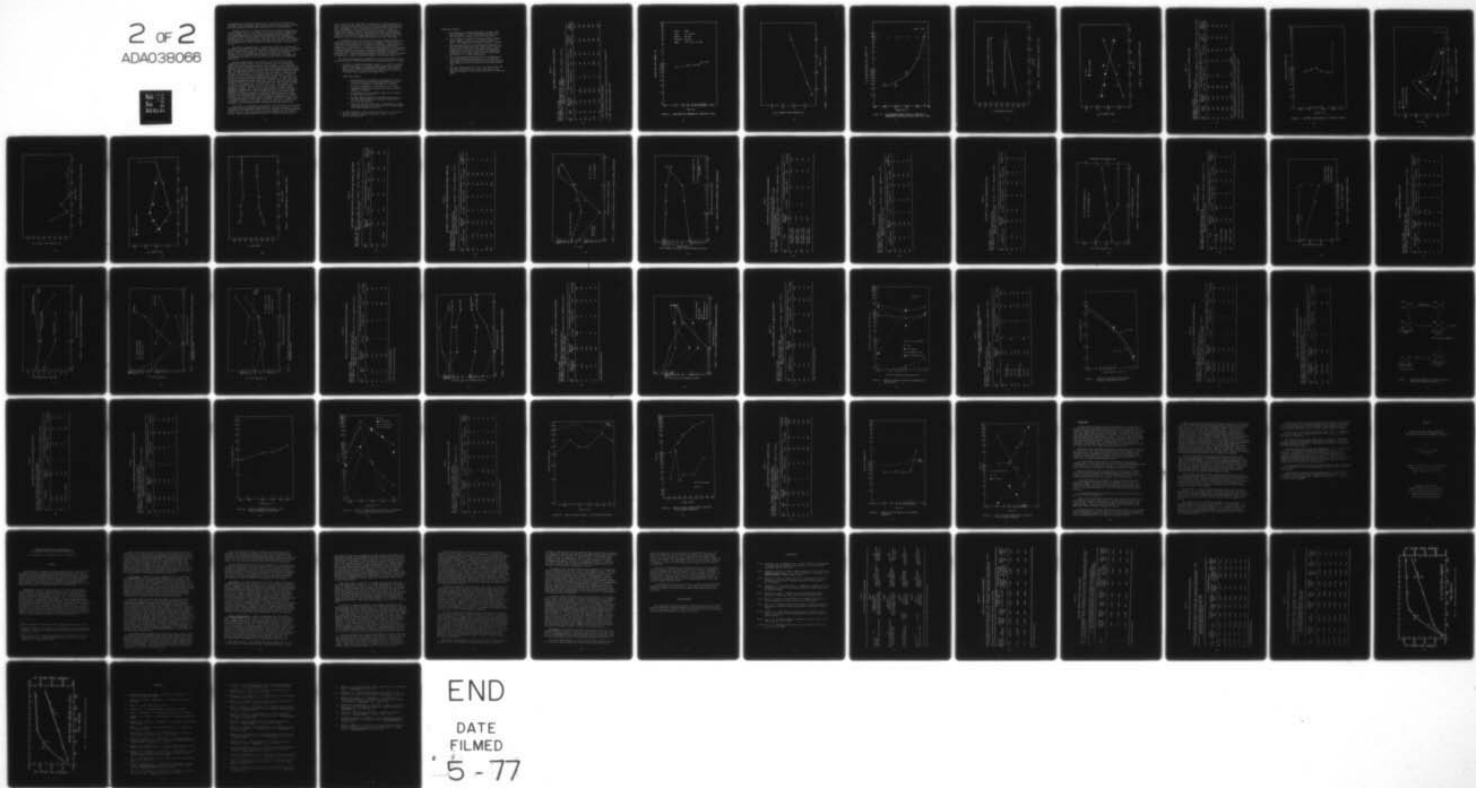
The observed behavior of the product distribution suggests that although similar characteristics can be found between the temperature series and the speed series, there are some differences. The pyridine-soluble iron and iron oxide formation rates suggest that the transition temperature of 300° to 400°F is reached between 600 and 800 r.p.m. For 800 and 1000 r.p.m. runs, probably the inorganic film is protecting the metal surface. At 1500 and 2000 r.p.m., the speed is high, and the resulting high temperatures in an oxygen-limited system probably induce other chemical reactions to become contributing. Similar behavior in the base oil is also observed when black carbides are formed instead of organometallic compounds under similar conditions.

The continuous rise in iron particles may be explained as follows. In the slow-sliding, temperature varying series, the shear stresses are low compared with the 600 r.p.m. or higher speeds. The inorganic phosphorus oxides are strong enough to withstand the low sliding shear at 2.9 r.p.m. As the shear stress is increased hundreds-fold by increasing the speed, the inorganic film breaks down under the tremendous stresses providing asperity-asperity contact. This results in high surface contact rate, high amounts of iron particles, and subsequently higher temperatures. The high temperatures at the same time accelerate the reaction rate to produce more phosphorus oxides which in turn, when they reach the critical film thickness, are sheared away. This kind of sacrificial oxide lubrication mechanism has been proposed for the air-iron-system (dry sliding). In this case, the oxide is not the iron oxide but rather the phosphorus oxide which comes from the additive.

One interesting point to be noted here is that the hydrocarbon reaction seems to be very sensitive to temperature. Figures 49 and 51 both indicate that the formation rate of the oil-insoluble organo-metallic iron is very sensitive to temperature. Assuming the hydrolytic mechanism to be qualitatively correct (Forbes and Battersby presented supporting evidence pointing to the hydrolytic mechanism in reference (33) to provide effective lubrication,

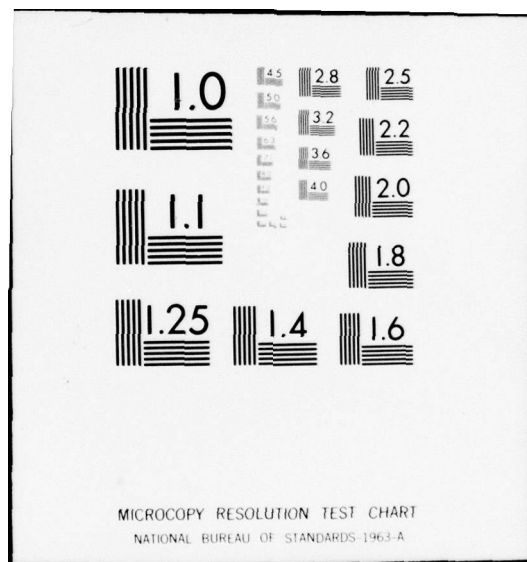
AD-A038 066 PENNSYLVANIA STATE UNIV UNIVERSITY PARK PETROLEUM RE--ETC F/G 11/8  
FLUIDS, LUBRICANTS, FUELS AND RELATED MATERIALS. (U)  
NOV 76 E E KLAUS, E J TEWKSBURY, E CVITKOVIC F33615-73-C-5101  
UNCLASSIFIED AFML-TR-74-201-PT-3 NL

2 OF 2  
AD-A038066



END

DATE  
FILMED  
5-77



the temperature must be high enough so that the reaction can proceed at a sufficient rate to generate enough products to protect the surface. This may partially explain the various wear rates observed at different speeds.

Changing the load at a constant speed varies the shear stresses and the contact pressure which in turn affect the friction and contact temperatures. In the preceding sections, some definite trends have been established. If the trends observed are real, then the same behavior will be observed in changing the load. The precision of these wear tests and their subsequent debris analysis, as explained before, has some built-in difficulties. However, if a trend manifests itself in several different experiments, the trend may be real.

The effect of varying load at a fixed speed of 600 r.p.m. on wear and its product distribution is shown in Table 35 and Figures 52 and 53. The gross wear as illustrated in Figure 52 indicates a transition load between 90 and 120 kg. This is an increase over the base fluid which under similar conditions, has a transition load of between 75 and 90 kg. The higher load carrying characteristics of TBP illustrate its principal use in industrial application.

The oil-soluble organic-iron, again as in the previous case, shows insignificant formation rate. The oil-insoluble iron, as illustrated in Figure 53, shows a decreasing trend as load increases. This is completely opposite the trend observed in the base fluid, but agrees quite well with the observed trend in the speed and slow-sliding series conducted with one percent TBP. As temperature increases with the load, the inorganic phosphorus oxide formation rate increases. At increasing load, the amount of additives and the base oil with its water and oxygen content also decreases. Finally at 120 kg, the wear rate abruptly increases about 10 fold. At that point, the amount of iron particles from rubbing also increases by 16 times indicating the ineffectiveness of antiwear protection of TBP at those conditions. When compared with the base fluid, at the same conditions, the wear scar diameter is about 1.1 mm compared with 1.85 mm in TBP's case. This suggests that the sacrificial antiscuff action of TBP is functioning by forming inorganic phosphorus "oxides." The formation of these "oxides" has shown a strong dependence on temperature. One reasonable speculation would be that under a temperature range of 75° to 350°F, the TBP functions as an antiwear agent primarily by forming organometallic phosphorus-containing reaction product with iron via hydrolysis which is quite sensitive to temperature in terms of reaction rate. From 350°F and above, the competing/complementing reactions of forming phosphorus "oxides" begin to dominate. While this inorganic film is capable of antiwear action under certain mild conditions, its principal advantage is scuff-preventing under extreme pressures and temperatures.

The trend in iron oxide and iron particles is consistent with the previous observation and the hypothesis proposed above. There is a continuous rise in the amount of iron particles formed as the load increases indicating increasing surface contacts. The iron oxide goes through a maximum and rises again at 120 kg. From the data presented in Table 35, it appears that 40 kg load is

in the transition load range where one mechanism is competing against the other. This partially explains the fact that the chemical data obtained at this load appear to have a far greater inconsistency than the rest of the data. The decrease in iron oxide formation can be due to either the insufficient supply of oxygen or the protective action of the phosphorus "oxide" film. From the data at 120 kg, 805  $\mu\text{g}$  of iron oxide was formed. Therefore, there must be enough oxygen around at a less severe case. The protective action of the inorganic phosphorus film is more reasonable.

In studying the lubrication mechanism of tributyl phosphite (TBP), the technique that was used so successfully in the mineral oil study fails to reveal the junction temperature by chemical conversions. This points to one limitation of the method, i.e., the ability of the extracting solvent to dissolve the reaction products. On the other hand, because of this particular solubility situation, one is able to demonstrate dramatically the transition of the TBP lubrication mechanism from organic phosphites to inorganic phosphorus film. There are strong indications that this transition is induced by temperature. Oxygen concentration appears to be playing a role, too.

The lubrication mechanism of phosphites from the data obtained in this study and the work by Forbes and Battersby (33) may be postulated as follows:

- 1) In the low to moderate temperature region, 75° to 350°F, tributyl phosphite functions as an antiwear agent reacting with oxygen and water to give organic iron-phosphorus compounds. The reaction takes place at the lubricating contacts which indicates that TBP is preferentially adsorbed on the metal surface.

**Supporting evidence:**

- a. The formation of the organic-iron compounds in the slow-sliding, externally-controlled temperature wear tests indicates the presence of organometallic compounds.
  - b. The strong dependence of the formation rate of these compounds on temperature suggests that the reactions are thermally controlled.
  - c. The maximum in the oil-insoluble organic-iron formation at about 300°F reinforces b.
  - d. The high formation rate of oil-soluble organic-iron in the slow-sliding experiments indicates the presence of polar reaction products.
  - e. Forbes and Battersby identified a large amount of alcohol formed during their static adsorption/reaction experiments with dibutyl phosphite with iron.
- 2) At high temperatures (above 350°F), TBP functions as an antiscuff agent by forming an inorganic phosphorus "oxides" film for sacrificial lubrication

**Supporting evidence:**

- a. The formation of a greyish white/brown coating on the ball-pot assembly in the slow-sliding wear tests above 300°F indicates a change in lubrication mechanism.
- b. This coating is insoluble in acetone, pyridine, benzene, xylene, naphtha, alcohol but is slightly soluble in water. This suggests the coating is inorganic in nature.
- c. The decreasing trend of the organometallic formation in both the slow-sliding wear tests (after 300°F); the load varying tests (after 21 kg); the speed varying series (after 600 r.p.m.) point to the fact that organometallic compounds are not being formed as the environment gets more severe, i.e., higher temperatures.
- d. The corresponding decreasing trend for iron observed for iron oxide and increasing trend for iron in the above tests support the idea that the surface is being protected from oxygen attack by the phosphorus containing inorganic film.
- e. The load carrying capacity of the oil is increased by the addition of TBP after c and d have taken place. This shows the inorganic film observed is working as an antiscuff agent.

Table 17  
WEAR PRODUCT ANALYSIS AS A FUNCTION OF LOAD

Test Fluid: MLO 7789A  
 Test Machine: GE/Brown Modified Wear Tester  
 Test Conditions: Speed = 600 r.p.m., Temperature = 167°F., Duration = 100 min.,  
 Atmosphere = Air @ .25  $\lambda$ /min

Run No.	Load, kg	Wear Scar Diameter, mm.	Iron Recovered from Wear Debris in $\mu$ g as - - -	Theoretical $\theta_m$ °F	Theoretical $\theta_m$ °C
		Oil Solu.	Pyridine. Solu.	Equa. [49]	Chemical Equa. [49]
67	21	0.82	2	4	35
BA	40	0.90	BDC***	14	89
89	60	0.93	Trace	49*	96
68*					184
69	75	0.93	Trace	16	58
70**	90	1.06*	Trace	2*	302*
71	120	1.10	Trace	52	275
					141
					121
					165
					426*
					690°

\* Run had abnormal friction behavior

\*\* Lower balls rolled and stopped, resulting in two wear scars on each ball

\*\*\* BDC = Below Detectable Concentration

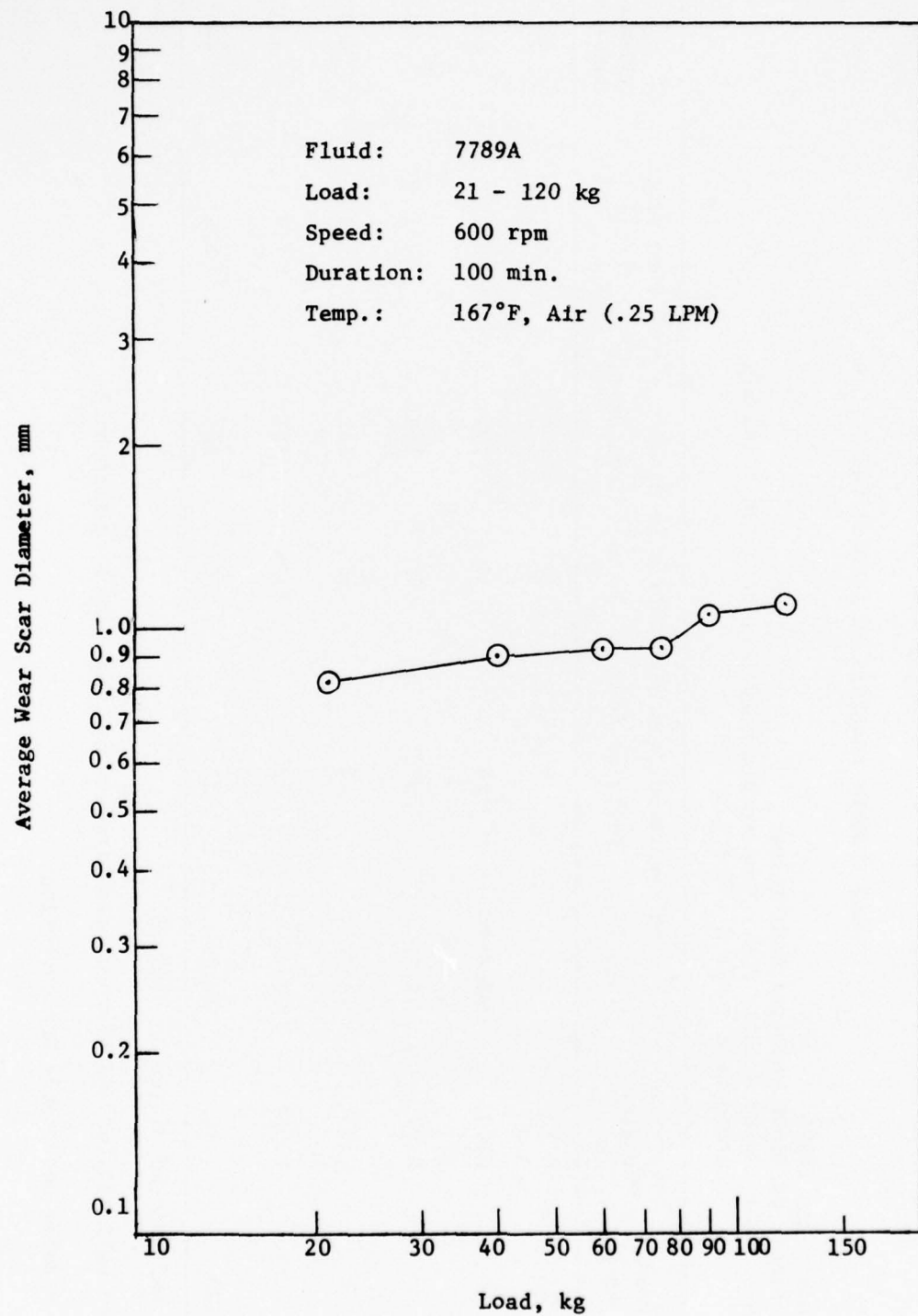


FIGURE 26. MEAN WEAR SCAR DIAMETER AS A FUNCTION OF LOAD.

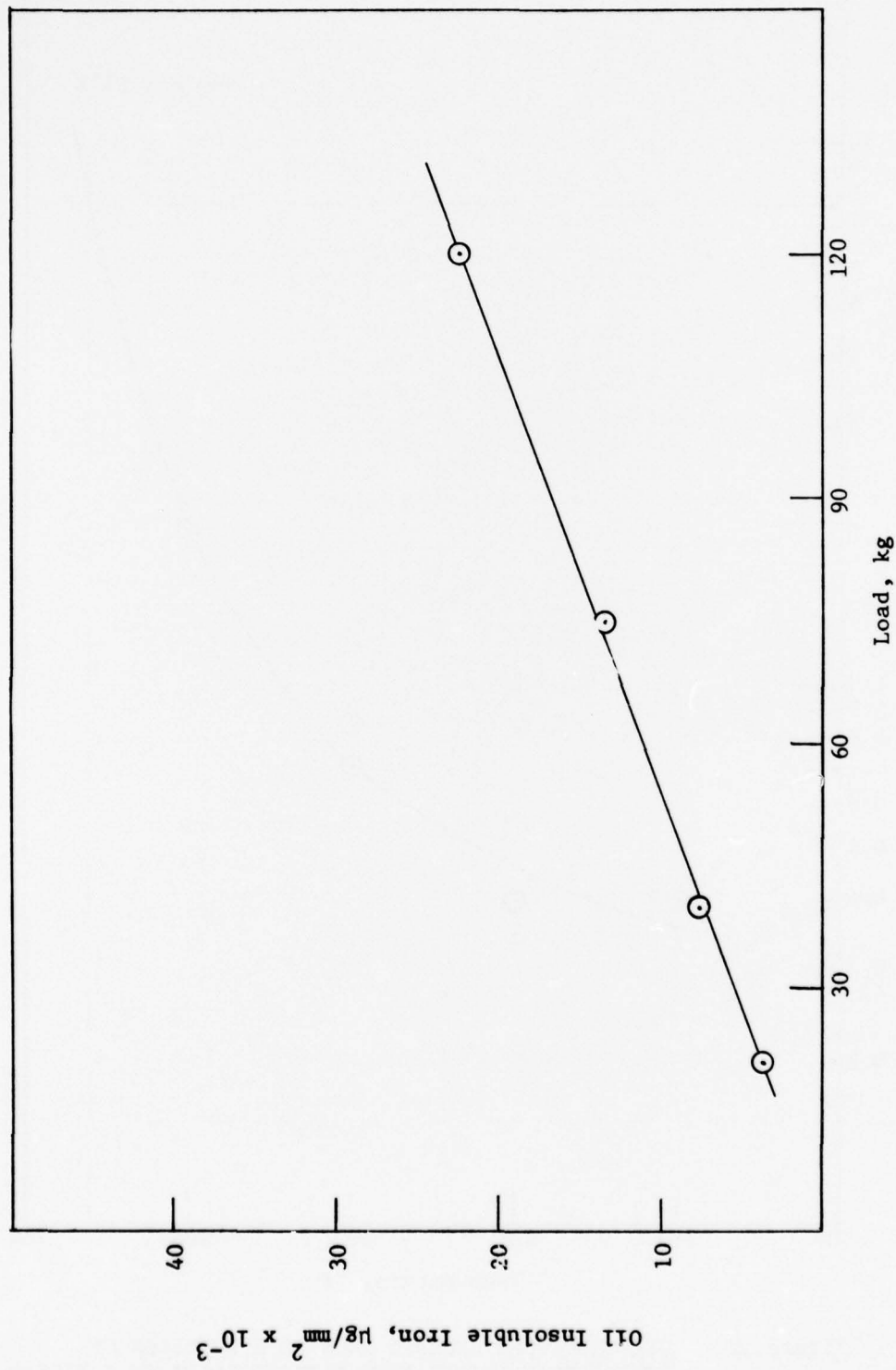


FIGURE 27. OIL INSOLUBLE IRON PER UNIT AREA AS A FUNCTION OF LOAD.

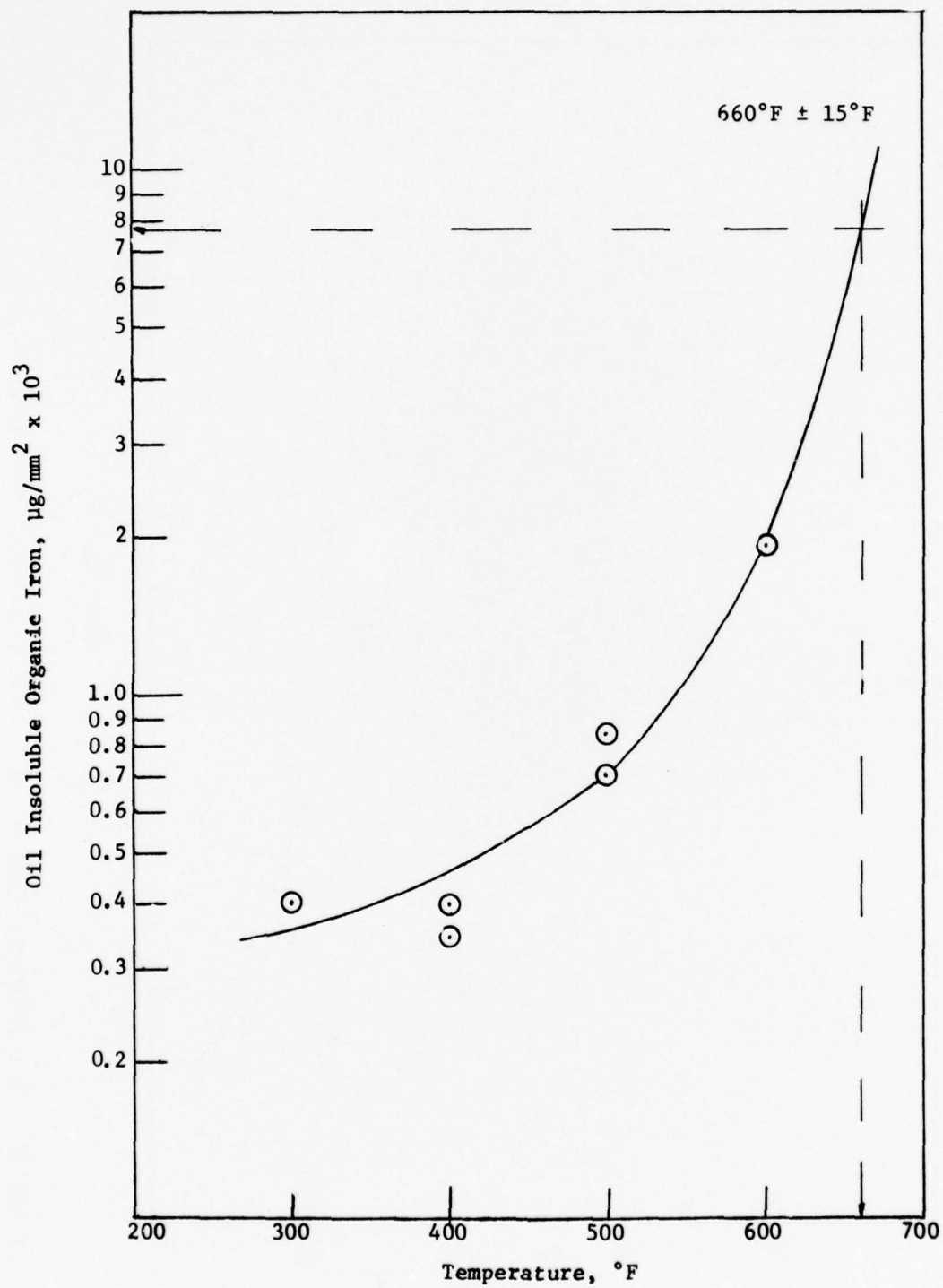


Figure 28. OIL INSOLUBLE ORGANIC IRON AS A FUNCTION OF TEMPERATURE IN THE SLOW-SLIDING TESTS (MLO 7789A).

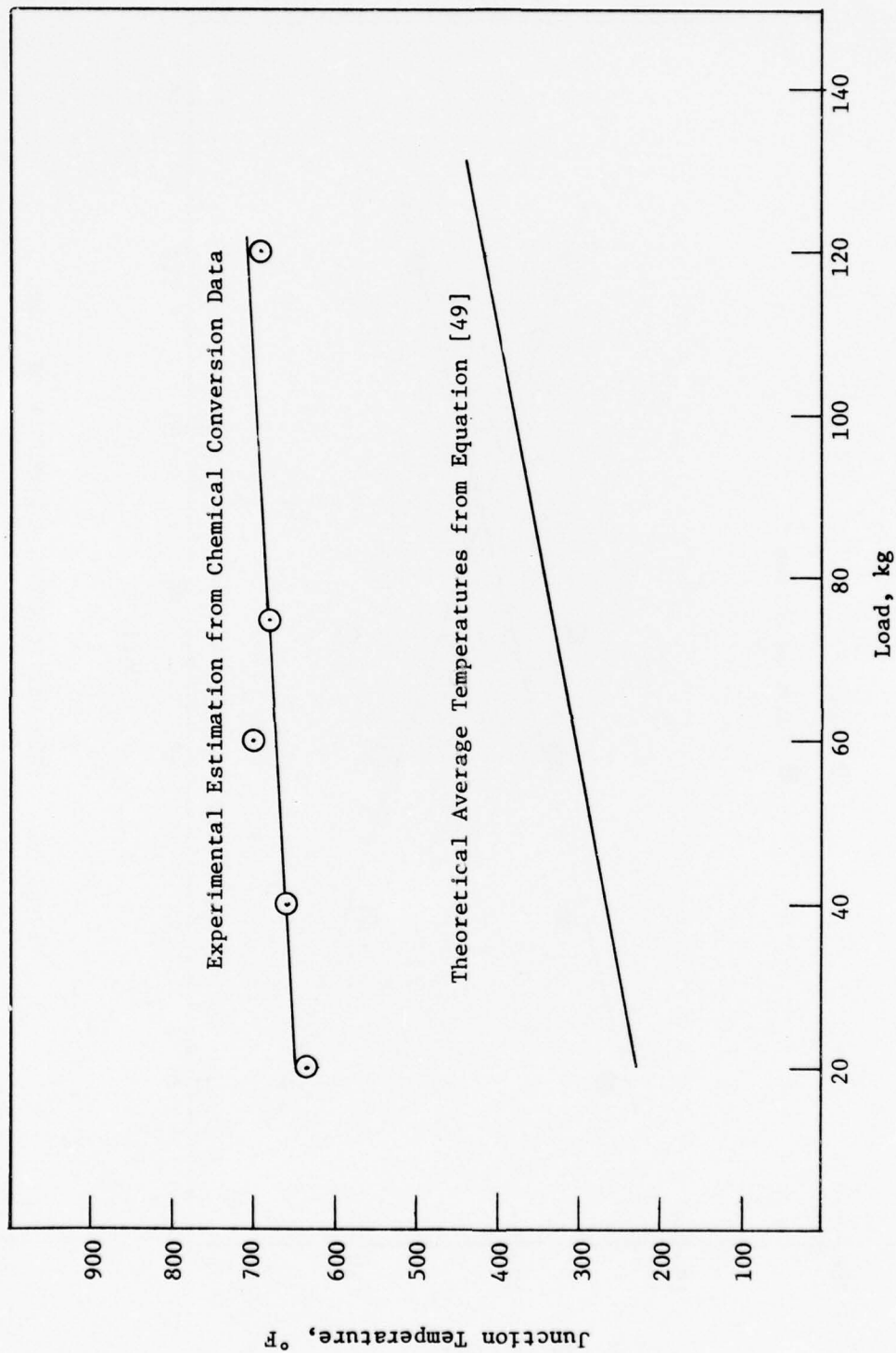


FIGURE 29. JUNCTION TEMPERATURES AS A FUNCTION OF LOAD.

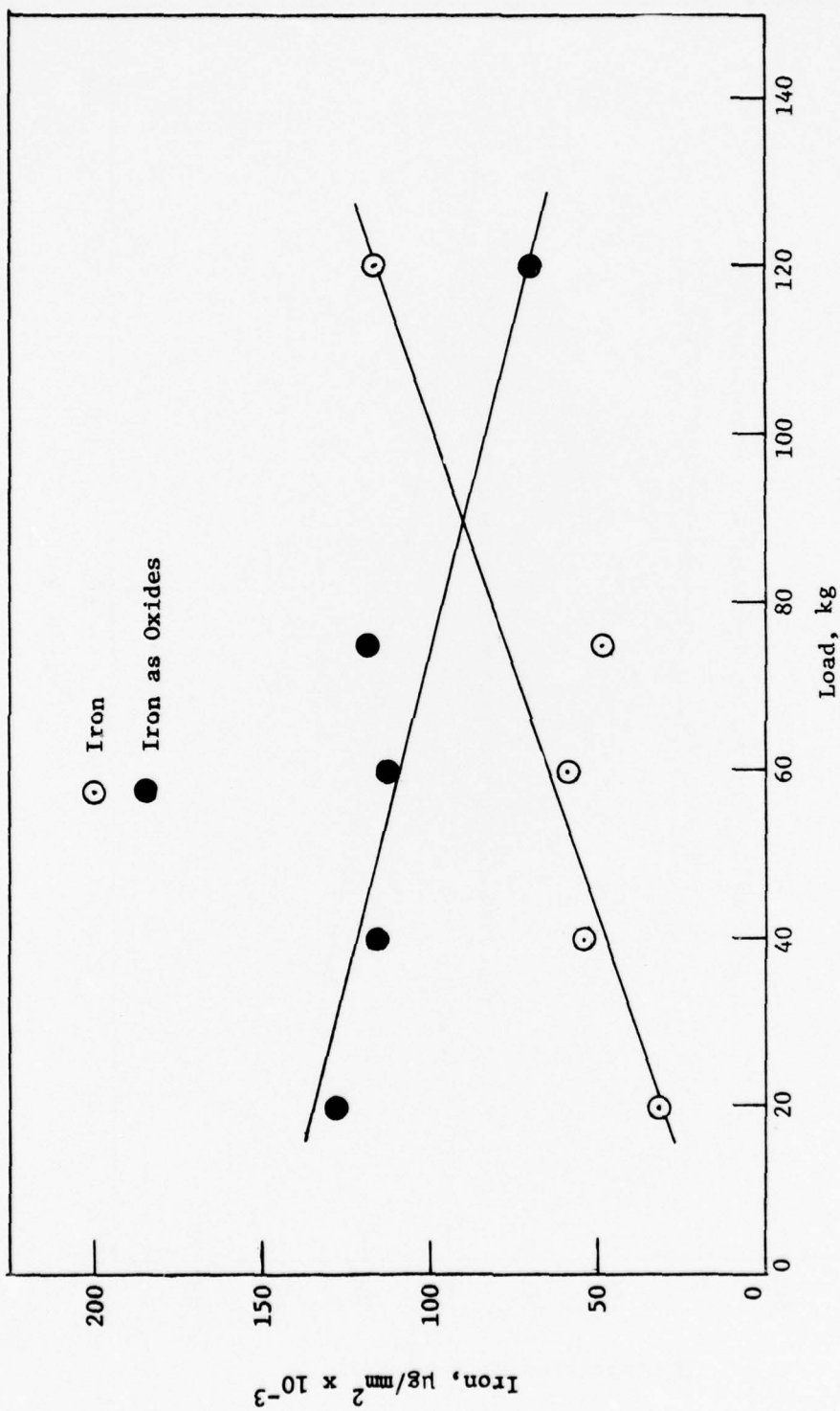


FIGURE 30. IRON PARTICLES AS A FUNCTION OF LOAD.

Table 18  
WEAR PRODUCT ANALYSIS AS A FUNCTION OF SPEED

Test Fluid: MLO 7789A  
Test Machine: GE/Brown Modified Wear Tester  
Test Conditions: Load = 40 kg., Duration = 100 min., Temperature = 167°F., Atmosphere = dry air @ 0.25 lb/min

Run No.	Speed, r.p.m.	Wear Scar Diameter, mm.	- - Iron Recovered from Wear Debris in $\mu$ g as - -			$\theta_m$ , °F	$\theta_m$ , °F
			Oil Solu.	Pyridine Solu.	Iron Oxides	From Equa. [47]	Chemical Conversion
62	400	0.78	BDC	51*	127	118	271
BA	600	0.90	BDC	14	89	191	321
95	790	0.94	BDC	37**	69	262	355
64	1000	0.79	BDC	4	54	123	340
65	1500	0.75	BDC	5	39	62	387
66***	2000	2.16***	1***	4***	4,500***	132***	

\* Possible contamination by residual aromatic compounds from Run 60

\*\* Abnormal friction curve indicating possible vibration problems

\*\*\* Ran for six minutes before seizure

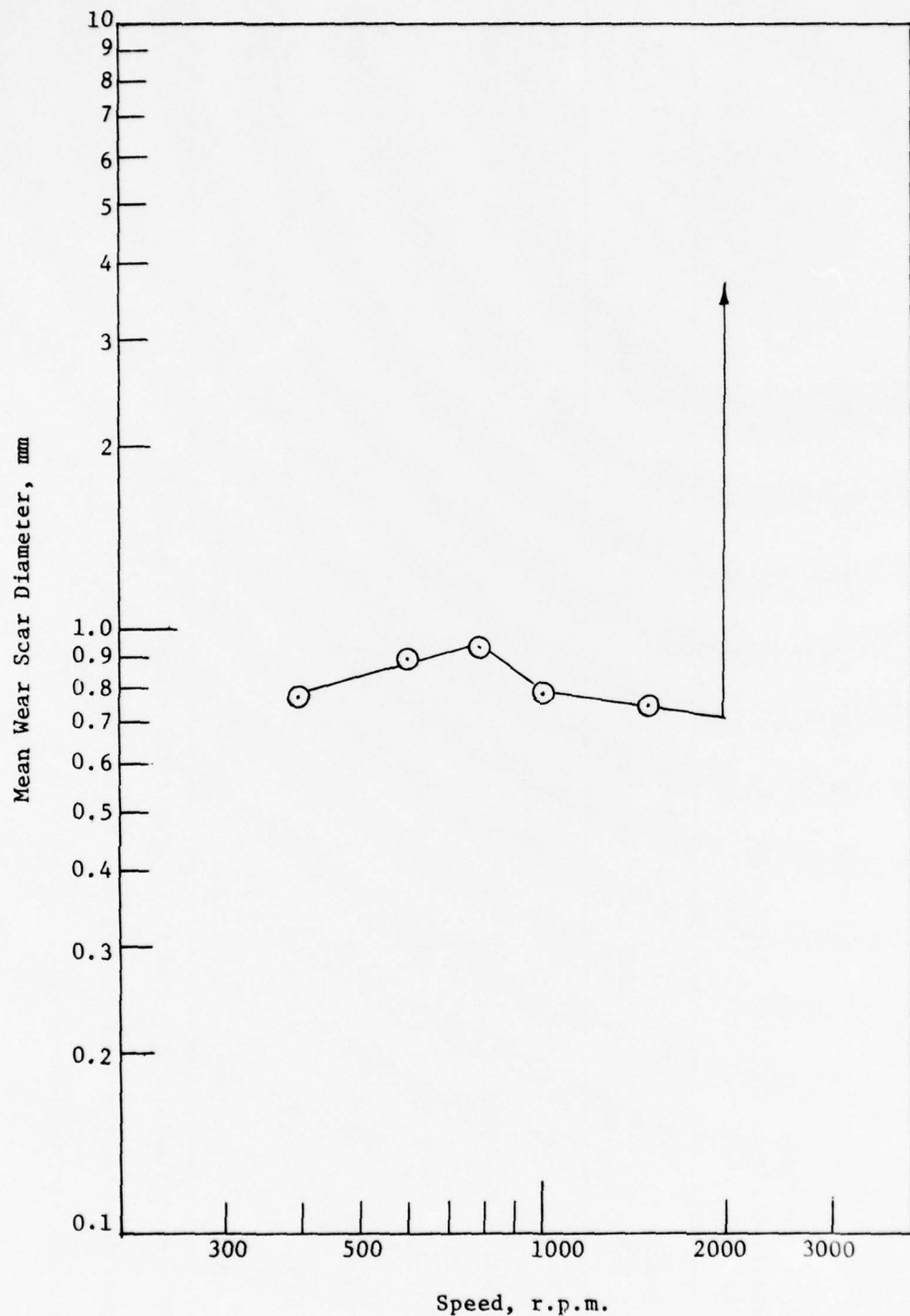


FIGURE 31. MEAN WEAR SCAR DIAMETER AS A FUNCTION OF SPEED.

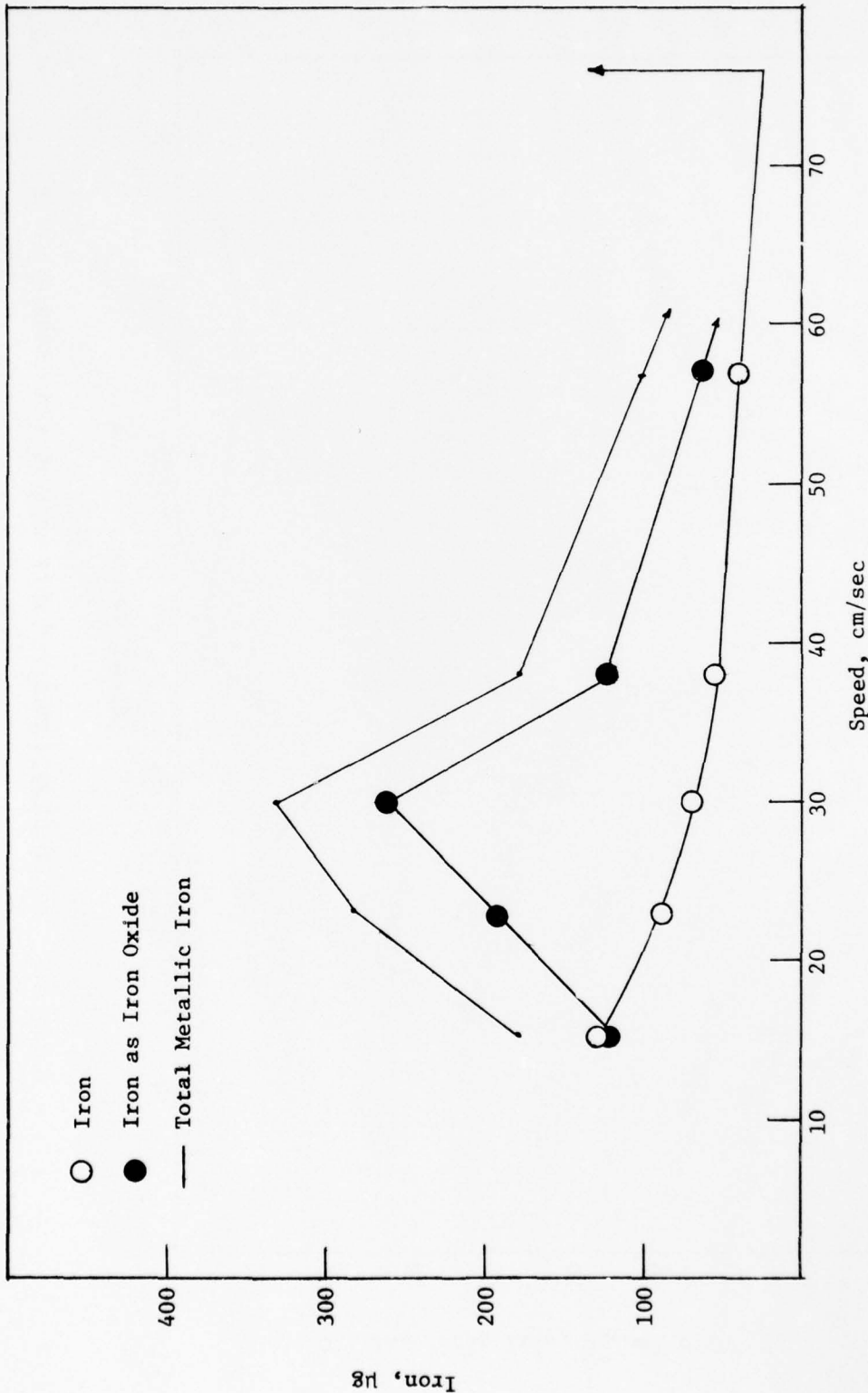


FIGURE 32. IRON PARTICLES AS A FUNCTION OF SPEED.

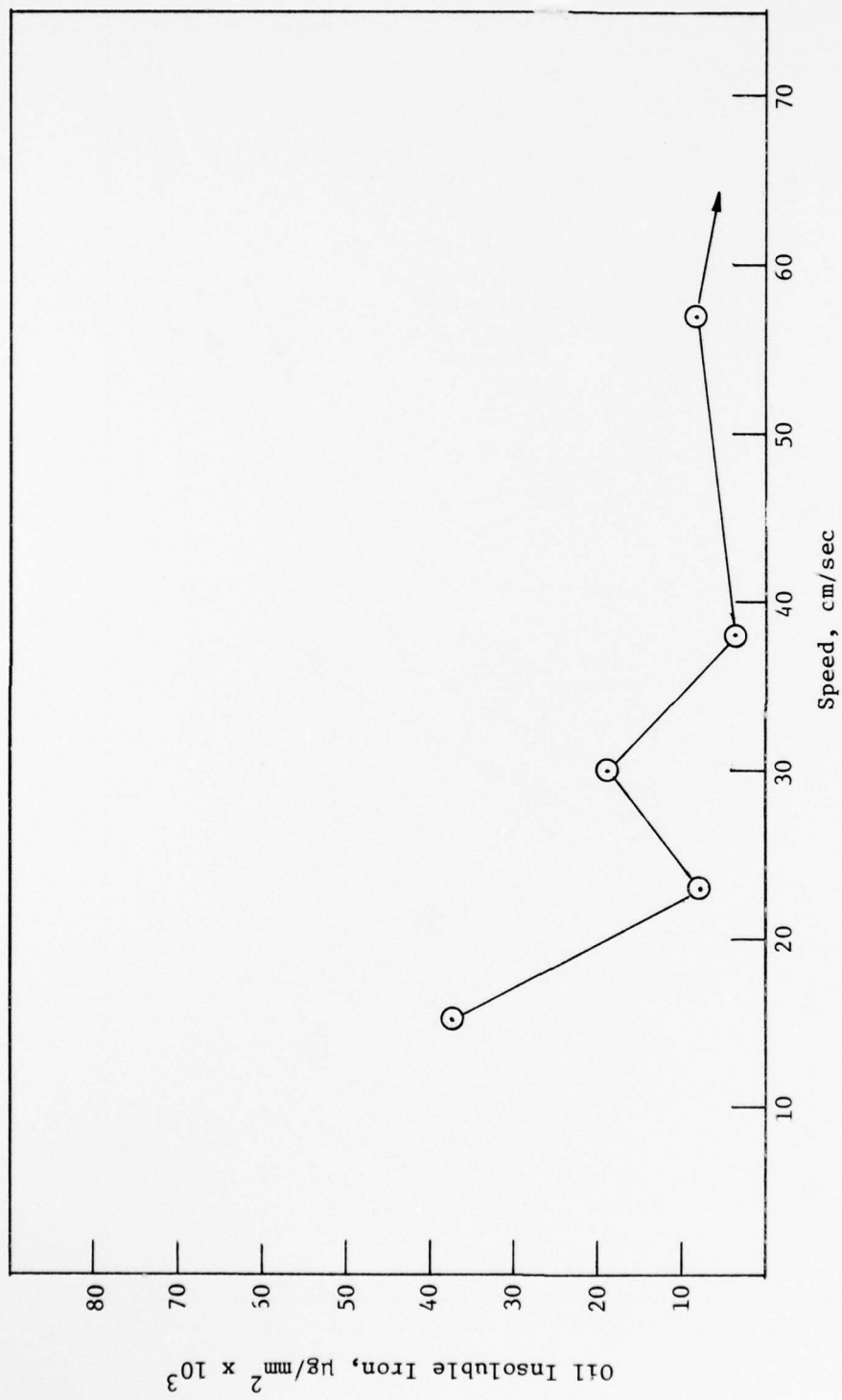


FIGURE 33. OIL INSOLUBLE IRON PER UNIT AREA AS A FUNCTION OF SPEED.

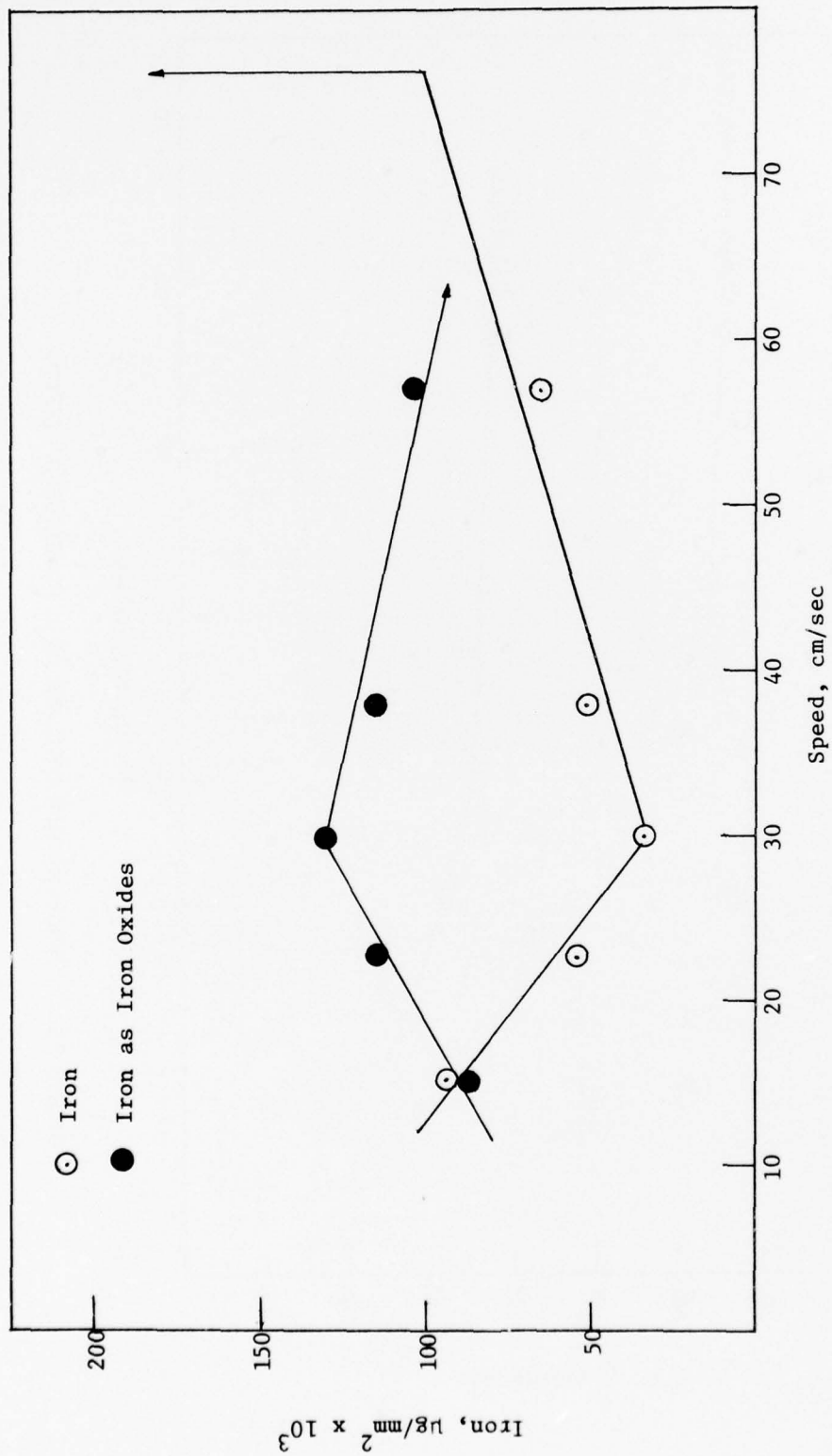


FIGURE 34. IRON PARTICLES PER UNIT AREA AS A FUNCTION OF SPEED.

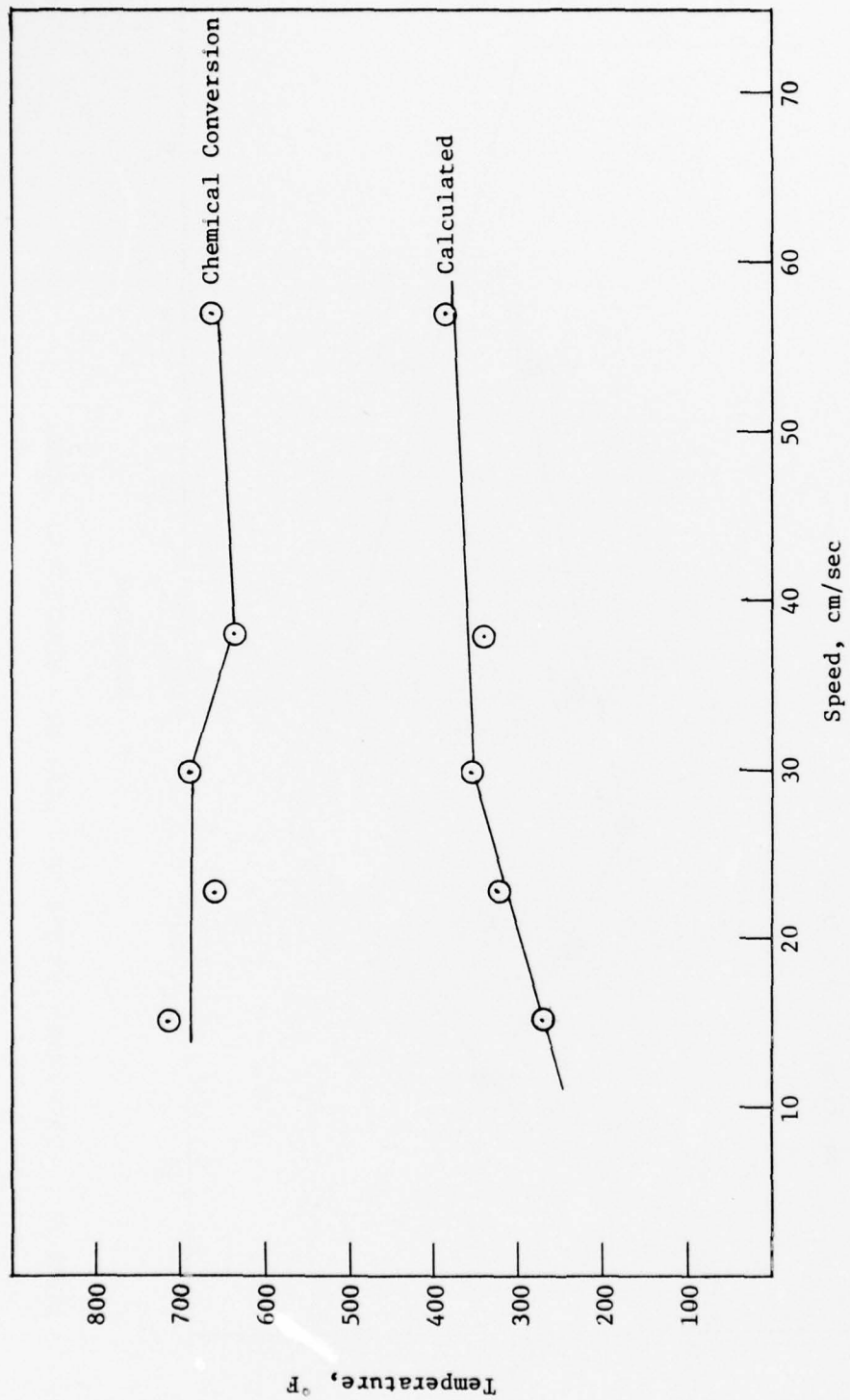


FIGURE 35. JUNCTION TEMPERATURES AS A FUNCTION OF SPEED.

Table 19

## WEAR PRODUCT COMPOSITION OF MLO 7789A IN THE SHELL FOUR-BALL WEAR TESTER

Test Fluid: MLO 7789A  
 Test Conditions: Load = 40 kg., Speed = 630 r.p.m., Duration = 100 min., Temperature = 167°F.,  
 Atmosphere = dry air (0.7 l/hr)

Run No.	Wear Scar Diameter, mm.	Oil Solu.	Pyridine Solu.	Wear Debris in $\mu$ g as - - -	Iron Oxides	Total Iron Recovered, $\mu$ g
K23	0.81	15		41	58	128
K24	0.83	16	28		66	170
BAK Average	0.82	15.5	35		62	149
						261

Table 20

## THE EFFECT OF OCTADECYL ALCOHOL CONCENTRATION ON WEAR PRODUCT COMPOSITION

Base Fluid: MLO 7789A  
 Test Machine: Shell Four-ball Wear Tester  
 Test Conditions: Load = 40 kg., Speed = 600 r.p.m., Duration = 100 min., Temperature = 167°F.,  
 Atmosphere = dry air (0.7 l/hr)

Run No.	Wt. % Octadecyl Alcohol	Wear Scar Diameter mm.	Oil Solu.	Pyridine Solu.	Iron	Iron Oxides	Organometallic Iron, %
BAK	0	0.82	1.6	35	62	149	19
K22	0.01	0.85	1.6	31	73	294	11
K8	0.10	0.77	3	14	279	187	3
K5	0.27	0.79	10	21	14	140	17
K6AV	1.00	0.77	26	23	52	145	20
K7AV	5.00	0.53	81.5	73	106	198	75

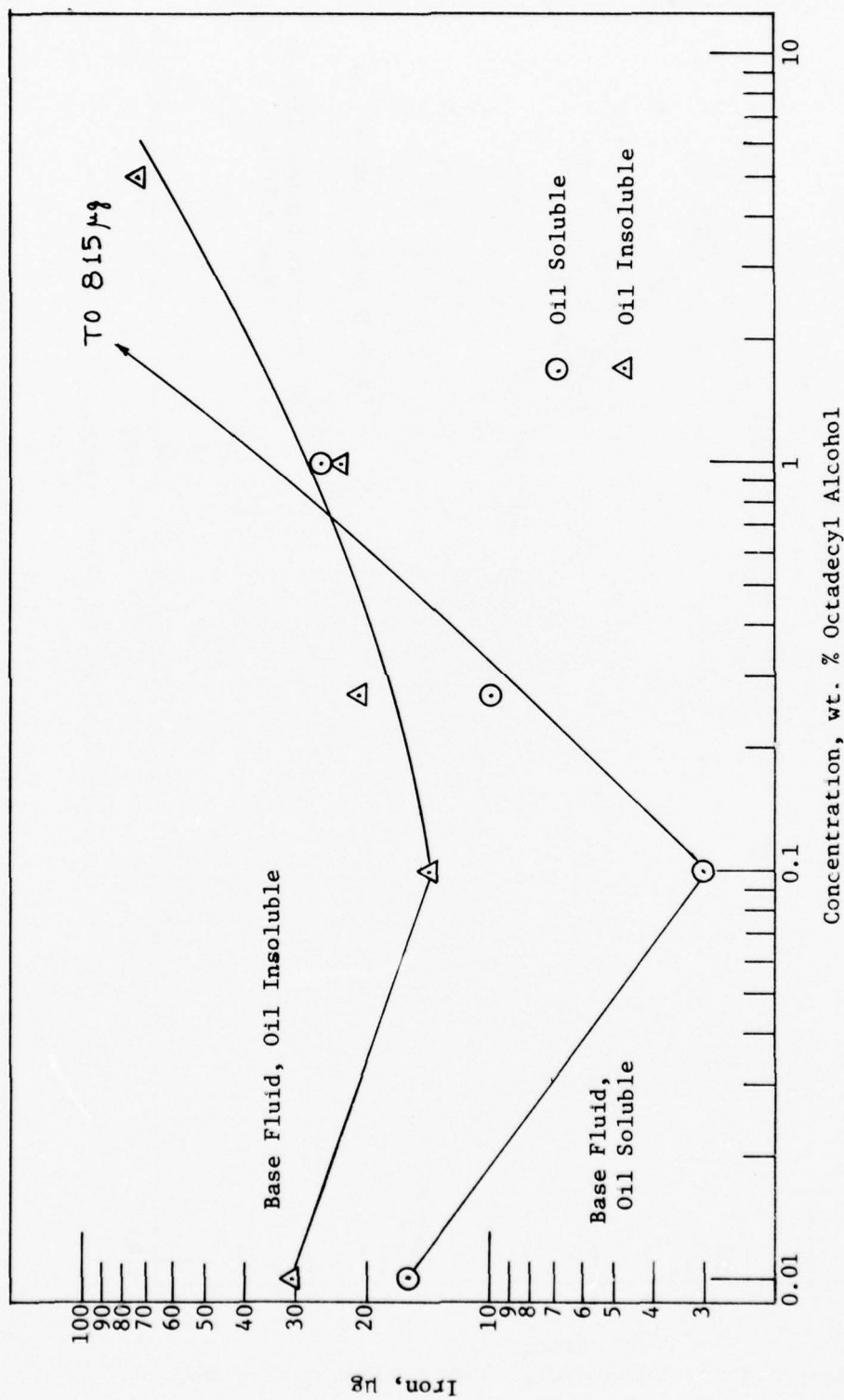


FIGURE 36. ORGANOMETALLIC IRON FORMATION AS A FUNCTION OF OCTADECYL ALCOHOL CONCENTRATION.

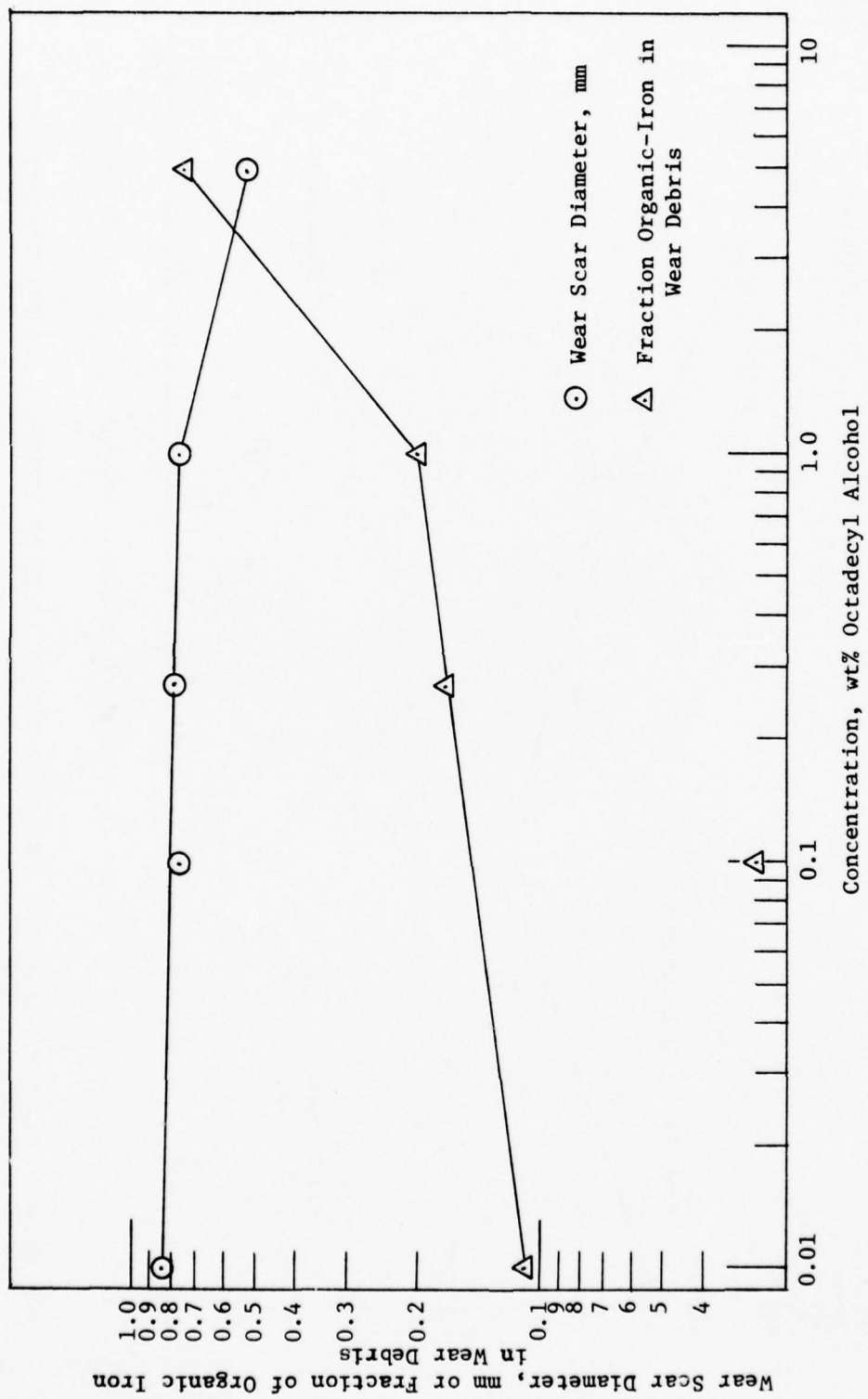


FIGURE 37. WEAR AS A FUNCTION OF OCTADECYL ALCOHOL CONCENTRATION.

Table 21

## THE EFFECT OF BASE FLUID PURITY ON ADDITIVE RESPONSE

Test Fluids: Super-refined Paraffinic Mineral Oil, MLO 7789  
 MLO 7789 Percolated through Activated Alumina, MLO 7789A

Test Machine: Shell Four-ball Wear Tester

Test Conditions: Load = 40 kg., Speed = 600 r.p.m., Duration = 100 min., Temperature = 167°F.,  
 Atmosphere = dry air (0.7 l/hr)

Run No.	Fluid	Wear Scar Diameter, mm.	Oil Solu.	Pyridine Solu.	Iron	Wear Debris in $\mu$ g as - - - - -	Iron Oxides
K8	MLO 7789A + 0.1% Octadecyl Alcohol	0.77	3	14	279	187	
K21	MLO 7789 + 0.1% Octadecyl Alcohol	0.94	1	28	91	157	
K6AV	MLO 7789A + 1.0% Octadecyl Alcohol	0.77	26	23	52	145	
K20	MLO 7789 + 1.0% Octadecyl Alcohol	0.82	2	19	69	131	

Table 22

## THE EFFECT OF OCTADECYL BROMIDE CONCENTRATION ON WEAR

Base Fluid: MO 7789A

Test Machine: Shell Four-ball Wear Tester

Test Conditions: Load = 40 kg., Speed = 600 r.p.m., Duration = 100 min., Temperature = 167°F.,  
Atmosphere = dry air (0.7 l/hr)

Run No.	Wt. % Octadecyl Bromide	Wear Scar Diameter mm	Iron Recovered from Wear Debris in $\mu\text{g}$	as - - - Iron Oxides	Organic Iron, %
K16	0.1	0.79	11	71	59
K15	1.0	0.89	4	53	93
K14	5.0	0.90	8	171	179
BAK	0	0.82	16	35	62
				149	149
					19

Table 23  
THE EFFECT OF STEARIC ACID CONCENTRATION ON WEAR

Test Fluid: MLO 7789A  
 Test Machine: Shell Four-ball Wear Tester  
 Test Conditions: Load = 40 kg., Speed = 600 r.p.m., Duration = 100 min., Temperature = 167°F.,  
 Atmosphere = dry air (0.7 l/hr)

Run No.	Wt. % Octadecanoic Acid	Wear Scar Diameter, mm.	- - Iron Recovered from Wear Debris in $\mu$ g as - -	Iron Oxides	Organic-Iron, %
BAK	0	0.82	35	62	149
K46	0.01	0.70	42	15	44
K13	0.1	0.50	3DC	20	133
K12	1.0	0.51	2	25	96
			47	47	5
			17	17	29

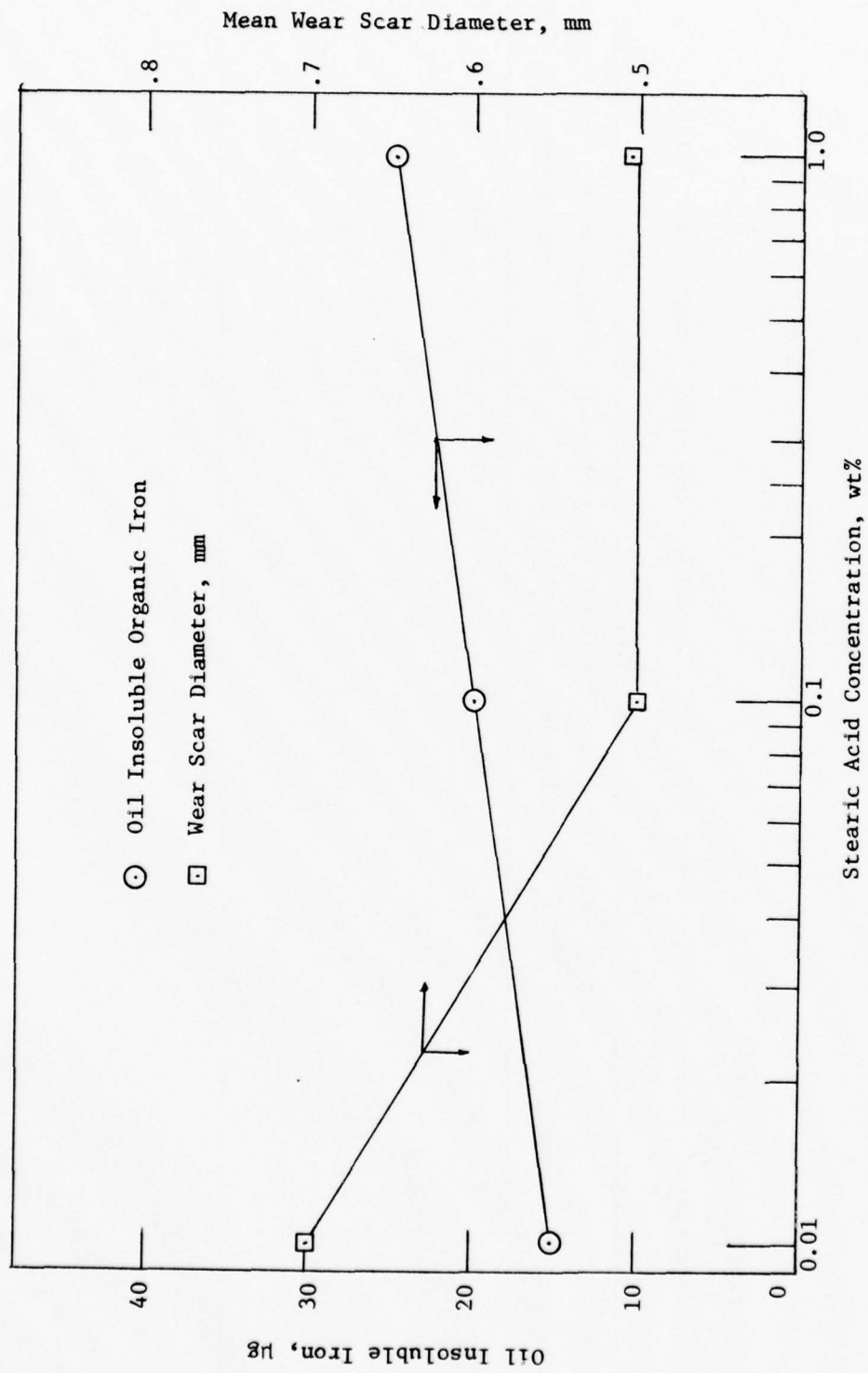


FIGURE 38. WEAR AS A FUNCTION OF STEARIC ACID CONCENTRATION.

Table 24

## EFFECT OF FLUID TYPE ON WEAR

Test Machine: GE/Brown Modified Wear Tester  
 Test Conditions: Load = 40 kg., Speed = 600 r.p.m., Duration = 100 min., Temperature = 167°F.,  
 Atmosphere = dry air (0.25 l/min)

Run No.	Fluid	Wear Scar Diameter, mm.	- - Iron Recovered from Wear Debris in $\mu$ g as - - -	Iron Oxides	Organic Iron Debris, %
BA	MLO 7789A	0.90	BDC	14	89
58	Dodecyl benzene	0.72	26	31	49
60	Triamylbenzene	0.79	62	52	42
59	Dodecyl toluene	0.88	88	74	26
				57	56

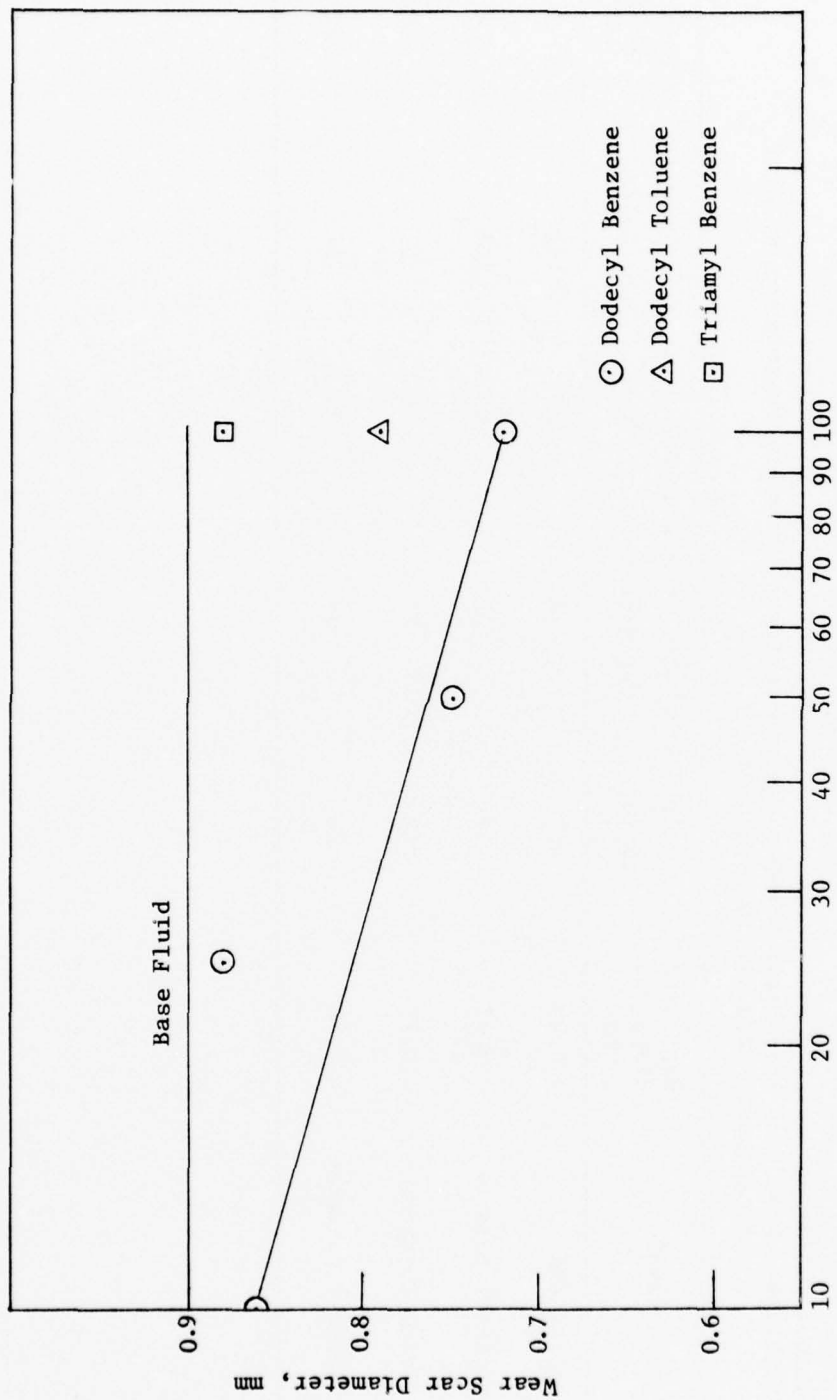


FIGURE 39. EFFECT OF AROMATIC COMPONENTS ON WEAR.

Table 25  
EFFECT OF AROMATIC COMPONENT ON WEAR

Base Fluid: MLO 7789A  
 Test Machine: GE/Brown Modified Wear Tester  
 Test Conditions: Load = 40 kg., Speed = 600 r.p.m., Duration = 100 min., Temperature = 167°F.,  
 Atmosphere = dry air (0.25 l/min.)

Run No.	Dodecyl benzene (Vol.)	Wear Scar Diameter, mm.	— Iron Recovered from Wear Debris in $\mu$ g as — — —	Organic Iron Debris, %				
BA	0	0.90	BDC	14	89	191	14	5
78	10	0.86	Trace	75	68	135	27	
79	25	0.88	Trace	42	59	125	19	
77	50	0.75	4	75	67	58	39	
58	100	0.72	26	31	49	285	14	

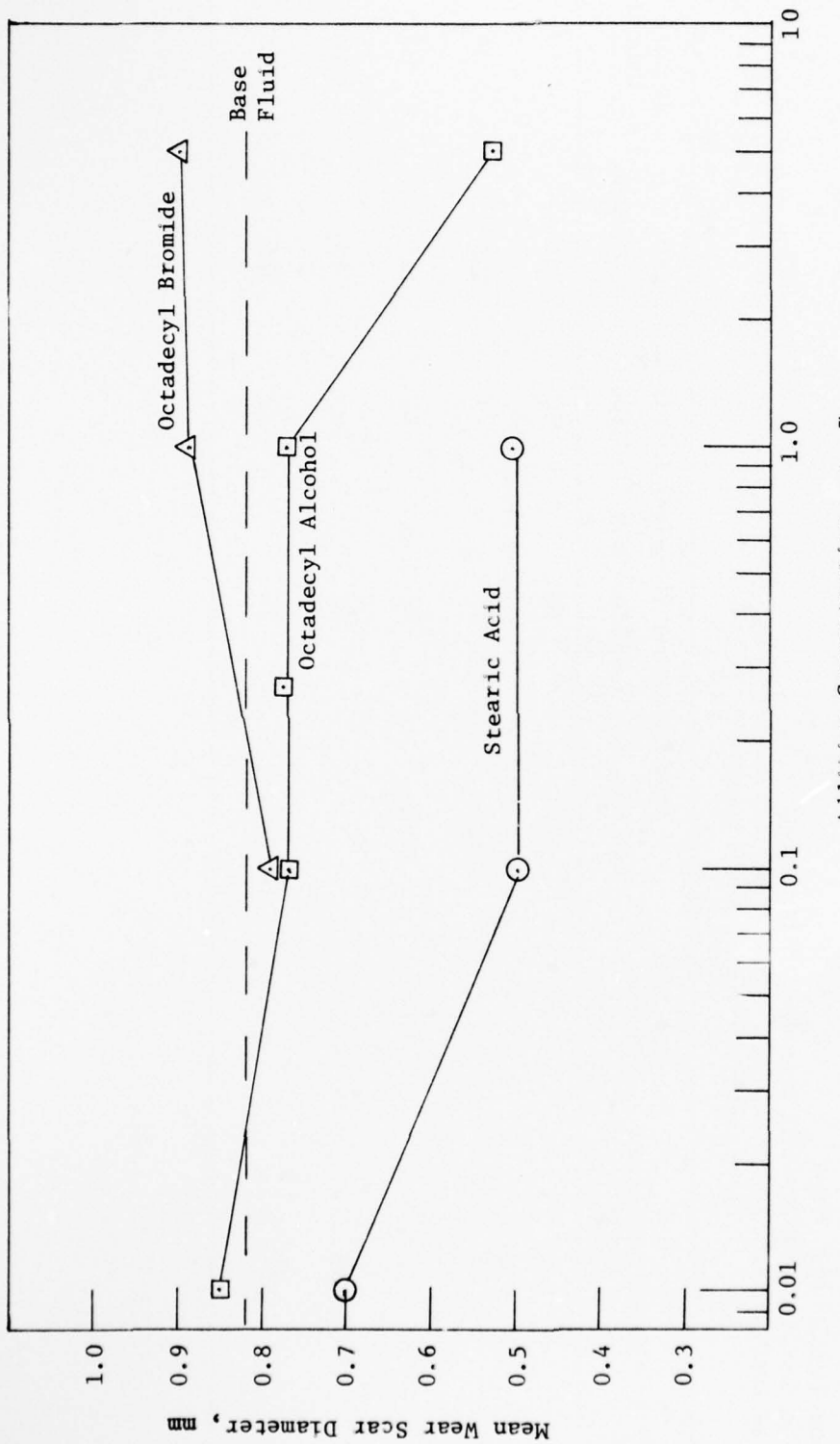


FIGURE 40. WEAR AS A FUNCTION OF THE VARIOUS ADDITIVE CONCENTRATIONS.

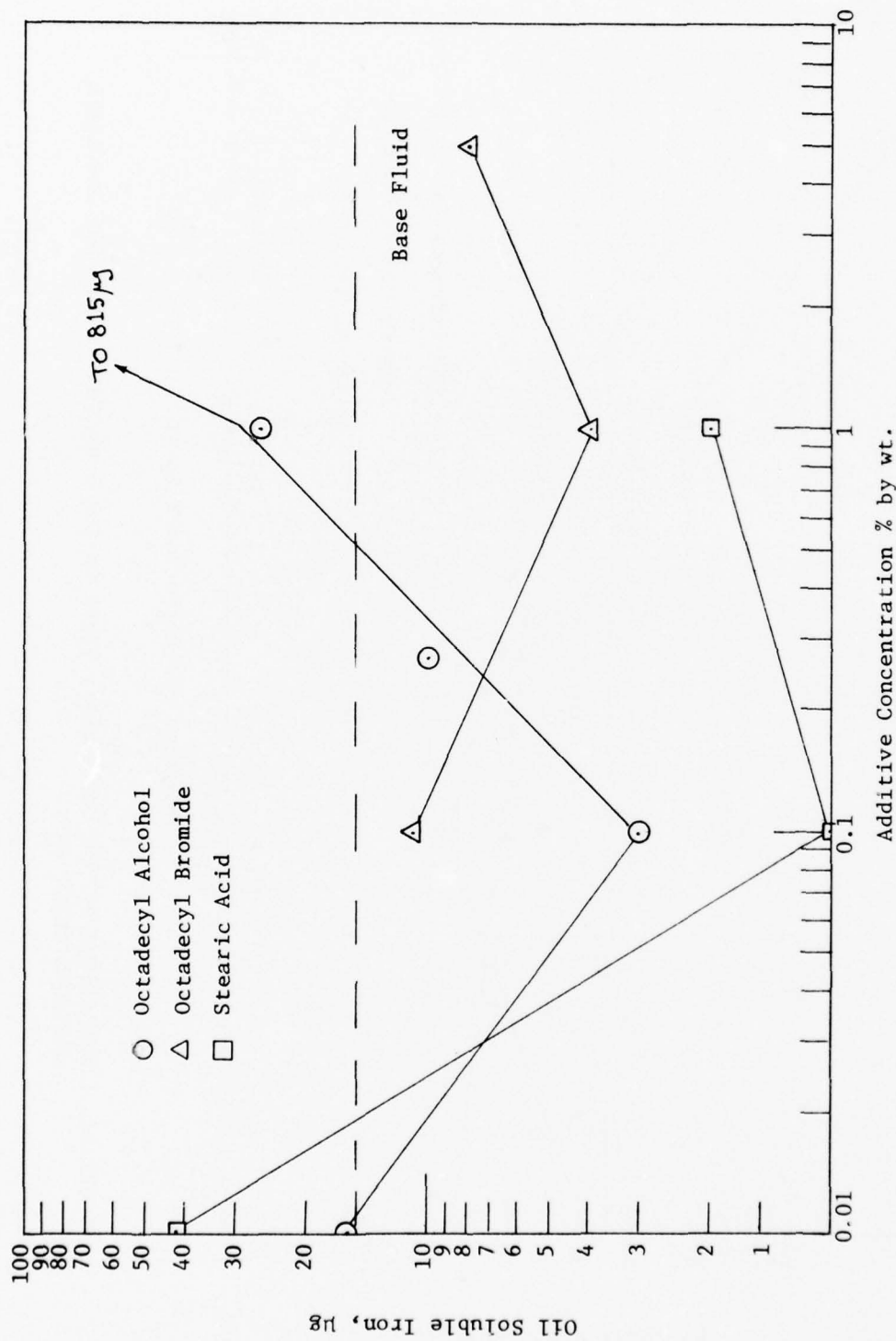


FIGURE 41. THE EFFECT OF THE FUNCTIONAL GROUPS ON THE FORMATION OF THE OIL SOLUBLE ORGANOMETALLIC IRON.

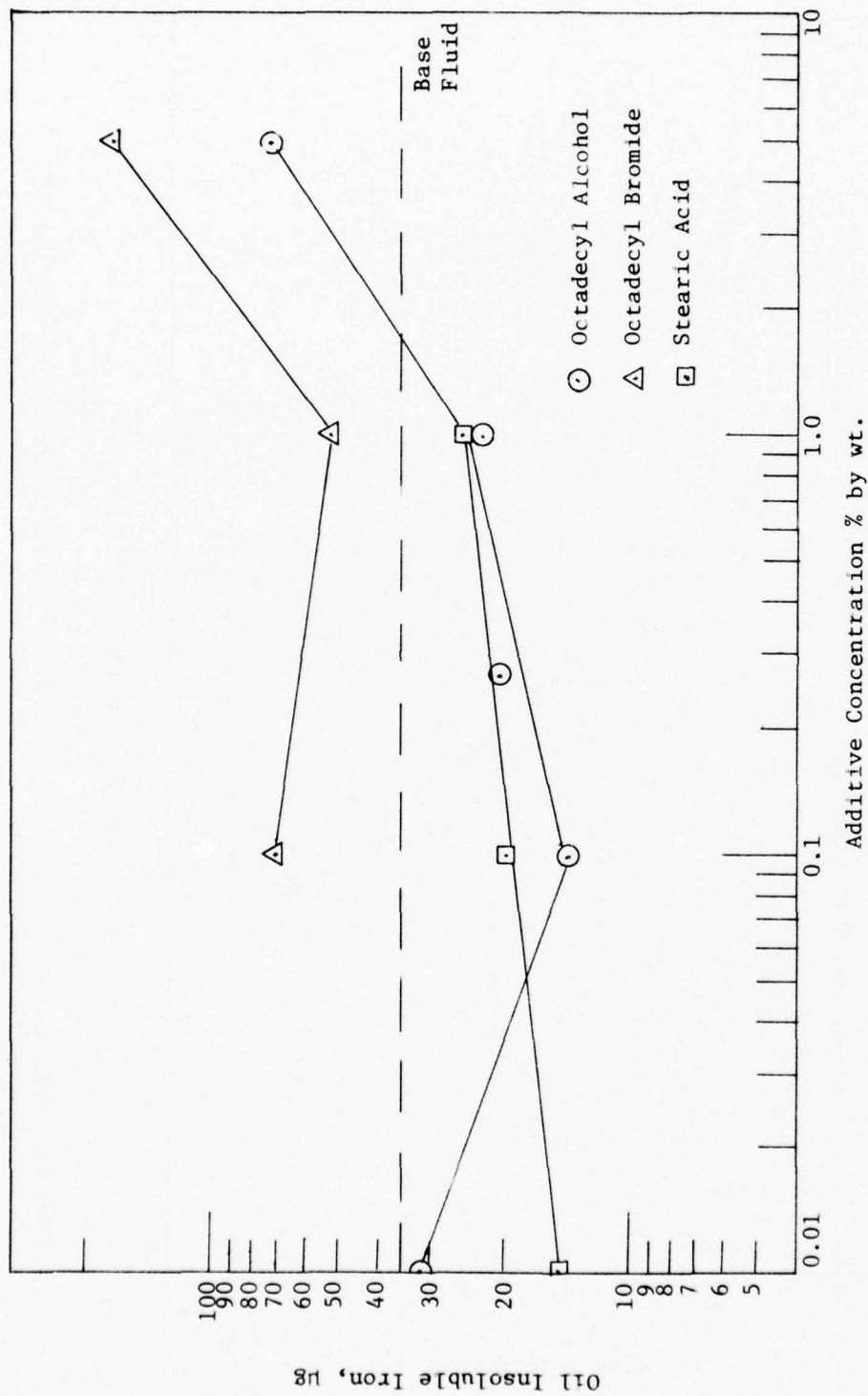


FIGURE 42. THE EFFECT OF THE FUNCTIONAL GROUPS ON THE FORMATION OF THE OIL INSOLUBLE ORGANOMETALLIC IRON.

Table 26  
EFFECT OF ZINC DIHEXYLDITHIOPHOSPHATE ON WEAR AND ITS PRODUCTS

Base Fluid: MLO 7789A  
 Test Machine: GE/Brown Modified Four-ball Wear Tester  
 Test Conditions: Load = 40 kg., Speed = 600 r.p.m., Duration = 100 min., Temperature = 167°F.,  
 Atmosphere = dry air (.25 l/min)

Run No.	Wt. % ZDP*	Wear Scar Diameter, mm.	BDC**	Oil Solu.	Pyridine Solu.	Iron	Iron Oxides
BA	0	0.90				14	191
61	0.01	0.70		3		10	42
57	0.1	0.56		1		6	110
56	1.0	0.46		2		5	31
55	5.0	0.50		5		8	124
						66	163
						22	35

\* ZDP = Zinc Dihexyldithiophosphate

\*\* BDC = Below Detection Concentration

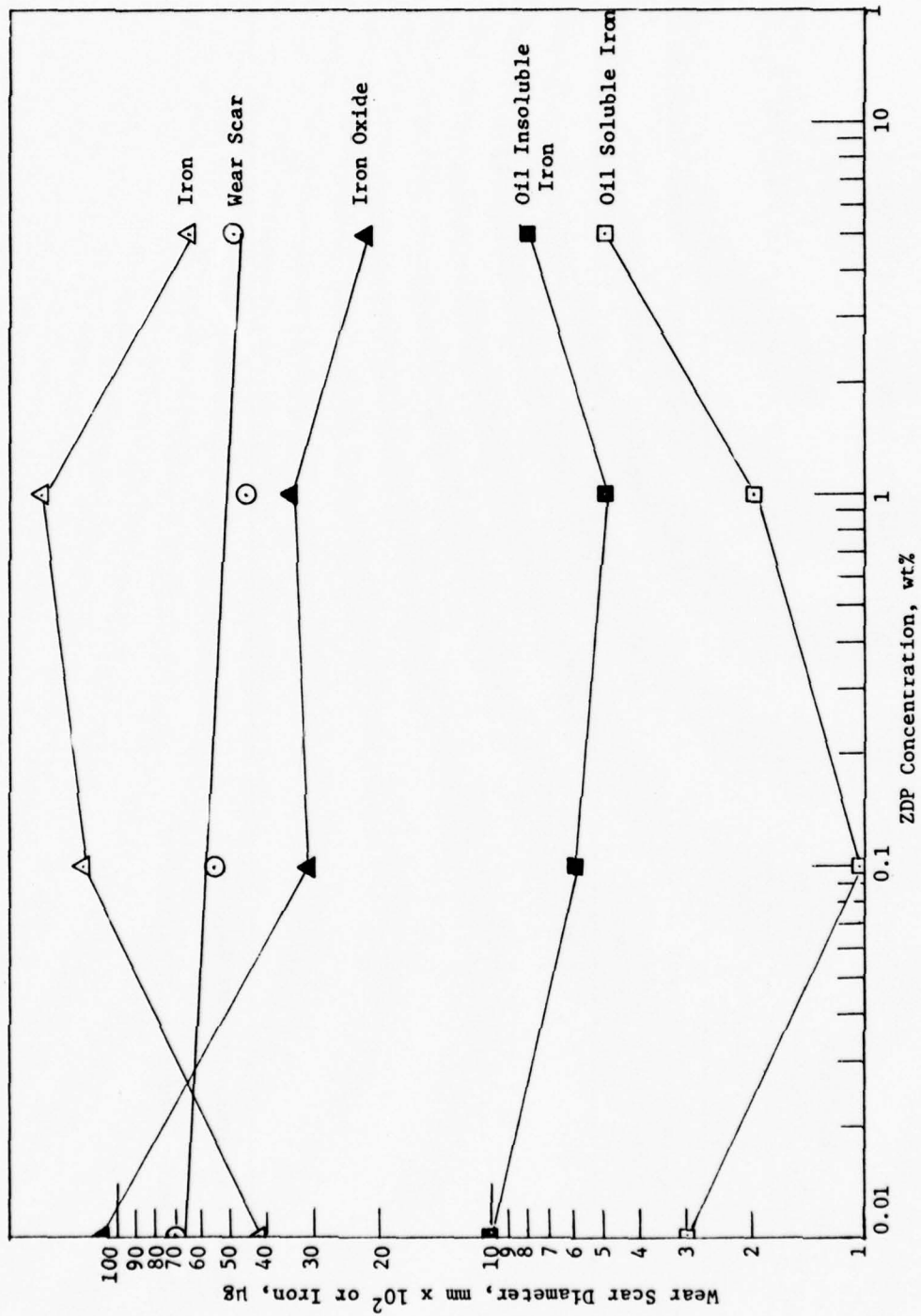


FIGURE 43. EFFECT OF ZINC DIHEXYLDITHIOPHOSPHATE CONCENTRATION ON WEAR PRODUCTS.

Table 27

## THE EFFECT OF DILAURYL ACID PHOSPHATE (DAP) ON WEAR AND ITS PRODUCTS

Base Fluid: MLO 7789A  
 Test Machine: GE/Brown Modified Four-ball Wear Tester  
 Test Conditions: Load = 40 kg., Speed = 600 r.p.m., Duration = 100 min., Temperature = 167°F.,  
 Atmosphere = dry air (0.25 l/min)

Run No.	Wt. % of Dilauryl Acid Phosphate	Wear Scar Diameter, mm.	BDC*	Oil Solu.	Pyridine Solu.	Iron	Iron Oxides
BA	0	0.90			14	89	191
54	0.01	0.93		2	55	132	258
52	0.1	0.40		2	5	69	11
51	1.0	0.45		19	8	22	48
49	5.0	0.44		40	50	35	65

\* Below Detectable Concentration

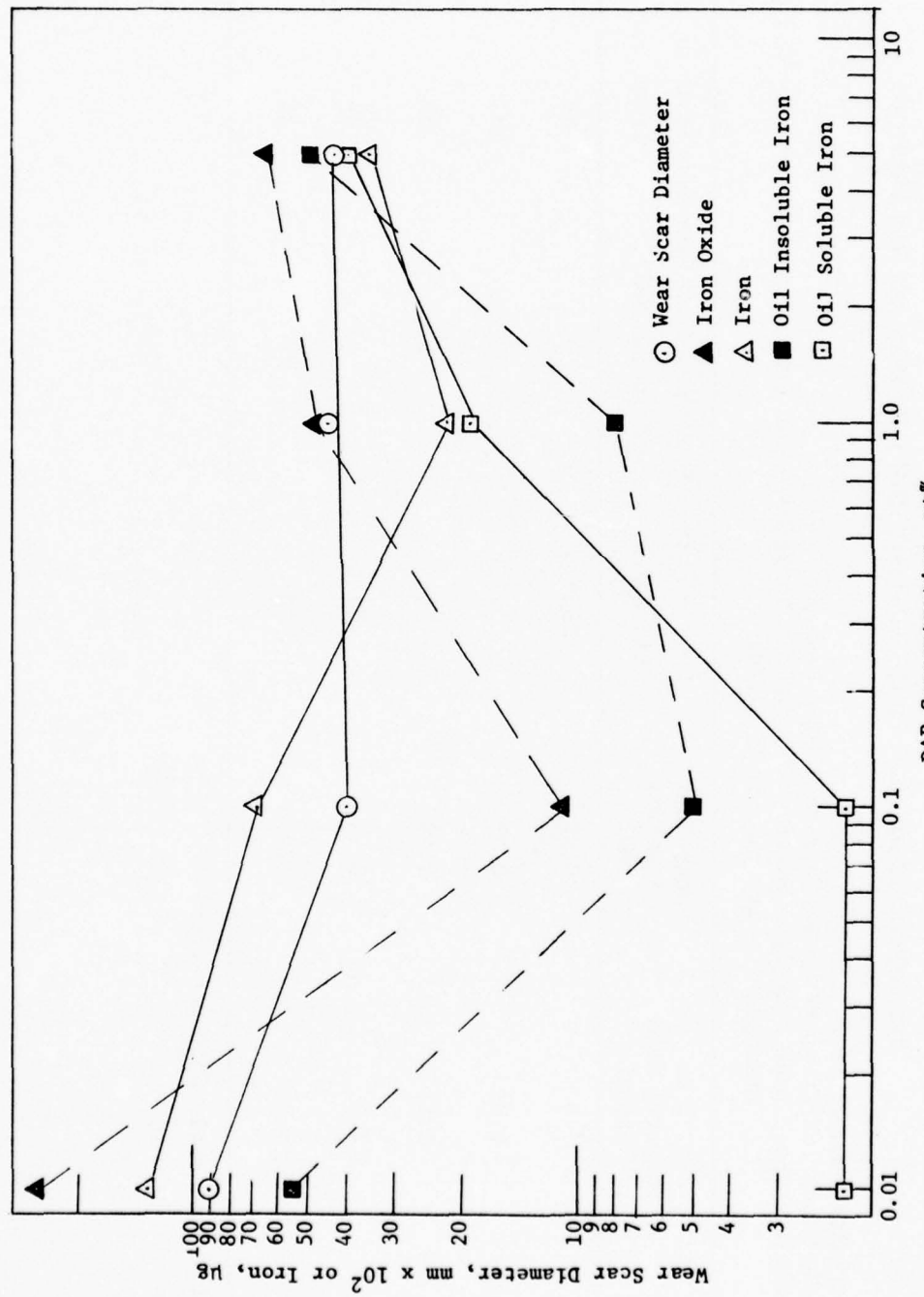


FIGURE 44. EFFECT OF DILAURYL ACID PHOSPHATE CONCENTRATION ON WEAR PRODUCTS.

Table 28  
EFFECT OF TRIBUTYL PHOSPHITE (TBP) ON WEAR AND ITS PRODUCTS

Base Fluid: MLO 7789A  
 Test Machine: GE/Brown Four-ball Wear Tester  
 Test Conditions: Load = 40 kg., Speed = 600 r.p.m., Duration = 100 min., Temperature = 167°F.,  
 Atmosphere = dry air (0.25 g/min)

Run No.	Wt. % Tributyl Phosphite	Wear Scar Diameter, mm.	0.1 Solu.	Pyridine Solu.	Iron	Recovered from Wear Debris in $\mu$ g as - - -	Iron Oxides
BA	0	0.90	BDC*	14	89	191	
46	0.1	0.75	BDC	3	183	151	
BAP	1.0	0.60	1	115	107	31	
48	5.0	0.74	2	1612	152	89	

\* BDC = Below Detection Concentration

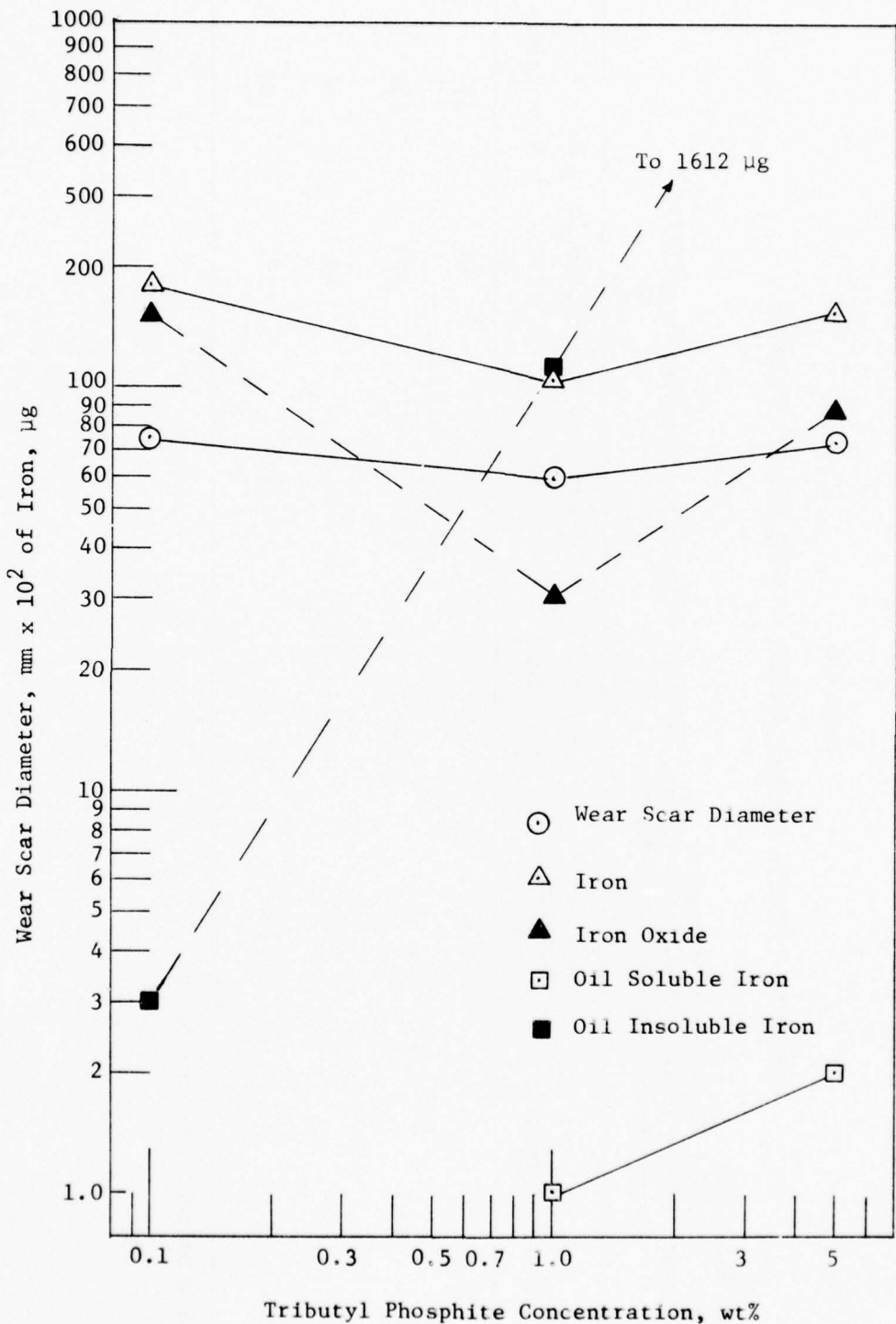


FIGURE 45. EFFECT OF TRIBUTYL PHOSPHITE CONCENTRATION ON WEAR PRODUCTS.

Table 29

EFFECT OF FLUID PURITY AND ITS RESPONSE TO TRICRESYL PHOSPHATE (TCP)  
CONCENTRATION ON WEAR AND ITS PRODUCTS

Base Fluid: MLO 7789

Test Machine: Shell Four-ball Wear Tester

Test Conditions: Load = 40 kg., Speed = 600 r.p.m., Duration = 100 min., Temperature = 167°F.,  
Atmosphere = dry air (0.7 l/hr)

Run No.	Fluid	Wear Scar Diameter, mm.	Oil Solu.	Pyridine Solu.	Iron	Debris in $\mu\text{g}$ as - - - -	Iron Oxides
BAK		0.82	16		35	62	149
K17	MLO 7789 + 0.1% (Wt.) TCP	0.97	1		21	148	227
K18	1.0% TCP	0.77		BDC	10	180	41
K19	5.0% TCP	0.50	2		10	14	32
K11	MLO 7789A + 0.1% (Wt.) TCP	0.94	1		46	113	213
K10	1.0% TCP	0.75		BDC	4	98	38
K9	5.0% TCP	0.47	1		14	20	26

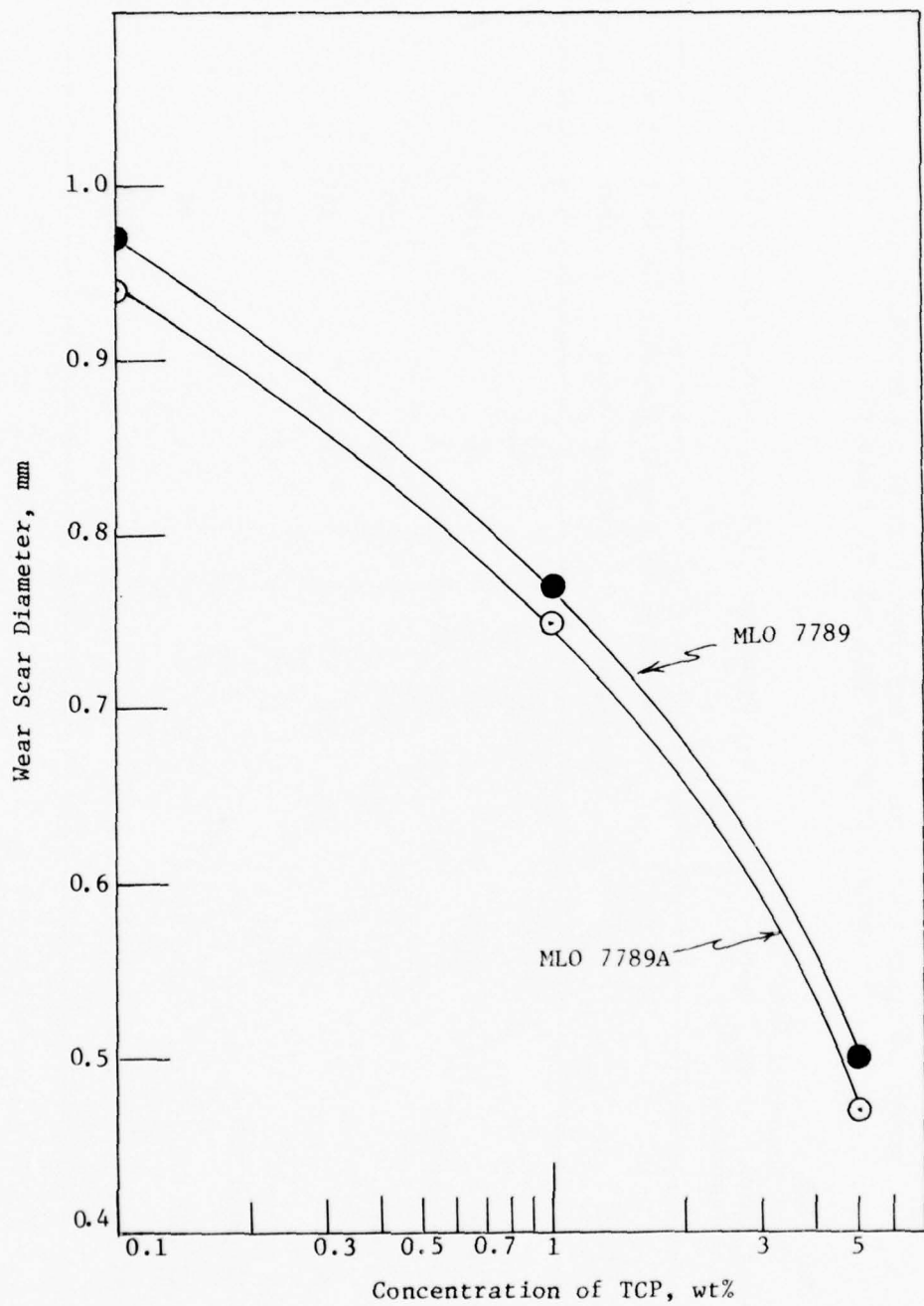


FIGURE 46. EFFECT OF FLUID PURITY AND TRICRESYL PHOSPHATE CONCENTRATION ON WEAR.

Table 30

## EFFECT OF BULK FLUID TEMPERATURE AND ATMOSPHERE ON WEAR

Test Fluid: MLO 7789A + 5% (Wt.) TCP  
 Test Machine: GE/Brown Modified Four-ball Wear Tester  
 Test Conditions: Load = 40 kg, Speed = 600 r.p.m., Duration = 100 min.,  
 Atmosphere = dry air or helium (0.25 l/min)

Run No.	Bulk Fluid Temperature, °F	Wear Scar Diameter, mm.	Oil Solu.	Pyridine Solu.	Iron	Iron Oxides
K38	100°F (Air)	0.62	7	7	26	78
K37	167°F (Air)	0.43	2	4	41	82
K40	300°F (Air)	0.47	2	4	23	137
K48	100°F (He)	0.44	6	9	29	49
K49	300°F (He)	0.53	3	4	24	37

Table 31

## EFFECT OF BULK FLUID TEMPERATURE AND ATMOSPHERE ON WEAR

Test Fluid: MLO 7789A + 2.25% (Wt.) TCP + 2.25% (Wt.) Octadecyl Bromide  
 Test Machine: GE/Brown Modified Four-ball Wear Tester  
 Test Conditions: Load = 40 kg., Speed = 600 r.p.m., Duration = 100 min.

Run No.	Bulk Fluid Temperature, °F	Wear Scar Diameter, mm.	Oil Solu.	Pyridine Solu.	Iron	Debris in $\mu$ g as - - - -	Iron Oxides
K47	100°F (Air)	0.54	10	4	4	27	27
K45	300°F (Air)	0.54	8	4	46	41	
K50	300°F (He)	0.76	11	7	99	85	

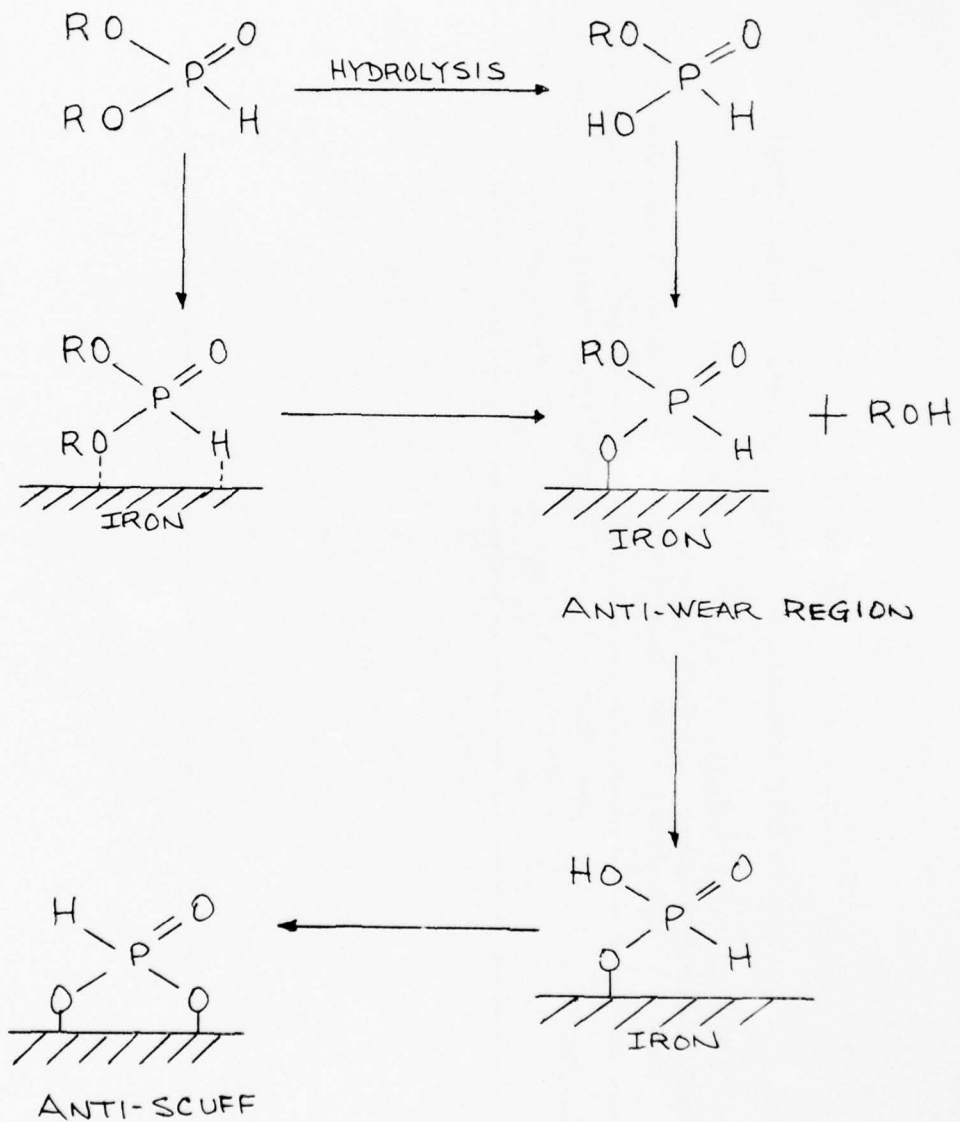


FIGURE 47. LUBRICATION MECHANISM OF DIALKYL PHOSPHITES AS PROPOSED BY FORBES AND BATTERSBY (33)

Table 32

## WEAR PRODUCT ANALYSIS OF TRIBUTYL PHOSPHITE IN MLO 7789A

Test Fluid: MLO 7789A + 1% (Wt.) Tributyl Phosphite  
 Test Machine: GE/Brown Modified Four-ball Wear Tester  
 Test Conditions: Load = 40 kg., Speed = 600 r.p.m., Duration = 100 min., Temperature = 167°F.

Run No.	Atmosphere	Wear Scar Diameter, mm.	- - - Iron Recovered from Wear Debris in $\mu$ g as - - -		
			Oil Solu.	Pyridine Solu.	Iron Oxides
47	Dry Air	0.60	1	80	137
53	Dry Air	0.59	1	149	77
BAP	Average	0.60	1	115	107
94	Helium (0.25 l/min)	0.46	2	34	249
				6	

Table 33

## EFFECT OF TEMPERATURE ON WEAR PRODUCT DISTRIBUTION AT SLOW SPEED

Test Fluid: MLO 7789A + 1% (Wt.) Tributyl Phosphate  
 Test Machine: GE/Brown Modified Four-ball Wear Tester  
 Test Conditions: Load = 40 kg., Speed = 2.9 r.p.m., Duration = 100 min.,  
 Atmosphere = dry air (0.25 l/min)

Run No.	Bulk Fluid Temperature, °F	Wear Scar Diameter, mm.	— — — Iron Solu.	— — — Pyridine Solu.	— — — Iron Recovered from Wear Debris in µg as — — —	Iron Oxides
110	167°	0.30	1	47	28	16
111	300°	0.36	38	392	638	72
112	400°	0.37	21	19	286	329
113	500°	0.40	6	2	169	169
114	600°	0.45	3	1	89	46

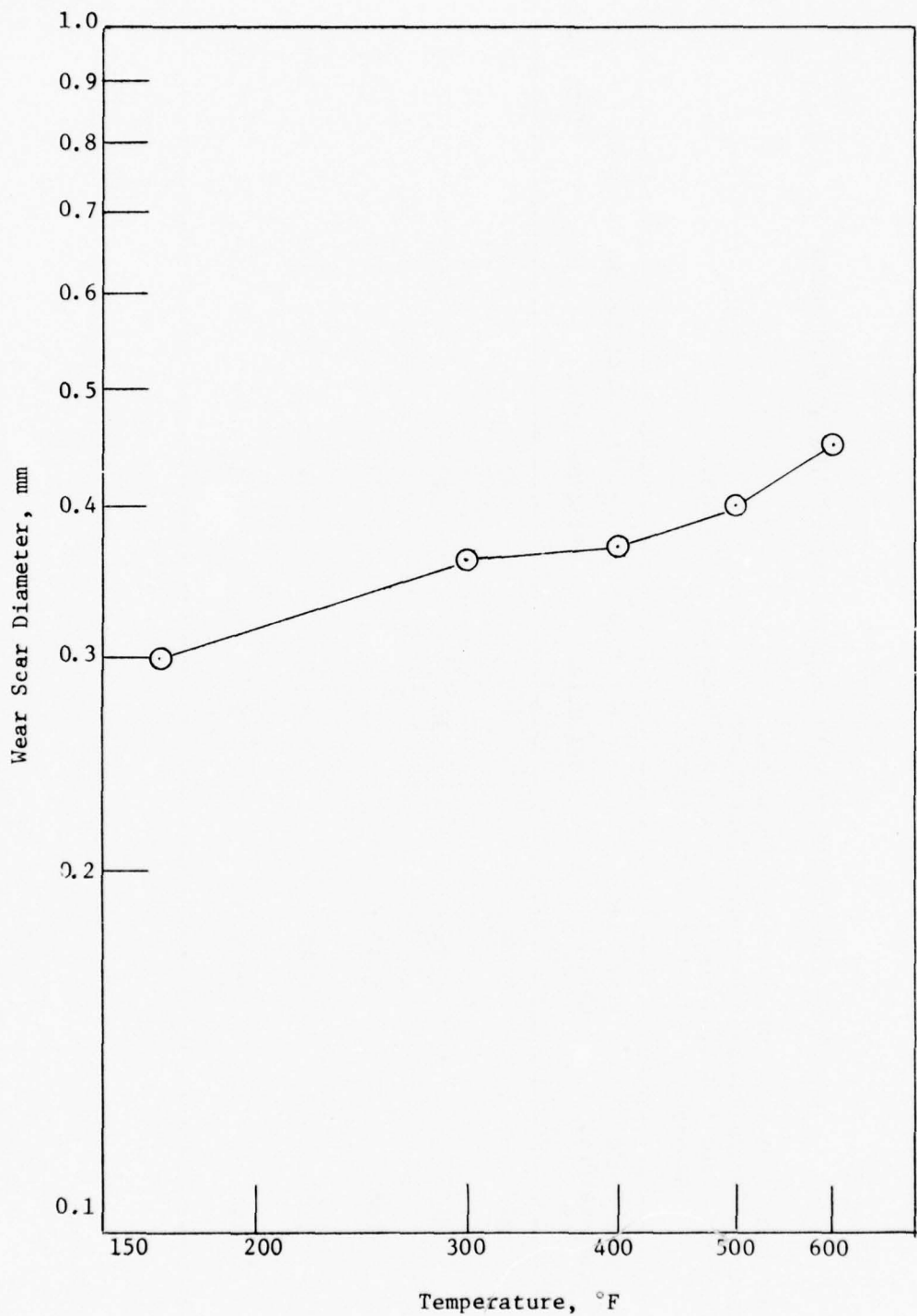


FIGURE 48. EFFECT OF TEMPERATURE ON WEAR, 1.0 WT% TRIBUTYL PHOSPHITE AT SLOW SPEED.

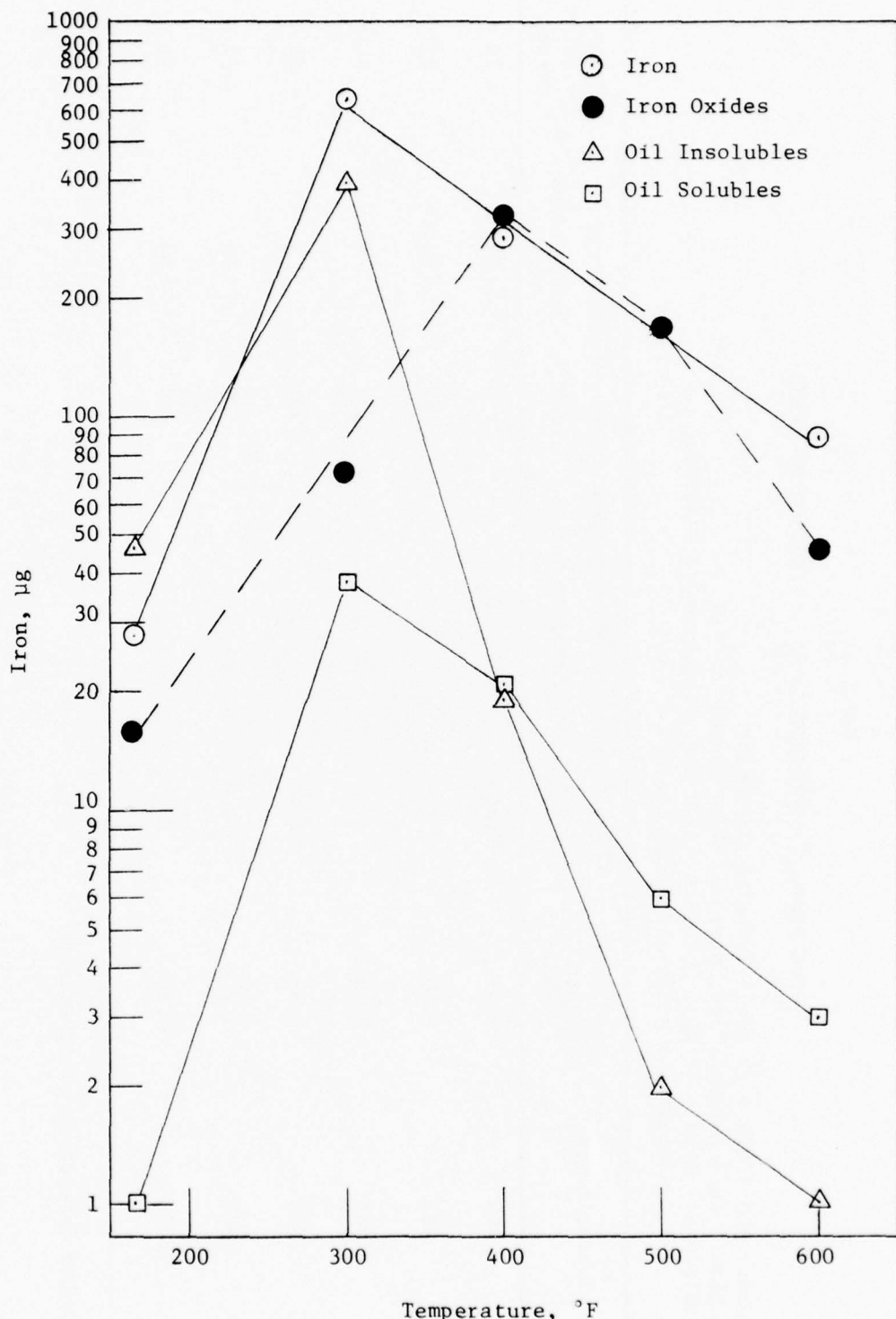


FIGURE 49. EFFECT OF TEMPERATURE ON WEAR PRODUCT DISTRIBUTION,  
1.0 WT% TRIBUTYL PHOSPHITE AT SLOW SLIDING.

Table 34

## WEAR PRODUCT DISTRIBUTION AS A FUNCTION OF SPEED

Test Fluid: MLO 7789A + 1% (Wt.) Tributyl Phosphite  
 Test Machine: GE/Brown Modified Four-ball Wear Tester  
 Test Conditions: Load = 40 kg., Duration = 100 min., Temperature = 167°F,  
 Atmosphere = dry air (0.25 l/min)

Run No.	Speed, r.p.m.	Wear Scar Diameter, mm.	Oil Solu.	Pyridine Solu.	Iron	Iron Oxides	Linear Velocity cm/sec
84	400	0.41	Trace	20	103	24	15
BAP	600	0.60	1	115	107	31	23
85	800	0.50	2	17	178	7	30
86	1000	0.49	BDC*	26	301	7	38
87	1500	0.72	Trace	25	509	36	57
88	2000	0.58	BDC	69	646	19	76

\*BDC = Below detectable concentration

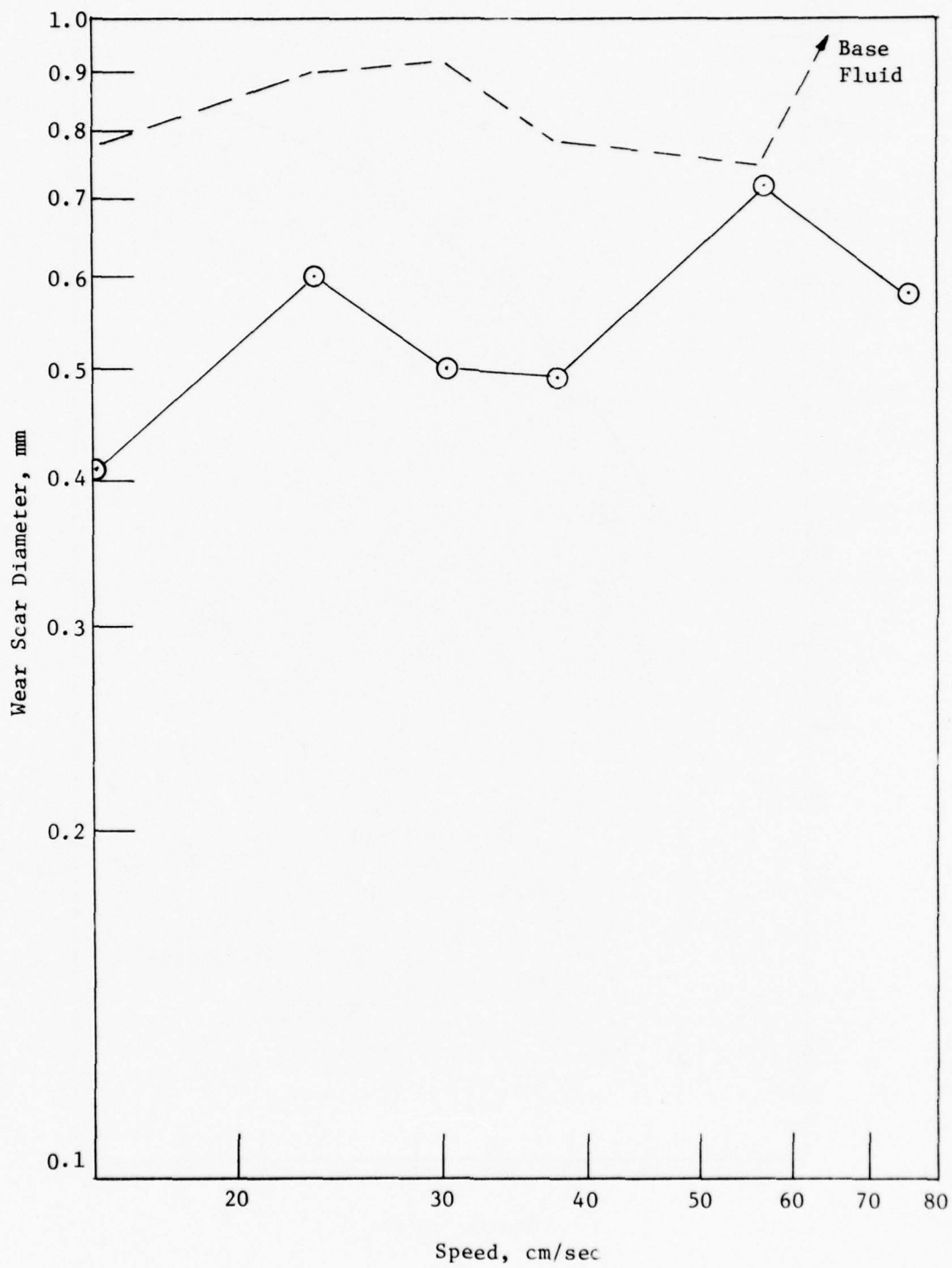


FIGURE 50. EFFECT OF SPEED ON WEAR, 1.0 WT% TRIBUTYL PHOSPHITE.

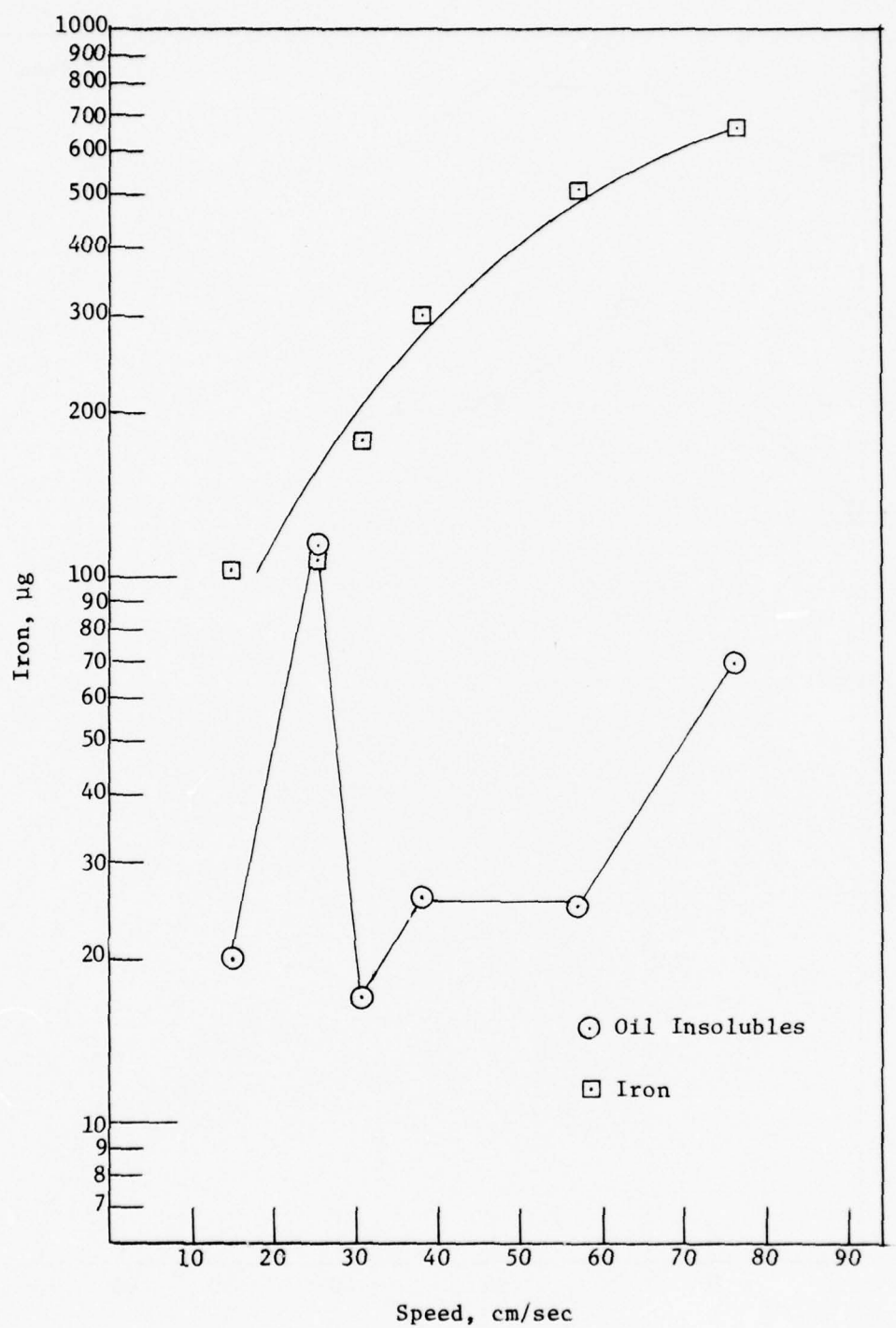


FIGURE 51. EFFECT OF SPEED ON WEAR PRODUCT FORMATION,  
1.0 WT% TRIBUTYL PHOSPHITE.

Table 35

## WEAR PRODUCT DISTRIBUTION AS A FUNCTION OF LOAD

Test Fluid: MLO 7789A + 1.0% (Wt.) Tributyl Phosphite  
 Test Machine: GE/Brown Modified Four-ball Wear Tester  
 Test Conditions: Speed = 600 r.p.m., Temperature = 167°F., Duration = 100 min.,  
 Atmosphere = dry air @ 0.25 l/min)

Run No.	Load, kg	Wear Scar Diameter, mm.	Oil Solu.	Pyridine Solu.	Recovered from Wear Debris in $\mu$ g as - - -	Iron	Iron Oxides	Iron Oxide to Iron Ratio
80	21	0.57	Trace	517	113	12	0.106	
BAP	40	0.60	1	115	107	31	0.290	
81	60	0.53	4	84	269	19	0.071	
82	90	0.59	2	30	324	10	0.031	
83	120	1.85	2	57	5265	805	0.016	

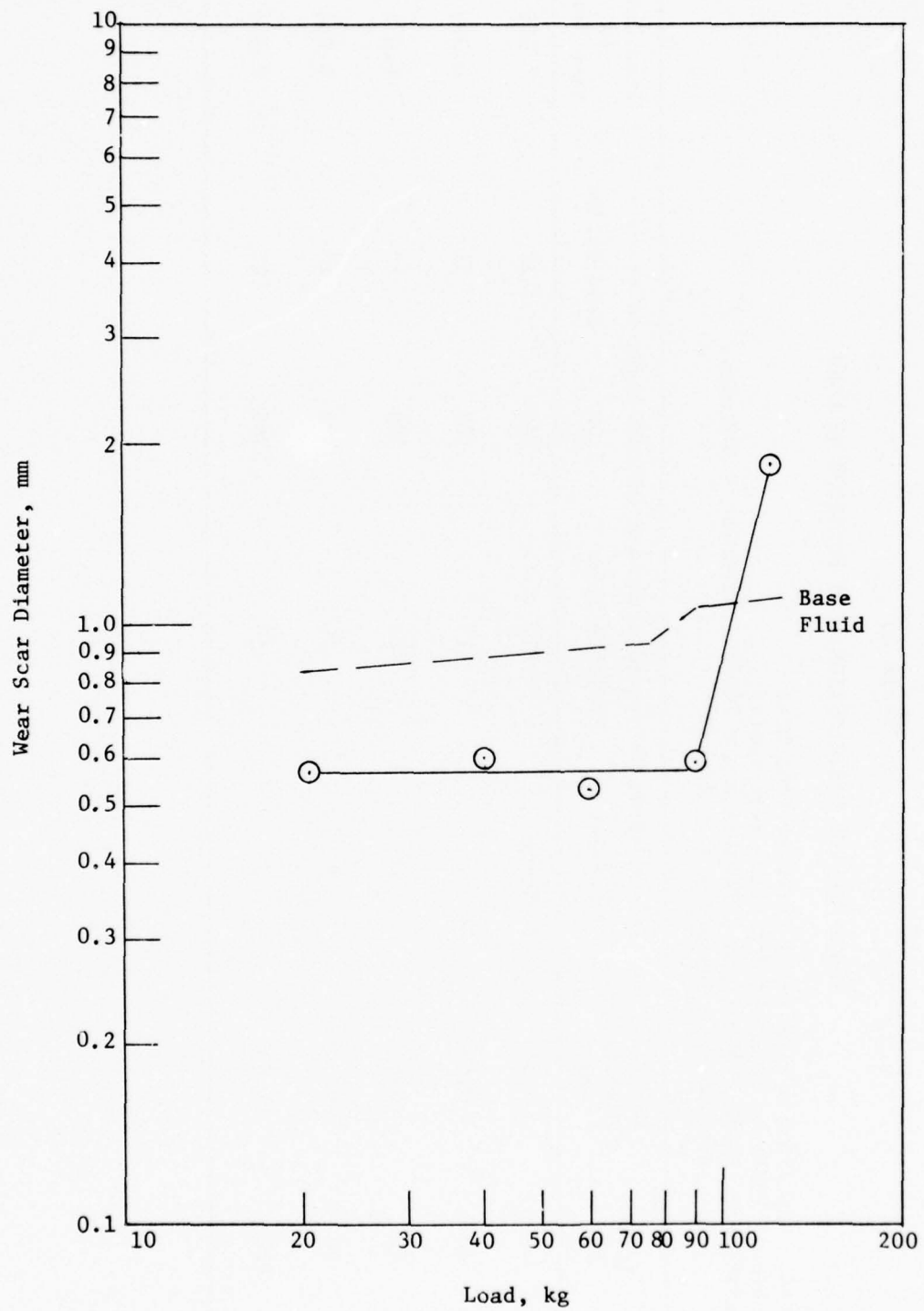


FIGURE 52. EFFECT OF LOAD ON WEAR, 1.0 WT% TRIBUTYL PHOSPHITE.

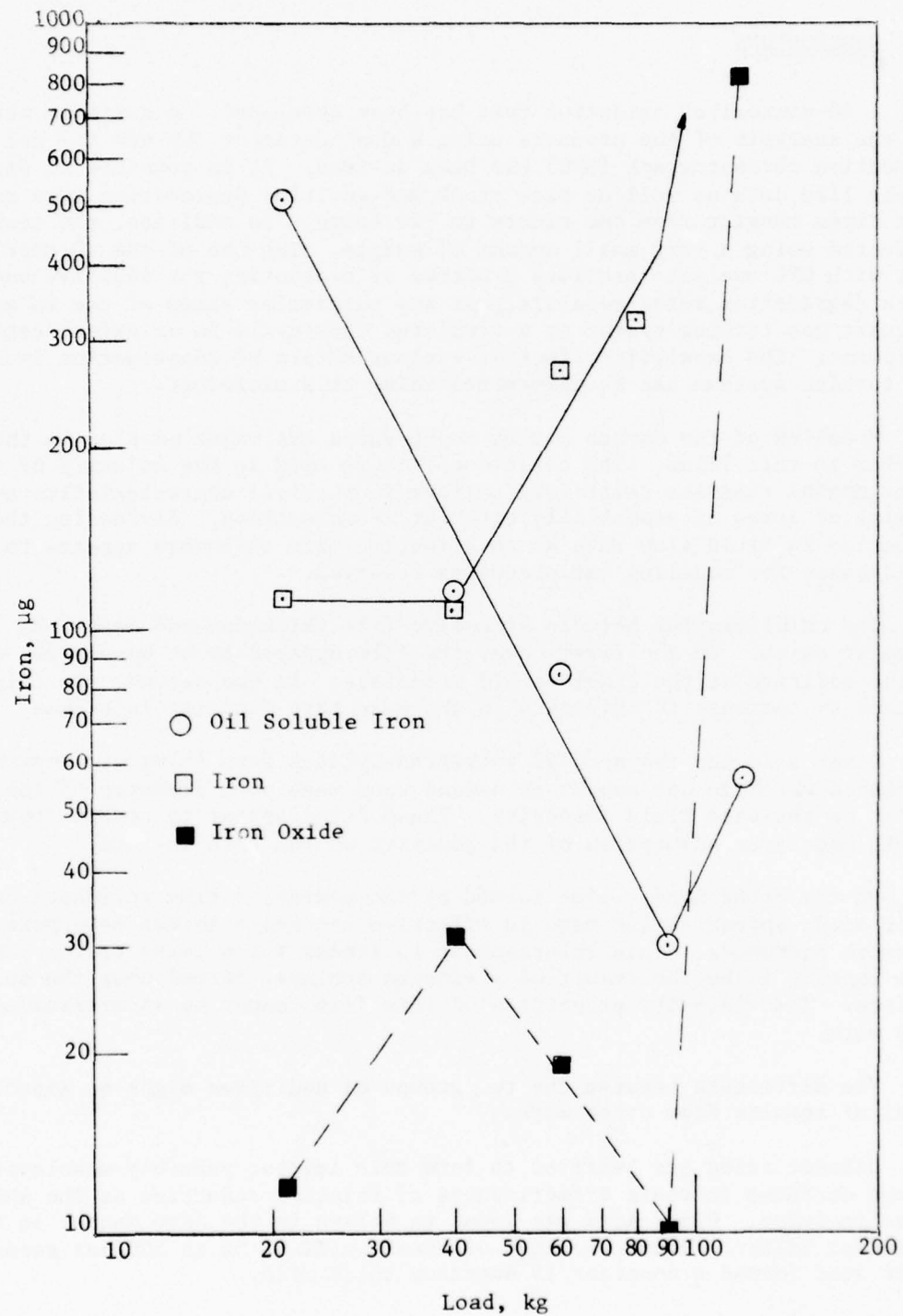


FIGURE 53. EFFECT OF LOAD ON WEAR PRODUCT FORMATION,  
1.0 WT% TRIBUTYL PHOSPHITE.

## 5. CONCLUSIONS

A 40-microliter oxidation test has been developed. A suitable method for the analysis of the products using a dual detector (UV and RI) gel permeation chromatograph (GPC) has been devised. It is possible to determine stable life data as well as base stock and additive degradation data using test times ranging from one minute to two hours. In addition, the test is conducted using a very small amount of sample. The use of the 40-microliter test with GPC analysis provides a method of evaluating the additive and base stock degradation rates separately at any particular stage of use in an aircraft gas turbine system or a simulated duty cycle in oxidation test equipment. The catalytic effect of various metals of construction in aircraft gas turbine systems can be determined using this microtest.

Modeling of the porous medium represented the major problem in the study of flow in thin films. The cellulose filters used in the majority of the experimental runs are relatively uniform in physical characteristics and consist of pores of essentially circular cross section. Expressing the reduction in fluid flow rate as an effective film thickness appears to be a valid basis for modeling the phenomena observed.

Two relationships between effective film thickness and mean pore diameter exist. In the first case, the film appears to be monolayer adsorption of the additive at the liquid-solid interface. In the second, the film appears to increase in thickness as the mean pore diameter increases.

Dimer acid and the n-octyl polymethacrylates form films of constant thickness which do not appear to depend upon mean pore diameter of the filter or the base fluid viscosity. These films appear to result from the simple monolayer adsorption of the additive on the pore surface.

On the other hand, films formed by the resins, barium sulfonate and oleic acid, appear to increase in effective thickness as the mean pore diameter increases. This relationship is linear for a heavy resin. This film appears to be the result of a viscous sublayer formed near the solid surface. The viscosity properties of this film cannot be ascertained from this work.

The difference between the two groups of additives might be expected in light of results from other work.

Dibasic acids are believed to form thin layers, possibly monolayer, that do not decrease in their effectiveness of friction reduction as the shear rates increase. Dimer acid was found to behave in the same manner in the cellulose filter. Over the range of shear rates of 50 to 500 per second, dimer acid formed a constant 15 Angstrom thick film.

Adsorption studies indicate essentially monolayer adsorption for polymers with the thickness of the polymer layer varying approximately as the square root of the molecular weight. In the case of n-octyl polymethacrylate-25 and n-octyl polymethacrylate-55, this behavior was found to be true.

Organic acids, on the other hand, are relatively ineffective at reducing friction at temperatures above their melting point. Oleic acid is also somewhat corrosive. Its effective film thickness varied from less than a monolayer to over two over the range of diameters studied. The resins and Acryloids, like oleic acid, have polar groups--acids or amines--that are readily accessible to groups on neighboring molecules. These additives exhibited effective film thicknesses that were larger than monolayer and generally increased as pore diameter increased. Stearic acid solutions below the melting point of stearic acid were found to provide relatively thick films on the order of 1500 Angstroms. Above the melting point, the effectiveness as a boundary lubricant decreased. In this study, stearic acid completely blocked flow through a 0.45 micron filter at 100 degrees Fahrenheit, yet flowed freely in a 0.1 micron filter at elevated temperatures. This type of behavior would be expected in light of adsorption studies where multilayer adsorption was found as the solubility limit was approached. The Acryloids effectively blocked the pores of an 0.45 micron filter. The structures formed by the Acryloids were much greater than a monolayer in thickness.

There are indications that additives may interfere with each other. That is, dispersing agents or antioxidants may interfere with the action of lubricity or antiwear agents. In the case of a dispersing agent and a heavy resin, there was a definite decrease in the effective film thickness for the combination of a barium sulfonated hydrocarbon (PRL 3530) and a heavy resin (MLO 7779) as compared with the heavy resin alone. In addition, di-2-ethylhexyl sebacate exhibited an effective viscosity increase over a nonpolar fluid in these filters. Oxidation products in the base fluid interfere similarly with the fluid flow in these cellulose filters.

Several tests with metal filters indicate that the cellulose filters behave in an equivalent manner. The cellulose filters have several advantages over the metal filters. In addition to being less costly, the cellulose filters provide a clean surface for adsorption, narrow pore size distributions, and pores that are nearly circular in cross section. Unfortunately, the filters are crushed under relatively low pressure drops, severely limiting the shear rates that can be studied.

An experimental technique has been developed to study the lubrication mechanism of oils. The method employs a Four-Ball Wear Tester, and the wear debris are subsequently analyzed with solvent extractions and atomic absorption spectroscopy. It offers insight into the chemical/mechanical interactions and pin points the critical role chemical reactions play in boundary lubrication.

The formation of the oil-soluble organometallic iron compounds is heavily influenced by the alcohol and the aromatic functional groups. The formation of the oil-insoluble organometallic iron compounds depends on the reactivity of the active functional groups, e.g., octadecyl bromide and stearic acid. It could be that the nature of the bonding and the density of the reacted molecules determine the film strength which in turn, controls the lubrication and wear.

Aromatics when mixed with paraffinic base stocks seem to have increased reactivity towards the iron surface as evidenced by the higher oil-insoluble iron generation than either of its components. Pure aromatics are more active chemically and more effective in wear reduction than are paraffins.

Stearic acid is a very effective antiwear agent. There is a saturation concentration above which further addition of the acid does not produce additional wear reduction.

The similarity of the chemical wear product distribution between the ZDP (zinc dialkyldithiophosphate), TCP (tricresyl phosphate), and the acid phosphate suggests that the acidic, phosphorus-containing impurities may be the effective antiwear agent.

Mixed additive studies indicate that depending on relative polarity and reactivity, one additive may blank other additives out of action. It illustrates the importance of preferential adsorption in lubrication processes. Oxygen does not seem to affect the working mechanism of the phosphorus-containing additives studied in this work. Sensitivity to additive concentration in terms of wear and organometallic compound formation suggests that there are multiple impurities/base stock interaction and competition for active sites at the metal surface.

The phosphite exhibits a different chemical mechanism than the phosphates studied in this work. A lubrication mechanism for tributyl phosphites has been proposed.

Temperature at the junction has been demonstrated to be the critical parameter in boundary lubrication. Mathematical models of wear, to be successful, have to recognize that temperature and chemical reaction rates are the critical parameters.

## APPENDIX

### EVALUATION OF WEAR PRODUCTS PRODUCED BY SOME CHEMICAL REACTIONS IN BOUNDARY LUBRICATION

by

A. C. Bose      E. E. Klaus  
E. J. Tewksbury

Prepared for Presentation at the JSLE-ASLE  
International Lubrication Conference  
Tokyo, Japan, June 9-11, 1975

Appendix of Annual Report  
AFML-TR-74-201, Part III, Prepared by  
Petroleum Refining Laboratory Division,  
Chemical Engineering Department  
The Pennsylvania State University

EVALUATION OF WEAR PRODUCTS PRODUCED BY  
SOME CHEMICAL REACTIONS IN BOUNDARY LUBRICATION

A. C. Bose<sup>(1)</sup>, E. E. Klaus<sup>(2)</sup>, and E. J. Tewksbury<sup>(3)</sup>

ABSTRACT

Previous studies of boundary lubrication with hydrocarbon-type lubricants and other "nonreactive" lubricants have identified the role of dissolved oxygen and water in the chemical reactions at the bearing surface. Additional studies with hydrocarbon-type lubricants and steel bearing surfaces have been used to show reaction products between constituents of the liquid lubricant and the metal bearing surface as well as between dissolved oxygen and the bearing surface. The test methods and analytical techniques necessary to show these small quantities of reaction products are also described.

Introduction. Boundary lubrication and/or thin film elastohydrodynamic lubrication have become increasingly important in recent years due to the general increase in bearing temperatures and loadings. Measured bearing surface temperatures and temperatures in the oil film in the conjunction are sufficiently high to promote chemical reactions (1). In fact the work of Larsen and Perry (2) suggested a large number of possible reactions that can take place under boundary lubrication conditions. The boundary lubrication process comprises these reactions that take place among the lubricant components or between the lubricant components and the metal bearing surface. It has been shown for saturated hydrocarbon lubricants (nonreactive lubricants) that dissolved oxygen, from the air above the lubricant, is an effective lubrication additive (3). It has also been demonstrated that the addition of an effective lubricity additive such as an alkyl acid phosphate will dominate the apparent chemical activity between the lubricant and the bearing surface (4).

---

(1) Chemical Engineer, Hooker Chemical Corp., Niagara Falls, New York 14302.

(2) Professor of Chemical Engineering in the Department of Chemical Engineering, College of Engineering, The Pennsylvania State University, University Park, Pennsylvania 16802.

(3) Associate Professor of Chemical Engineering in the Department of Chemical Engineering, College of Engineering, The Pennsylvania State University, University Park, Pennsylvania 16802.

Microcorrosion studies have been used to relate temperature and fluid composition to the reactions that occur between a fluid and a metal or metal oxide surface (5). These studies have demonstrated a temperature sensitive reaction sequence that produces organometallic compounds which progress from a relatively simple reaction product, which in many cases appears to be soluble in the test fluid, to a sludge or varnish similar to wear debris described as "friction polymer" (6). This study uses the four-ball wear tester to provide the boundary lubrication conditions to produce the surface chemical reactions. The analytical techniques developed to look at the organometallic products formed in corrosion have been adapted to the measurement of the relative amounts of organometallic, metal oxide and metal wear particles produced in the boundary lubrication process (7).

Test Procedure. The wear tests were conducted with a four-ball wear tester modified to provide a controlled atmosphere over the system. The tests were conducted in accordance with conventional test procedures. The preparation of the tester and the treatment of the wear debris after the test comprise the principal areas of interest. Prior to this test program, all the parts of the tester that come in contact with the test fluid and the vapor space above the fluid are cleaned with solvents and abrasives until no further material containing iron can be detected in the hot pyridine wash used to clean the test system. Pyridine is used in the test program to dissolve sludge and varnish produced in the tests. The pyridine solution is then evaluated for iron content using atomic absorption spectrometry.

Following a test in the four-ball wear tester the used fluid and the system parts are subjected to a special procedure to determine the oil soluble metal-containing compounds, the metal content in the sludge and varnish deposits soluble in pyridine, and the metallic and metal oxide particles resulting from the wear process. A flow plan for this procedure is shown in Table A.1. The first step in the separation of the wear products is the filtration of the liquid residue from the four-ball wear test through a 0.45 micron porosity filter that is resistant to hydrocarbon solvents but soluble in pyridine. The wear debris from the test system is washed onto the filter with petroleum naphtha, and the filtrate is used for the determination of oil soluble iron compounds. The filter paper, after the thorough wash with petroleum naphtha (220°F endpoint), is dried in a convection oven at 200°F and allowed to cool in a dessicator. The paper was previously tared in a similar manner. The weight gain of the filter is considered to be the total of the metal and metal oxide particles as well as the organic and organometallic insolubles. The total weight is determined to  $\pm$  2 micrograms. The organic debris is determined as the difference between the total weight and the metal found in the analysis.

The pyridine-soluble organometallic material and organic sludge is then separated from the metal and metal oxides which are not soluble in pyridine. Twenty milliliters of pyridine is used to wash the ball and ball pot. This pyridine is then used as a hot solvent for the filter paper containing the total insoluble wear debris. The pyridine solution is then filtered through a filter system insoluble in pyridine. Additional pyridine is used as the wash for the filter paper. This pyridine solution represents the soluble organometallics from the oil insoluble sludge.

The solid residue is assumed to be primarily metal and metal oxide particles. The iron oxide is removed from the iron in this procedure by a four normal HCl solution containing an acridine pickling inhibitor. The integrity of this separation was evaluated with known iron-iron oxide mixtures and the use of nitric acid to dissolve the iron without affecting the iron oxide. The final iron particles were dissolved in excess acid solution.

The oil-naphtha solution, the pyridine-organometallic solution and the two aqueous acid solutions were then evaluated for iron content in the atomic absorption spectrograph. Iron concentrations to less than 0.1 part per million can be measured in this unit. In all cases the analysis was made by comparing solutions of known metal concentrations with solutions containing the same solvents and at the same viscosity level. Tests on the four-ball wear tester that show good repeatability in wear values generally exhibit repeatability in metal distribution in the products of  $\pm 10$  percent.

Test Fluids. The test fluids used in this study include di-2-ethylhexyl sebacate and two super-refined mineral oils. The di-2-ethylhexyl sebacate used is a high quality, lubricant grade ester. This material shows excellent tricresyl phosphate response for lubrication improvement. Tricresyl phosphate response has been used to demonstrate the quality of the ester in terms of the low level of polar impurities present. The two super-refined mineral oils used are completely saturated white oils which contain no appreciable quantities of sulfur, nitrogen or oxygen in the form of polar impurities. Saturated hydrocarbons of this type show a strong response to dissolved oxygen as a lubricity additive. Super-refined mineral oil MLO 7789 has a 100°F viscosity level of 13 centistokes which is designed to match the 100°F viscosity of the di-2-ethylhexyl sebacate. The MLO 7625 super-refined mineral oil has a viscosity of 75 centistokes at 100°F. The two mineral oils differ in viscosity and molecular weight but contain the same type saturated hydrocarbon molecules. These two mineral oils were chosen to demonstrate the same chemical reactions in boundary lubrication and at the same time to provide different film thicknesses under elastohydrodynamic lubrication conditions.

Results and Discussion. A series of experiments was conducted with super-refined mineral oil MLO 7789 (13 centistokes at 100°F) to evaluate the role of oxygen in the fluid. The dissolved oxygen content was controlled by the atmosphere above the test fluid during the wear process. The data for these tests are shown on Table A.2. The oxygen concentration in the test fluid is estimated to be 40 ppm by weight in the tests under air (8), 0.5 ppm for the tests with nitrogen and less than 0.1 ppm for the tests under argon. The wear level indicates approximately equal severity for the three test conditions. The material balance for metals was compared by metal weight loss from the balls as well as total analysis of the fractions of the wear debris and test fluid under atomic absorption spectrographic techniques. The excellent correlation between these two test systems is typical of the demonstrated analytical capability of this method of debris analysis.

The organic portion of the insoluble wear debris ranges from 77 to 85 percent of the total in these three tests. The high percentage of organic

constituents is typical for scuffing wear on the four-ball wear tester. The indications are that the environment in the wear conjunction favors chemical reactions even when oxygen and polar constituents in the lubricant are at low concentrations. The results of the analysis for iron reacted with the lubricant can be compared with results from corrosion studies at moderate temperatures. The corrosion studies (5) show the formation of oil soluble organometallic compounds under mild conditions which upon further reaction become oil insoluble. More severe conditions tend to produce the oil insoluble (pyridine soluble) organometallic compounds more rapidly. The presence of pyridine soluble but no oil soluble organometallic compounds may reflect the severity of the environment in which these products are formed. Recent studies suggest that elastohydrodynamic film temperatures are of the order of 650°F (1) and there is evidence of higher temperatures in boundary lubrication in four-ball wear testers.

These data do show a sensitivity to oxygen concentration in both iron oxide and organometallic formation. It has been suggested that the effect of oxygen in nonreactive lubricants is that of lubricity additive. It has been shown that oxygen diffusion in some studies can provide the necessary oxygen at the metal surface to provide an iron oxide film (9,10). The data on Table A.2 suggest that the interaction of the liquid lubricant with the oxygen and the metal surface may play a critical role in the wear process. While all of the debris systems containing metal respond to the concentration of oxygen dissolved in the fluid, the largest response is in the formation of organometallic material. This product would appear to be related to corrosive wear.

The effect of oxidation inhibitors on the chemical reactions in the bearing conjunction has been evaluated for two super-refined mineral oils and di-2-ethylhexyl sebacate as shown in Table A.3. The wear tests were conducted at 40 kilograms to provide severe boundary conditions and an appreciable wear scar. For these tests the iron and iron oxide in the wear debris were analyzed as a single measurement. In all three cases the amount of organic and organometallic debris is substantially reduced by the addition of the oxidation inhibitor (Table A.4). The reduction of chemical activity by the oxidation inhibitor in the super-refined mineral oils also appears to reduce the total amount of iron involved in total wear debris. In fact the reduction in reactivity in the formation of all wear debris by the use of an oxidation inhibitor appears to be parallel to the effect of lowering oxygen availability for the uninhibited fluid shown in Table A.2. These data indicate that the lack of chemical reaction between the lubricant and the bearing surface may well result in a reduction in wear from metal particles and oxide formation.

The ester studied shows the same reduced trend for reaction between the metal and the lubricant in the presence of the inhibitor. However, the total wear including metal particles and metal oxide formation is not reduced. Tests with the ester in a nitrogen atmosphere show corrosion tendencies as severe or more severe than those of the uninhibited ester in the presence of oxygen. Both microcorrosion tests (5) and wear tests with di-2-ethylhexyl sebacate under a nitrogen atmosphere show corrosive characteristics.

Microcorrosion studies (5) with steel surfaces and mild oxidation conditions at 347°F produce an oil soluble organometallic product which is then converted by further reaction with oxygen to an oil-insoluble, pyridine-soluble organometallic material. Indications are that the more severe the test conditions the faster the conversion of the organometallic to the oil insoluble phase. The presence of an oxidation inhibitor has the effect of reducing the rate of production of organometallic product at a given temperature and level of oxygen. One effect of the presence of oxidation inhibitor in the test fluids is the reduction of total organometallic compounds produced as shown on Table A.3. In two of the three tests with inhibited fluids some oil soluble organometallic product is evident. These data suggest that wear control may be more closely related to the oxygen-fluid activity than to the activity between the oxygen and the metal of the bearing surface. These data show that the same general results can be achieved by reducing the rate of reaction between the dissolved oxygen and the liquid lubricant as by reducing the amount of oxygen available. Based on these data the role of direct action between the bearing surface and the dissolved oxygen does not appear to be the controlling factor in wear.

A significant problem in the evaluation of wear debris as a function of condition in the wearing conjunction of the four-ball wear tester is the continuous change in unit loading in the bearing as the wear surface changes. The changing pressure will also influence the film thickness in the conjunction and the temperature and pressure conditions contributing to the chemical reaction that might take place as well as the kinetics of the reaction. The choice of a 40-kilogram load in the four-ball wear tester is designed to produce a large wear scar and a more significant volume of fluid in the reaction zone. However, at the start of each test the load and temperature in the conjunction are at the maximum value and the volume of lubricant in the conjunction at a minimum. At the end of the one-hour test the load and temperature of the conjunction are probably at a minimum value and the volume of the liquid lubricant at a maximum.

In order to observe the differences between the behavior of the fluid lubricant and the conditions in the wear conjunction, a series of sequential tests have been used. A single, one-hour four-ball wear test is used as the severe portion of the sequential test. The analysis from this one-hour test is carried out using the analytical procedures described with minor modifications. The wear scars are measured without removing the balls from the ball pot. The debris is removed from the ball pot and spindle without disturbing the geometry of the four-ball wear tester. A second one-hour wear test is then conducted with the same bearing system with a new charge of test fluid. The second hour test starts on the wear scar generated by the first hour and shows only a small change in scar size during this portion of the test. Sequential tests for di-2-ethylhexyl sebacate and the two super-refined mineral oils are shown in Tables A.4 and A.5. Tests are shown for both air and nitrogen atmospheres.

The results of the reduction of environmental severity (temperature and pressure) on the reaction between the oxygen, the fluid and the metal is

consistent. The second test in the sequence produces a much smaller quantity of organometallic product than the first test where conditions are more severe. The reduction in test severity for the second test in the sequence also changes the type of organometallic product formed. In all of the second sequential tests there is evidence of oil soluble organometallic product. As suggested previously, this type of organometallic product is associated with test conditions that are less severe than those producing only oil-insoluble, pyridine-soluble organometallic product.

The amount of iron and iron oxide particles generated in the sequential tests is substantially the same for both of the sequential tests. The large quantity of surface area of iron and iron oxide generated under the fluid surface has been considered to be a potential catalytic source for the reactions involving the generation of organic and organometallic products found in the wear debris. The presence of the large surface areas on the wear scar and metal wear debris for the second run in the sequence obviously did not contribute to the generation of increased quantities of organometallic product. The production of these organometallics appears to follow the predicted reduction in surface temperatures with increasing bearing area. The most notable point of data to illustrate this trend is the case of the high viscosity super-refined mineral oil MLO 7625 (75 centistokes at 100°F) which shows by far the largest reduction in the generation of organometallics in the second test in the sequence.

A series of tests, starting in each case with a new set of test balls, has been run to evaluate the effect of test time and severity on a cumulative basis. These tests also provide a series of check points to establish the repeatability of this test method. A series of tests between 5 and 140 minutes have been utilized to evaluate the role of the reaction producing the organometallic product in the run-in of a four-ball wear tester. For these tests only the total organometallics and the sum of metal and metal oxide wear debris are determined. The wear values for di-2-ethylhexyl sebacate are shown in Figure A.1 and those for MLO 7625 super-refined mineral oil are shown on Figure A.2. Both figures show the same general trends. That is, the formation of iron and iron oxide in the insoluble wear debris increases linearly with test time. The concentration of the organometallic products shows a typical wear-in period followed by a period of little additional activity in the formation of these products. These data suggest that the chemical activity associated with boundary lubrication may be determined by the organometallic product formed. Adhesive wear on the other hand may be less directly related to chemical reaction at the bearing surface.

Conclusions. The four-ball wear tester can be used successfully as a boundary lubrication tester for the study of the chemical effects that take place at the wearing surfaces. Relative amounts of metallic and metal oxide as well as organometallic and organic wear debris can be measured repeatably for lubrication under a variety of load and environmental conditions.

For super-refined mineral oils where dissolved oxygen has been shown to be an effective lubricity additive, a significant reaction between the

lubricant; oxygen; and the metal appears to play an important role in the lubrication mechanism. The reduction in the formation of organometallic product as well as a reduction in iron oxide debris with reduced oxygen concentration demonstrates the separate chemical reaction paths of oxygen in boundary lubrication. The improvement in wear with reduced oxygen concentration appears to indicate a relationship between chemical reaction and the wear mechanism.

The relative concentrations of organometallic product as a function of test time indicates that the chemical reaction producing the organometallic products determines the relative severity of wear. The use of oxidation inhibitors which control the rate of reaction between oxygen, the fluid, and the metal surface has an effect similar to that of lowering the oxygen concentration. Conditions which, based on elastohydrodynamic theory, tend to lower the environmental severity in the concentrated contact zone also lower the chemical activity noted.

The trends noted in this activity are all consistent with the predicted qualitative trends of reaction kinetics. More quantitative data could be produced with additional analytical refinements using these general test techniques.

#### ACKNOWLEDGEMENT

This research was supported in part by the United States Air Force under Contracts AF33615-69-C-1183 and AF33615-73-C-5101 monitored by the Air Force Materials Laboratory, Nonmetallic Materials Division, Lubricants and Tribology Branch, Wright-Patterson Air Force Base, Ohio 45433.

## BIBLIOGRAPHY

- (A.1) Turchina, V., D. M. Sanborn and W. O. Winer, "Temperature Measurements in Sliding Elastohydrodynamic Point Contacts," *J. of Lubrication Technology*, 96, pp. 464 (1974).
- (A.2) Larsen, R. G. and G. L. Perry, "Chemical Aspects of Wear and Friction," Mechanical Wear, Chapter V, pp. 73-94. Edited by J. T. Burwell, Jr., American Society of Metals, January 1950.
- (A.3) Klaus, E. E. and H. E. Bieber, "Effect of Some Physical and Chemical Properties of Lubricants on Boundary Lubrication," *ASLE Trans.*, 7, pp. 1-10 (1964).
- (A.4) Bieber, H. E., E. E. Klaus, and E. J. Tewksbury, "A Study of Tricresyl Phosphate as an Additive for Boundary Lubrication," *ASLE Trans.*, 11, pp. 155-161 (1968).
- (A.5) Klaus, E. E. and E. J. Tewksbury, "Microcorrosion Studies with Functional Fluids," *Lubr. Engr.*, 29 (5), pp. 205-211, May 1973.
- (A.6) Fein, R. S. and K. L. Kreuz, "Chemistry of Boundary Lubrication of Steel by Hydrocarbons," *ASLE Trans.*, 8, pp. 29-38 (1965).
- (A.7) Bose, A. C., "Studies of Chemical Reactions in Boundary Lubrication," M.S. Thesis, The Pennsylvania State University, University Park, PA (1973).
- (A.8) Smith, D. B., "Some Effects of Dissolved Gases on Boundary Lubrication," M.S. Thesis, The Pennsylvania State University, University Park, PA (1964).
- (A.9) Tao, F. F., "A Study of Oxidation Phenomena in Corrosive Wear," *ASLE Trans.*, 12, pp. 97-105 (1969).
- (A.10) Tao, F. F., "The Role of Diffusion in Corrosive Wear," *ASLE Trans.*, 11, pp. 121-130 (1968).

Table A.1

## FLOW PLAN FOR SEPARATION OF WEAR DEBRIS

<u>Step 1</u>	(A) Test Fluid Wear Debris Wear Tester Ball Pot and Spindle	Wash with Petroleum Naphtha Solvent Filter through 0.45 Micron Hydrocarbon Resistant Filter	(B) Filtrate of Oil + Solvent + Oil Soluble Reaction Products	(C) Insoluble Sludge + Iron Oxides Iron Particles
<u>Step 2</u>	(C) Wear Tester Ball Pot and Spindle Filter Containing Sludge, Iron Oxide, and Iron	Wash with Pyridine Solvent Filter through 0.45 Micron Pyridine Resistant Filter	(D) Filtrate of Pyridine + Pyridine Soluble Organo- metallic Products	(E) Iron Oxide + Iron Pyridine Insolu- ble Sludge
<u>Step 3*</u>	(E) Iron Oxide, Iron, and Pyridine Insoluble Sludge	4 N HCl + 0.001 N Acridine	Filter through 0.45 Micron Filter	(F) Filtrate Containing Dissolved Fe Oxides as $FeCl_3$
<u>Step 4*</u>	(E) Iron Oxide Iron Pyridine Insoluble Sludge	+ 6N $HNO_3$	Filter through 0.45 Micron Filter	(G) Insoluble Sludge and Iron on Filter
				(H) Filtrate Containing Dissolved Fe as $Fe(NO_3)_3$
				(I) Insoluble Sludge and Iron Oxide on Fil- ters

\*Order of these steps can be reversed without altering analytical results.

Table A.2

## EFFECT OF ATMOSPHERE ON WEAR PRODUCTS

Four-Ball Wear Test Conditions Include: Test Speed = 600 r.p.m.; Load = 40 kg.; Test Temp. = 167°F;  
 Fluid Charged = 20 ml.; Test Time = 1 hr.; and Balls = 52-100 Steel, PRL Batch No. 15.

Test Fluid: Super-refined Paraffinic Mineral Oil (MLO 7789)

Average Wear Scar Diameter, mm.	Test Atmosphere	Pyridine Soluble Metal, mg.	Oil Soluble Metal, mg.	Fe-Oxide Metal, mg.	Fe-Metal mg.	Pyridine Insoluble Metal, mg.		by bearing weight difference (B)	by adding all soluble and insoluble metals (A)	Total Metal Loss, mg.	Organic Debris, mg. (A-B)
						by bearing weight difference (B)	by adding all soluble and insoluble metals (A)				
0.78	Dry Air	0.0752	BDL*	0.1287	0.0167	0.22	0.2206	1.50	1.28		
0.71	Nitrogen	0.0427	BDL*	0.0948	0.0292	0.18	0.1667	1.05	0.87		
0.73	Argon	0.0198	BDL*	0.0806	0.0450	0.15	0.1454	0.64	0.49		

\* Below limit of detection.

Table A.3

## WEAR DEBRIS FORMED BY SEVERAL INHIBITED FLUIDS

Four-Ball Wear Test Conditions Include: Test Speed = 600 r.p.m.; Load = 40 kg.; Test Temp. = 167°F.; Test Time = 1 hr.; Fluid Charged = 20 ml.; Test Atmosphere = Dry Air at 0.7 liter/hour; and Bearings = 52-100 Steel, PRL Batch No. 15.

Test Fluids: 1. Di-2-Ethylhexyl Sebacate (MLO 7710) + 0.5 Weight Percent Phenothiazine

2. Super-refined Paraffinic Mineral Oil (MLO 7789) + 1.0 Wt.% Hindered Phenol

3. Super-refined Naphthenic Mineral Oil (MLO 7625) + 1.0 Wt.% Hindered Bisphenol

Test Fluid	Average Wear Scar Diameter, mm.	Pyridine Soluble Metal, mg.	Oil Soluble Metal, mg.	Pyridine Insoluble Metal, mg.	by bearing weight	by adding 1ml. soluble difference and insoluble metals	Total Debris, mg.	Organic Debris, mg. (A-B)	Total Metal Loss, mg.
									(A)
1	0.83	0.0073	0.0040	0.1493	0.18	0.1606	0.253	0.073	
2	0.70	0.0346	0.0031	0.1117	0.15	0.1494	1.20	1.051	
3	0.54	0.0066	BDL*	0.0765	0.09	0.0831	0.65	0.567	

\* Below limit of detection.

Table A.4  
WEAR PRODUCTS FROM FIRST HOUR RUN IN THE FOUR-BALL WEAR TESTER

Four-Ball Wear Test Conditions Include: Test Speed = 600 r.p.m.; Load = 40 kg.; Test Temp. = 167°F.; Fluid Charged = 20 ml.; Test Time = 1 hr.; and Bearings = 52-100 Steel, PRL Batch No. 14.

Test Fluids: Super-refined Paraffinic Mineral Oil (MLO 7789)  
Super-refined Naphthenic Mineral Oil (MLO 7625)  
Di-2-Ethylhexyl Sebacate (MLO 7710)

Test Fluid	Average Wear Scar Diameter, mm.	Test Atmos.	Pyridine Soluble Metal, mg.	Oil Soluble Metal, mg.	Pyridine Insoluble Metal, mg.	Total Metal Loss, mg.		Organic Debris, mg. (A-B)
						by bearing weight difference (B)	by adding all soluble and insoluble metals (A)	
MLO 7710	0.74	Dry Air	0.0782	BDL*	0.1114	0.16	0.1896	1.17
MLO 7789**	0.78	Dry Air	0.0752	BDL*	0.1454	0.22	0.2206	1.50
MLO 7625	0.53	Dry Air	0.0658	BDL*	0.1075	0.22	0.1733	1.09
MLO 7710	0.70	Nitrogen	0.0740	BDL*	0.1166	0.21	0.1906	1.17
MLO 7789	0.71	Nitrogen	0.0427	BDL*	0.1240	0.18	0.1667	1.05
MLO 7625	0.47	Nitrogen	0.0633	BDL*	0.0921	0.17	0.1554	0.54
								0.37

\* Below limit of detection.

\*\* Data also appears on Table A.2.

Table A.5

## WEAR PRODUCTS FROM A SECOND HOUR TEST USING "RUN-IN" BEARING SYSTEM

Four-Ball Wear Test Conditions Include: Test Speed = 600 r.p.m.; Load = 40 kg.; Test Temp. = 167°F.; Fluid Charged = 20 ml.; Test Time = 1 hr.; and Bearings = 52-100 Steel, PRL Batch No. 15

Test Fluids: Di-2-Ethylhexyl Sebacate (MLO 7710)  
Super-refined Paraffinic Mineral Oil (MLO 7789)  
Super-refined Naphthenic Mineral Oil (MLO 7625)

Test Fluid	Average Wear Scar Diameter, mm.	Test Atmosphere	Pyridine Soluble Metal, mg.	Oil Soluble Metal, mg.	Pyridine Insoluble Metal, mg.	Total Metal Loss, mg.	Total Debris, mg. (A)	Organic Debris, mg. (A-B)
MLO 7710	0.99	Dry Air	0.0029	0.0023	0.1585	0.1637	3.24	3.08
MLO 7789	0.84	Dry Air	0.0130	0.0022	0.1655	0.1807	1.17	0.99
MLO 7625	0.58	Dry Air	0.0168	0.0029	0.0350	0.0539	3.40	3.35
MLO 7710	0.93	Nitrogen	0.0030	0.0089	0.1448	0.1567	3.33	3.17
MLO 7789	0.84	Nitrogen	0.0119	0.0011	0.0885	0.1015	1.41	1.31
MLO 7625	0.53	Nitrogen	0.0051	0.0005	0.0295	0.0351	2.94	2.90

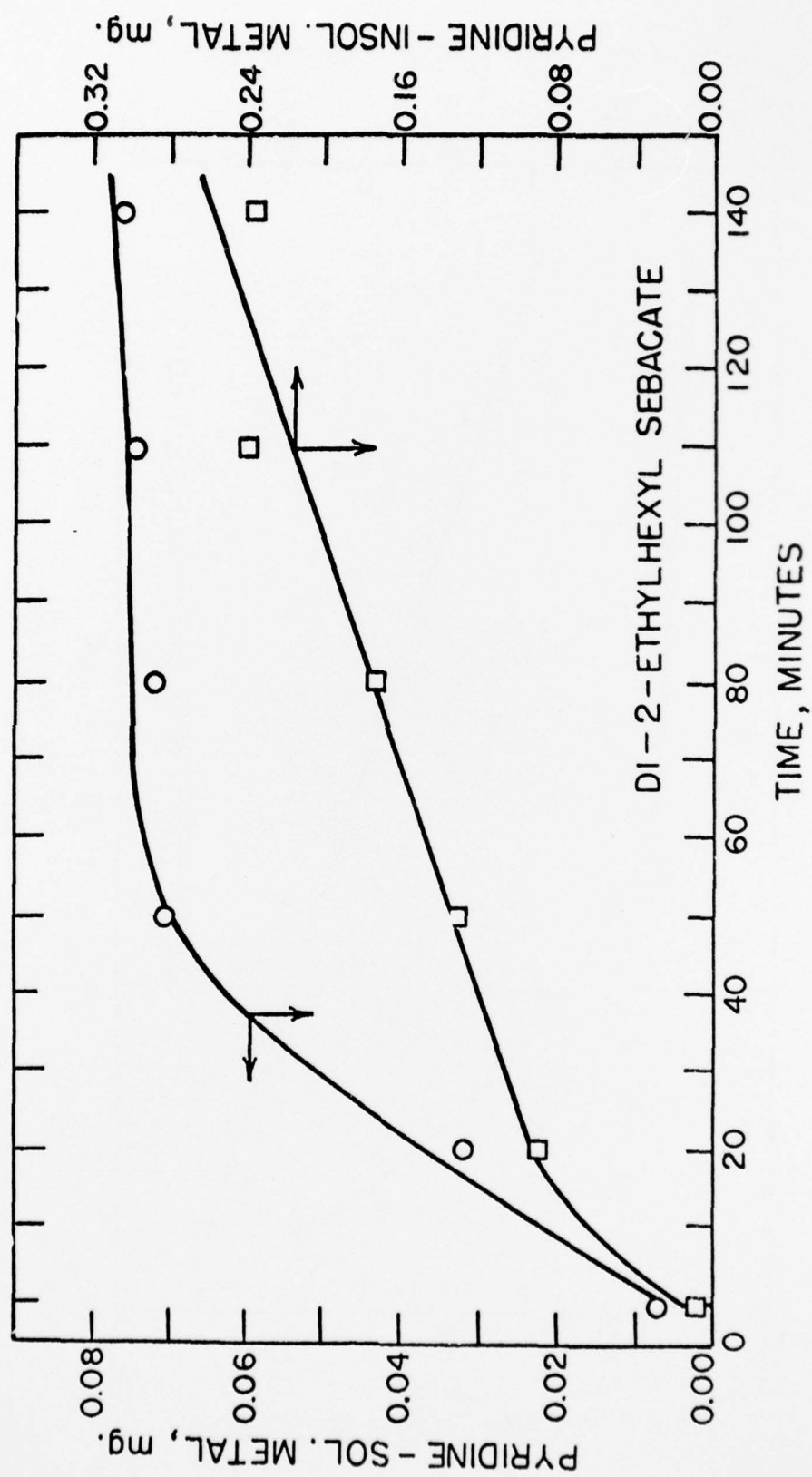


Figure A.1 METALLIC WEAR PRODUCTS AS A FUNCTION OF TIME

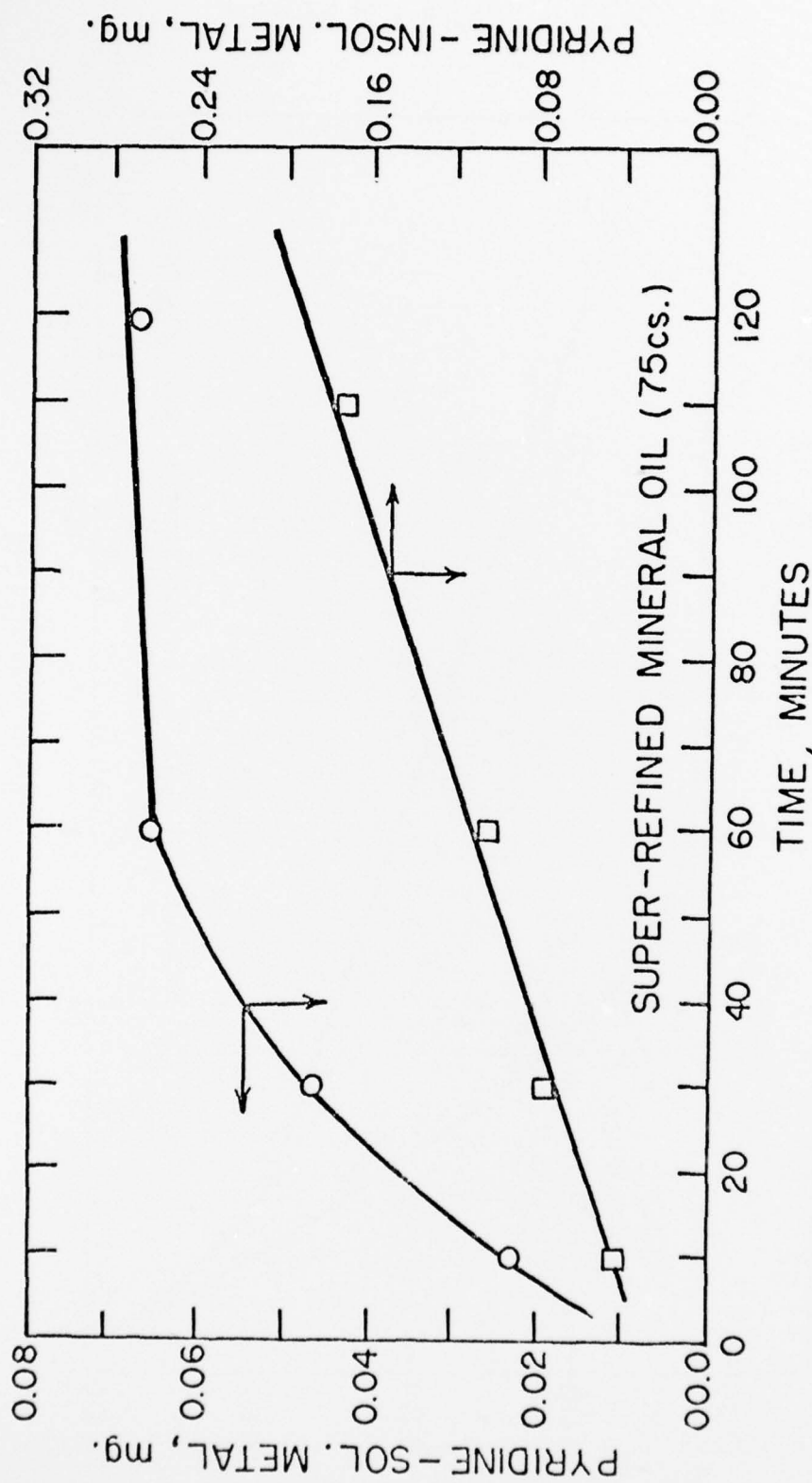


Figure A.2 METALLIC WEAR PRODUCTS AS A FUNCTION OF TIME

#### REFERENCES

1. Benoit, H., Grubisic, Z., Rempp, P., Decker, D., and Zilliox, J. G., *J. Chim. Phys.*, 63, 1507 (1966).
2. Grubisic, Z., Rempp, P., and Benoit, H., *J. Polym. Sci., Part B*, 5, 753 (1967).
3. Haley, G. A., *Anal. Chem.*, 43, 371 (1971).
4. Freeman, D. H., *J. of Chromatographic Science*, 11, 175 (1973).
5. Cazes, J., and Gaskill, D. R., *Separation Science*, 4 (1), 15 (1969).
6. Gogswell, T. E., McKay, J. F., and Latham, D. R., *Anal. Chem.*, 43, 645 (1971).
7. Freeman, D. H., Angeles, R. M., Enagonio, D. P., and May, W., *Anal. Chem.*, 45, 768 (1973).
8. Hazell, J. E., Prince, L. A., and Stapelfeldt, H. E., *J. Polym. Sci., Part C*, 21, 43 (1967).
9. Dullien, F. A. and Batra, V. K., "Determination of the Structure of Porous Media," *Ind. and Eng. Chem.*, 62 (10), (1970).
10. Zorin, Z. B., Sobolev, V. D. and Churaev, N. B., "The Measuring of Capillary Pressure and Viscosity of Fluids in Quartz Microcapillaries," *Doklady Akademii Nauk, SSSR*, 193 (3), (1970).
11. Karasev, V. V. and Deryagin, B. V., "Study of Boundary Viscosity by the Method of Blowing Away," *Kolloid I. Zhurnal*, 15 (5), (1953).
12. Deryagin, B. U., Karasev, V. V., Lavygin, I. A., Skorokhodov, I. I. and Khromova, E. N., "Boundary Viscosity of Some Polydimethylsiloxanes," *Doklady Akademii Nauk, SSSR*, 187 (4), (1969).
13. Bos, A., "The Temperature at the Wear Scars of the Four-Ball Apparatus," *Wear*, 31, pp. 17-27, 1975.
14. Cameron, A. and Gentle, C. R., "Mechanics and Thermodynamics in Lubrication." NASA Sym. Preprint, Interdisciplinary Approach to Liquid Lubricant Technology, Cleveland, Ohio, Jan. 1972.
15. Bailey, M. W. and Cameron, A., "The Effects of Temperature and Metal Pairs on Scuffing." ASLE Trans., 16, 2, 121-131, 1973.

16. Groszik, A. J., "Wear-Reducing Properties of Mineral Oils and Their Fractions." Proc. Inst. Mech. Engr., 182, Pt. 3N, 160-168, 1967-68.
17. Appeldoorn, J. K. and Tao, F. F., "The Lubricity Characteristics of Heavy Aromatics." Wear, 12, 117-130, 1968.
18. Beerbower, A. and Goldblatt, I. L., "An Interpretation of Wear Observed with Natural Hydrocarbons." Wear, 18, 421,
19. Whitby, R. D., "Comments on 'An Interpretation of Wear Observed with Natural Hydrocarbons'." Wear, 20, 235-236, 1972.
20. Beeck, O., Givens, J. W. and Smith, A. E., "On the Mechanism of Lubrication. I. The Action of Long-Chain Polar Compounds." Proc. Roy. Soc., Vol. A177, pp. 90-102, 1940.
21. Beeck, O., Givens, J. W. and Williams, E. C., "On the Mechanism of Lubrication. II. Wear Prevention by Addition Agents." Proc. Roy. Soc., Vol. A177, pp. 103-118, 1940.
22. Davey, W., "Extreme Pressure Lubricants. Phosphorus Compounds as Additives." Ind. Eng. Chem., Vol. 42, pp. 1841-7, 1950.
23. Bieber, H. E., Klaus, E. E. and Tewksbury, E. J., "A Study of Tricresyl Phosphate as an Additive for Boundary Lubrication." ASLE Trans. 11, pp. 155-161, 1968.
24. Bennett, P. A. and Kabel, R. H., "The Anti-Scuff Performance of Metal Organo-dithiophosphate Additives." Lubrication Eng., Vol. 19, No. 9, pp. 365-370, 1963.
25. Gallopoulos, N. E., "Thermal Decomposition of Metal Dialkyldithiophosphate Oil Blends." ASLE Trans. 7, pp. 55-63, 1964.
26. Rowe, C. N. and Dickert, J. J., Jr., "The Relation of Anti-Wear Function to Thermal Stability and Structure for Metal 0,0-Dialkylphosphoro-dithioates." ASLE Trans. 10, pp. 85-90, 1967.
27. Furey, M. J. and Kunc, J. F., Jr., "A Radiotracer Approach to the Study of Engine Valve Train Lubrication." Lub. Engr., 14, pp. 302-309, 1958.
28. Loeser, E. H., Wiquist, R. C., and Twiss, S. B., "Cam and Tappet Lubrication III - Radioactive Study of Phosphorus in the EP Film" ASLE Trans. 1, 329-335, 1958.
29. Loeser, E. H., Wiquist, R. C., and Twiss, S. B., "Cam and Tappet Lubrication. IV - Radioactive Study of Sulfur in the EP Film." ASLE Trans. 2, 199-207, 1959.

30. Furey, M. J., "Film Formation by an Anti-Wear Additive in an Automotive Engine." ASLE Trans. 2, 91-100, 1959.
31. Bennett, P. A., "A Surface Effect Associated with the Use of Oils Containing Zinc Dialkyl Dithiophosphate." ASLE Trans. 2, 78-90, 1959.
32. Barton, D. B., Klaus, E. E., Tewksbury, E. J., and Strang, J. R., "Preferential Adsorption in the Lubrication Process of Zinc Dialkyl dithiophosphate." ASLE Trans., 16, 3, 161-167, 1973.
33. Forbes, E. S. and Battersby, J., "The Effect of Chemical Structure on the Load-Carrying and Adsorption Properties of Dialkyl Phosphites." ASLE Trans., 17, 4, pp. 263-270, 1974.
34. Davey, W., "Extreme Pressure Lubricants. Phosphorus Compounds as Additives." Ind. Eng. Chem., Vol. 42, pp. 1841-7, 1950.
35. Eberhardt, E., Keil, G., and Weber, K., "Zur Wechselwirkung Phosphorhaltiger EP-Additivs mit Metalloberflächen." Schmierungstechnik 1, 101-107, 1970.
36. Weber, K., Eberhardt, E., and Keil, G., "Zur Wirkungsweise Phosphorhaltiger EP-Additivs unter Mechanischer Belastung in Vierkugelapparat." Schmierungstechnik 1, 300-310, 1970.